Dynamic Wetting of Aqueous Surfactant Solutions on Hydrophobic Solids and Water Subphases

Ph.D. Thesis

M. Phil. Xiang Wang | Matrikelnummer: 1830583
Maschinenbau, Technische Universität Darmstadt

TECHNISCHE
UNIVERSITÄT
DARMSTADT

Dynamic Wetting of Aqueous Surfactant Solutions on Hydrophobic Solids and Water Subphases

Vom Fachbereich Maschinenbau

an der Technischen Universität Darmstadt

zur

Erlangung des akademischen Grades eines

Doktors rerum naturalium (Dr. rer. nat.)

genehmigte

Dissertation

vorgelegt von

M. Phil. Xiang Wang

aus HeNan, China.

Berichterstatter: Prof. Dr.-Ing. Cameron Tropea

Mitberichterstatter: Prof. Stephen Garoff

Prof. Hans-Jürgen Butt

Tag der Einreichung: 21.10.2014

Tag der mündlichen Prüfung: 09.12.2014

Darmstadt 2014

D17

Erklärung

Hiermit erkläre ich, dass ich die vorliegende Arbeit, abgesehen von den in ihr ausdrücklich genannten Hilfen, selbständig verfasst habe.

Darmstadt, den 21.10.2014

Xiang Wang

Acknowledgements

As I look back to the past time for my Ph.D. study, I want to acknowledge the success of the long journey to many parties, the research group, collaborators, the administration team, friends and family members, and so on. Without their help and encouragement, there is no doubt that I would not have finished the thesis so smoothly.

Firstly, I would like to express my heartfelt gratitude to my supervisor, PD Dr.rer.nat. Elmar Bonaccurso, who offered me the chance to explore the Ph.D. journey in the Experimental Interface Physics (EIP) group at the Center of Smart Interfaces (CSI) of the Technische Universität Darmstadt. As an excellent group leader, he was always ready for discussion and support with team members. I benefited much from the weekly discussion with him, which helps guiding me on the right track of research. His enthusiastic passion in research and positive attitude in work inspired me to move forward. Therefore, I appreciate much for his supervision in the past three years.

Secondly, I thank, Prof. Dr.-Ing. Cameron Tropea, the director of our institute, for initiating the interdisciplinary CSI. Thanks to the groups with different research fields in the institute, my research views were broadened. I also give acknowledgement to Prof. Dr.-Ing. Cameron Tropea for advising me during my Ph.D. study. Moreover, it was my honor to collaborate with Dr. Joachim Venzmer from Evonik Industries AG, Germany. The beneficial discussion with him helped me to understand the research topics from a practical point of view. It was also my pleasure to cooperate one project with Dr. Kai Zhang (LOEWE Soft Control, Technische Universität Darmstadt).

Thirdly, thank Prof. Stephen Garoff and his group members for hosting me at the Carnegie Mellon University in Pittsburgh for two months. The research life there was productive, although the time was short. Also, thank Prof. Stephen Garoff for giving me valuable comments on my thesis. I appreciated the beneficial discussion with Prof. Hans-Jürgen Butt from the Max-Planck-Institute for Polymer Research. I also would like to thank Prof. Weijia Wen from the Hong Kong University of Science and Technology for his encouragement in the past years.

Meanwhile, I express my gratitude to all former members of the EIP group. They were all nice partners and cultivated a friendly work atmosphere. They helped me a lot in both work and life. It was great to work with them together as colleagues and close friends. Special thanks were given to Dr. Lars Heim, Dr. Julien Petit and Dr. Longquan Chen for commenting my thesis. I also thank the CSI committee for organizing the monthly seminars. My scientific view was broadened through the talks and discussions. As a member of the CSI committee from year 2013, I was pleased to work with other committee members as a team. Acknowledgements were also given to the administrative and technical staff in CSI, Monika Medina, Angela Berger, Sebastian Keuth, Marcus Keiner, Jana Müller and Felix Seipp. You all helped much with my Ph.D. journey in CSI.

Moreover, I am grateful that I had the opportunity to supervise a brilliant bachelor student, Simon Negash. With his diligence and smartness, he went along very well with the project and obtained a relevant share of results. I also thank my friends here without whom I would not have spent such a colorful life. I enjoyed eating together, drinking together and hanging out together with you guys. Particular thanks are given to my boyfriend, Weidong Chen, for being a great partner. He shared many good and bad moments of my life. Therefore, I thank him a lot for his help and encouragement during my Ph. D. life.

Last but not least, I would like to express my sincere appreciation to my family members, my parents and my brothers, for their continuous love and support since I was born. They sacrificed much to my education from elementary to Ph.D. for as long as 21 years. I owe a lot to them, which I may never be able to pay back. My parents always taught me to be diligent, to be persistent, and to be positive. Their encouragements, which drove me forward in the past, will also keep me optimistic in the future. Thank you, my dear parents!

Dynamic Wetting of Aqueous Surfactant Solutions on Hydrophobic Solids and Water Subphases

Abstract

Wetting is the ability of liquids to maintain contact with solids or other liquids. It is a commonly observed phenomenon in numerous natural and technological processes. Efficient wetting of liquids is crucial to painting, coating, printing, and drug delivery applications. Surface active agents (surfactants) are amphiphilic compounds which can lower the surface tension of liquid solvents. Adding surfactants to liquids is one common method to enhance wetting. Since the 1960s organomodified trisiloxane surfactants have been recognized as effective wetting agents for aqueous pesticide formulations because they fasten foliar uptake and wet larger leaf surface areas. Trisiloxane surfactants that possess the ability to promote rapid and extensive spreading of water on hydrophobic solids are known as superspreaders, and their wetting phenomenon is referred to as superspreading.

Numerous studies have been performed to reveal the peculiar properties of superspreaders and the underlying mechanisms of superspreading. The wetting area of superspreader solutions was found to increase linearly with time within the first several seconds. The highest wetting velocity was observed at a critical surfactant concentration. In the course of the years, the superspreading ability of trisiloxane surfactants was attributed to their molecular structure and to the way they aggregate in solutions. It was proposed that the driving force for superspreading is surface tension gradient over the spreading drop, which can be maintained for longer time by superspreaders than by non-superspreaders. Most of previous experiments were performed with video camera at low speeds (e.g., 500 frames per second or less). However, the investigation of early wetting with time scale of milliseconds is crucial

to understand rapid adhesion phenomena. It also allows us to know when surfactants start to become effective in the wetting systems, which helps to understand the wetting mechanisms behind. The goal of this experimental thesis is to shed light on the early wetting stage of aqueous surfactant solutions on hydrophobic solids and water subphases. Different surfactants and solids are used for comparative investigations. The superspreading stage of surfactant solutions is systematically studied by changing the factors that are assumed to influence the surface tension gradient, such as surfactant concentration and relative humidity.

The experiments within this thesis are performed using high-speed video imaging with temporal resolution up to 0.02 milliseconds. The results show that the wetting processes of hydrophobic solids by surfactant-laden drops can be described by one, two, or three stages, depending on physicochemical properties of the surfactants and the solids used. Surfactants do not play a role in the early wetting stage, which is mainly dominated by inertia. After a characteristic time, inertial wetting goes over in viscous wetting. This stage has also a characteristic duration and is influenced by surfactants. Afterwards a superspreading stage is observed for superspreading drops only. The driving force in this stage is the surface tension gradient, which is influenced by the dynamic surface tension of the spreading drop. The superspreading dynamics depends strongly on the surfactant concentration, on the relative humidity, as well as on the substrate wettabilities. It is found that superspreader solutions only superspread on substrates whose wettability falls within a narrow range. Conversely, on water subphases superspreader and non-superspreader solutions behave similarly.

The work in this Ph. D. project completes one gap - early wetting dynamics of surfactant solutions – in prior work. The findings reveal different wetting stages with different characteristic duration. The action times of surfactants during the wetting process have been assessed. Moreover, this study provides more evidence for the surface tension gradient as a driving force in the superspreading stage. Therefore, the findings represent a significant step forward for surfactant-enhanced wetting and superspreading. They can also offer guidance on practical applications, e.g., crop spraying. By using superspreaders under proper conditions, the wetting performance can be maximized and a cost reduction can be achieved.

Dynamische Benetzung Wässriger Tensidlösungen auf Festen Oberflächen und an der Wasser/Luft-Grenzfläche

Zusammenfassung

Mit Benetzung wird das Verhalten von Flüssigkeiten bezeichnet mit Festkörperoberflächen oder anderen Flüssigkeiten in Kontakt zu treten. Es ist ein vielfältig beobachtbares Phänomen in natürlichen wie auch in technischen Prozessen. Effiziente Benetzung ist entscheidend für Prozesse wie beispielsweise dem Lackieren, Beschichten, Drucken oder auch der Arzneimittelapplikation. Tenside (von lat. tensus gespannt) sind amphiphile Substanzen, die die Oberflächenspannung von Flüssigkeiten herabsetzen können. Die Zugabe von Tensiden ist eine gängige Methode um die Benetzungseigenschaften von Flüssigkeiten zu verbessern. In den sechziger Jahren des letzten Jahrhunderts wurde die Bedeutung spezieller Trisiloxane für die Formulierung wasserlöslicher Pestizide erkannt, da sie die Benetzungseigenschaften auf Pflanzenblättern verbesserten. Solche Tenside, die die Benetzung beschleunigen und intensivieren sind unter dem Begriff Superspreader bekannt und das Phänomen dieser verbesserten Benetzung als Superspreading.

Vielfältige Untersuchungen wurden durchgeführt, um die besonderen Eigenschaften und die zugrundeliegenden Mechanismen dieser Tenside zu entschlüsseln. Es wurde erkannt, daß die Fläche, die diese Tenside benetzten, in den ersten Sekunden linear zunimmt. Die höchste Geschwindigkeit wurde dabei bei einer bestimmten Konzentration gefunden. Im Laufe der Zeit wurde die molekulare Struktur sowie das Aggregationsverhalten der Trisiloxane in Lösung für dieses Verhalten verantwortlich gemacht. Als treibende Kraft wurde der Gradient der Oberflächenspannung über der sich ausbreitenden Tropfenoberfläche angeführt, der bei diesen Tensiden einen längeren Bestand hat als bei anderen Tensiden, die diese Eigenschaft nicht ausweisen. Die meisten der bisherigen Untersuchungen wurden mit Filmaufnahmen mit relativ

geringer zeitlicher Auflösung (ca. 500 Bilder pro Sekunde oder geringer) durchgeführt, wobei gerade die erste Phase der Benetzung mit einer Zeitauflösung im Millisekunden-Bereich für das Verständnis des Verhaltens wesentlich ist. Es erlaubt zu erkennen, wann Tenside beginnen eine Rolle zu spielen und welche grundlegenden Prozesse im Hintergrund ablaufen. Vornehmliches Ziel diese experimentelle Arbeit ist es, Licht in die erste Phase der Benetzung von hydrophoben Festkörpern und wäßrigen Grenzschichten zu bringen. Zu diesem Zweck wurden Untersuchungen mit unterschiedlichen Tensiden und Oberflächen durchgeführt. Das besondere Verhalten der Superspreader wurde dabei systematisch untersucht, wobei die den Gradienten der Oberflächenspannung beeinflussenden Parameter, wie Tensidkonzentration und relative Feuchtigkeit variiert wurden.

Die Untersuchungen im Rahmen dieser Arbeit wurden mit einer Videokamera durchgeführt, die eine zeitliche Auflösung von bis zu 0.02 Millisekunden ermöglicht. Es zeigte sich, daß die Benetzung von tensidhaltigen Tropfen auf hydrophoben Oberflächen mit einer, zwei oder drei Phasen beschrieben werden kann, abhängig von den physikalischen und chemischen Eigenschaften der verwendeten Tenside und Oberflächen. Tenside beeinflussen nicht die allererste Phase der Benetzung; diese ist im wesentlichen trägheitsdominiert. Nach einer charakteristischen Zeitpanne erfolgt ein Übergang von trägheitsdominiert zu viskosedominiert. Diese Phase wird durch die Tenside beeinflußt, auch sie hat eine charakteristische Dauer. Im Falle von Superspreading wird eine weitere, dritte Phase beobachtet. Federführend in dieser Phase ist der Gradient der Oberflächenspannung, welcher durch die Dynamik der Oberflächenspannung des sich ausbreitenden Tropfens beeinflußt wird. Diese Dynamik ist abhängig von der Tensidkonzentration, der relativen Luftfeuchtigkeit sowie der Benetzbarkeit der Oberfläche. Es zeigte sich, daß das Phänomen des Superspreading nur auftritt, wenn die Benetzbarkeit der Oberfläche in einem bestimmten Bereich liegt. Auf wäßrigen Oberflächen verhalten sich Superspreader und Nicht-Superspreader vergleichbar.

Diese Arbeit füllt eine Lücke bisheriger Untersuchungen – die frühe Phase der Benetzungsdynamik von Tensidlösungen. Es wurden unterschiedliche Phasen der Benetzung gefunden, die unterschiedliche charakteristische Zeiten aufweisen. Der

Zeitpunkt, ab wann Tenside im Benetzungprozeß eine Rolle spielen, konnte bestimmt werden. Diese Arbeit untermauert die These, daß der Gradient der Oberflächenspannung die treibende Kraft in der Phase der Benetzung ist, die mit Superspreading beschrieben wird. Die Ergebnisse bieten eine solide Grundlagen für ein besseres Verständnis des durch Tenside verbesserten Benetztens und sogenanntes Superspreading. Sie können als Grundlage dienen, praktische Anwendungen zu generieren, wie beispielsweise bei der Schädlingsbekämpfung in der Argrarwirtschaft. Durch den Einsatz von entsprechenden Tensiden unter entsprechenden Randbedingungen könnte das Benetzungsverhalten verbessert und somit der Aufwand gemindert werden.

Contents

List of Figures

List of Tables

List of Symbols

$A(t)$ surface area [m^2]

a air phase

a_0 cross-sectional area occupied by a hydrophilic group [m^2]

C power law coefficient

Ca Capillary number

D diffusion coefficient

D_0 diameter of Petri dish

$d(t)$ advancing distance with time [m]

d^* spreading diameter [m]

d_0 initial drop diameter [m]

d^*_{max} maximum wetting diameter [m]

F capillary force [N]

g gravitational acceleration [m/s^2]

H_0 height of water subphases

h height of drop [m]

z vertical height of drop from reference plane [m]

h_m microscopic height

K_0 molecular jump frequency [Hz]

k Boltzmann constant [J/K]

k_* wavenumber

L macroscopic length scale

L_C capillary length [m]

L_α lamellar phase

L_3 sponge phase

L_s slip length

l liquid phase

l_b length of a hydrophobic group [m]

We Weber number

l_c critical height for strong surface tension gradient [m]

n number of the molecules

P packing parameter

ΔP_0 Laplace pressure [Pa]

r spreading/contact radius [m]

r_0 initial drop radius [m]

r_{max} maximum wetting radius [m]

R radius of curvature

R_1 main radius of curvature

R_2 main radius of curvature

R_a average deviation of roughness

Re Reynolds number

s solid phase

S spreading coefficient

t spreading time [s]

t_0^* dimensionless time $t/\sqrt{\rho r_0^3/\gamma}$

t_m^* dimensionless time $t/\sqrt{\rho r_{max}^3/\gamma}$

T absolute temperature [K]

V drop volume [m^3]

V_H volume occupied by a hydrophobic group [m^3]

v velocity of capillary wave on curved water surfaces [m/s]

v_{min} minimum propagating velocity of capillary waves [m/s]

v_p phase velocity of capillary waves

v_g group velocity of capillary waves

u_0 impact velocity [m/s]

U spreading velocity [m/s]

θ dynamic contact angle

θ_A advancing contact angle

θ_{eq} equilibrium contact angle

θ_0 static contact angle

θ_H contact angle hysteresis

θ_R receding contact angle

θ_m microscopic contact angle

θ_0^{MKT} fitted static contact angle from MKT

θ_0^{HD} fitted static contact angle from HDT

Pe Péclet number

ξ distance travelled by expanding surfactant

u expanding velocity of surfactant

β dimensionless spreading factor

β_{max} maximum spreading factor

τ actual inertial time [s]

τ_c characteristic inertial time [s]

α wetting exponent

γ liquid surface tension [N/m]

$\Delta\gamma(t)$ surface tension difference

$\nabla\gamma(t)$ surface tension gradient

γ_c characteristic critical surface tension of solids [N/m]

γ_{sl} solid/liquid interfacial tension [N/m]

γ_{sa} solid/air interfacial tension [N/m]

ρ liquid density [kg/m^3]

$\Delta\rho$ liquid density difference [kg/m^3]

μ dynamic viscosity [Pa·s]

λ molecular displacement [m]

λ^* wavelength of capillary wave [m]

λ_c^* critical wavelength of capillary wave

ω angular frequency [rad/s]

ϵ correlation coefficient

List of Abbreviations

AFM	Atomic force microscope
AOT	Dioctyl sodium sulfosuccinate
CMC	Critical micelle concentration
CTAB	Cetyltrimethyl ammonium bromide
DLS	Dynamic light scattering
DST	Dynamic surface tension
HDT	Hydrodynamic theory
LSM	Least square method
MKT	Molecular kinetic theory
MFC	Mass flow controller
PAT	Profile analysis tensiometer
PC	Polycarbonate
PDMS	Polydimethylsiloxane
PET	Polyethylene terephthalate
PMMA	Polymethyl methacrylate
PP	Polypropylene
PS	Polystyrene
RDS	Respiratory distress syndrome
RH	Relative humidity
SANS	Small-angle neutron scattering
SAXS	Small-angle X-ray scattering
SDS	Sodium dodecyl sulfate
SRT	Surfactant replacement therapy
TPCL	Triple phase contact line

1 Introduction and Motivation

Wetting refers to the study of how a liquid deposited on a solid or liquid subphase spreads out. The phenomenon is pertinent to the house we live in, the cosmetics we use, the food we eat and the books or newspapers we read. Motivated by numerous technical applications, such as coating, oil recovery, pesticide spraying, lubrication and many others, the topic of wetting has been systematically investigated for more than two centuries. In many fields like agricultural spraying and industrial printing, liquids are required to wet hydrophobic solids rapidly and even completely. In textile industry, for example, increasing the wettability of fibers is required for effective dyeing and cleaning. Due to the high surface tension of water, surface active agents (surfactants) are widely added to liquids to decrease the surface tensions and thus to turn non-wetting into a wetting solutions, even on hydrophobic solids. Surfactants are a class of amphiphilic compounds that consist of a hydrophilic head group and a hydrophobic tail group. They are widely used in a number of commercial products, e.g. paints and coatings [1], herbicides and pesticides [2, 3], medical drugs [4], to enhance wetting and deposition on respective substrates. Thus, advancing our understanding about the underlying mechanisms of surfactant-enhanced wetting is crucial to the implementation of many technological processes.

Within tens of seconds, certain aqueous trisiloxane surfactant solutions spread over hydrophobic solids into a thin film with a final contact angle of around zero, and the overall wetting area can be as much as 50 times larger than that of water and 25 times larger than that of “conventional” surfactant solutions [5]. Trisiloxane surfactants with such unique wetting ability were discovered in the 1960s [6, 7], and their ability to rapidly and extensively wet hydrophobic surfaces (e.g. leaf’s surfaces or general hydrophobic plastics) is referred to as superwetting or superspreading [8-13]. The capability of trisiloxane surfactants to promote wetting on plant leaves is the basis of their use as wetting and spreading agents in pesticide formulations [2, 14, 15]. The superspreaders maximize the performance of agrochemicals by reducing spray drops’ tendency to bounce off plant foliage, by increasing the immediate penetration of the liquid into the naturally occurring plant openings, and by spreading the liquid to greater leaf areas. In this way, delivery of the pesticide into the plant is insured and a

later rainfall cannot dislodge the residue. In addition, the rapid uptake process allows the spray to reach locations that are usually not accessible by “conventional” surfactant solutions. Therefore, significant savings can be achieved as less water is required per area, either reducing energy cost or extending the area treated by a single spray tank.

Pioneered by the work of Ananthapadmanabhan and co-workers [16], numerous investigations have been performed to understand the superspreading behavior of aqueous trisiloxane solutions on hydrophobic solids [13, 15, 17-29]. It was found that trisiloxane surfactants, with similar chemical structure and similar ability to reduce liquid surface tension, exhibit different wetting performances on the same solids [12, 30, 31]. Researchers have put forward a number of factors influencing the superspreading ability of trisiloxane surfactants, such as their unique molecular structure, the aggregation of surfactant molecules (e.g. bilayers, vesicles, or lamellae), the adsorbability of surfactant molecules at the solid/liquid interface, and the atmospheric relative humidity (RH). Although surfactant-enhanced wetting and superspreading have been the subject of considerable research interests over the past decades [9, 19, 20, 32-37], the underlying mechanisms are still not completely understood. This is because wetting of aqueous surfactant solutions is a dynamic process, which is complicated by the fact that the liquid surface tension is a dynamic property as well. The liquid surface tension changes with time, also depending on surfactant concentration. The classical physical concepts for the spreading of liquids on solids can be classified into two basic mechanisms. The first one is based on thermodynamics [38]: a positive spreading coefficient leads the liquids to spread on solids until the surface tension balance is restored. The second one describes wetting in terms of a surface tension gradient [38, 39]. The spatial variation in surface tension at an air/liquid interface results in tangential stresses at the surface, which causes liquid flows from regions of lower to regions of higher surface tension. Surface tension gradient was suggested to be a major driving force for superspreading [8, 13, 17, 22, 24].

The liquid flows caused by the surface tension gradient have found applications in industry and science [40-48] because of its major relevance in large scale processes

like oil recovery in environment engineering [49] or for drying integrated circuits and liquid crystal displays in technical applications [50, 51]. It was reported that the surface tension gradient could move solid objects (e.g. particles) along a liquid subphase [41, 45, 52-54]. This has specific application in aerosol drug delivery and surfactant replacement therapy (SRT) [55-57]. Premature newborns with developmentally deficient lung surfactant in the alveoli suffer from the respiratory distress syndrome (RDS). The SRT treatment for this life-threatening syndrome involves pushing a bolus of surfactant-laden fluid into the lungs through an intubation tube. During the movement of the fluid deeper into the lung, the bolus breaks into a film, coating the lung airway surface. It is speculated that this film is moved forwards via the surface tension gradient as the surfactant in the bolus moves along the liquid in the lung airway surface.

Regarding the wetting of drops of simple liquids on solids, an early stage dominated by inertia was reported in a number of experimental and theoretical studies [58-62]. On partially and completely wettable solids, a second wetting stage dominated by viscosity was observed [63, 64]. However, there is little experimental data about the early wetting dynamics of aqueous surfactant solutions, which can help clarifying at what time scales surfactants play a role in enhancing wetting. In several studies trying to elucidate the mechanism of superspreading [17, 65, 66], either superspreader solutions at low concentrations (e.g. 10^{-4} wt%), or very hydrophobic solids (e.g. perfluorinated polymers) were used in experiments and no superspreading occurred. It was also found that superspreading was not observed at very low RH (e.g. dry air) [8, 67]. Understanding how surfactant concentration, substrate wettability, and atmospheric RH influence the superspreading can offer practical guidance in the applications of trisiloxane surfactants as pesticide additives. For instance, farmers will know whether it is better to spray the pesticides when the atmospheric RH is high.

This Ph.D. project aims to investigate the early wetting dynamics and impact dynamics of aqueous solutions of non-superspreaders and superspreaders on hydrophobic solids and water subphases, and to determine the effects of surfactant concentration, substrate wettability, atmospheric RH, and the surface tension gradient on superspreading. Through the comparative study of different types of surfactants,

the project attempts to reveal the physicochemical properties of a certain class of trisiloxanes that make them be so effective as wetting agents.

1.1 Outline of the Thesis

Chapter 2 presents the fundamentals of wetting on solids and liquids. It introduces wetting of simple liquids and aqueous surfactant solutions. Both static and dynamic wetting are addressed for the wetting of simple liquids. The dynamics of two wetting stages is described in the dynamic wetting part. Moreover, the chapter conveys the reader some fundamental knowledge about surfactants. Previous studies related to surfactant-enhanced wetting and superspreading are briefly reviewed in this chapter.

The experimental materials including surfactants and solids and water subphases used in the work are presented in Chapter 3. Methods and principles used to characterize the physicochemical properties of materials are explained. The experimental setups are schematically shown in this chapter. The program used to process the images and data analysis methods are described as well.

Chapter 4 introduces the wetting dynamics of different surfactant-laden drops on hydrophobic solids. Fitting models are applied to each wetting stage, and the experimental results are compared with existing work. This chapter mainly addresses the effects of surfactant concentration, substrate wettability and relative humidity on the wetting dynamics of trisiloxane surfactant solutions, especially of superspreader solutions.

Chapter 5 covers the investigation of surfactant-enhanced wetting on hydrophobic polypropylene substrates and flat water subphases. The first part aims to understand how surfactants spreads along curved air/water interfaces and how the surface tension gradient influences drop spreading. The experimental results on solids are compared with that in spontaneous wetting of surfactant solutions. The early wetting stage of aqueous surfactant solutions on flat water subphases constitutes the second part.

Chapter 6 presents experimental work about the impact of surfactant-laden drops on polypropylene substrates. The impact and wetting dynamics are analyzed with regard to different types of surfactants. The experimental data is compared with that in

spontaneous wetting of surfactants on similar substrates. This offers the reader a comprehensive picture of spontaneous wetting and drop impact of aqueous surfactant solutions.

The last chapter summarizes all the experimental results and conclusions of the Ph.D. project. The findings reveal some unknown aspects in surfactant-enhanced wetting and superspreading, and therefore represent important steps forward from a scientific point of view. The results can find applications in optimizing the use of surfactants in wetting and spraying processes.

2 Fundamentals of Wetting

Wetting is of key importance in life science and industry, such as waterproofing of concrete, drainage of water from highways, pesticide deposition on plant leaves, or rise of sap in plants. Enhancement of wettability by surfactants is important in cases where complete contact of a hydrophobic solid with a liquid is desirable. Thus, developing and furthering our understanding of the physicochemical processes that control the wetting dynamics of aqueous surfactant solutions will enable us to improve our knowledge of everyday events. This chapter briefly introduces the fundamentals of wetting on solids and liquid subphases. In the first part, wetting by simple liquids is described, addressing the equilibrium of a liquid drop on a solid, i.e. the static wetting case, and the dynamic wetting case. In the second part, wetting of aqueous surfactant solutions and superspreading are addressed.

2.1 Wetting of Simple Liquids

Wetting of one-component liquids or simple liquids (e.g. ultra-pure water) on solids has been addressed for over two centuries since the pioneering work by Young [68]. Thermodynamic and mechanical descriptions of capillarity have been put forward which help explaining a number of experimental observations, such as the shape of sessile drops and the spontaneous rise of liquid in a capillary. Static and dynamic wetting behaviors of simple liquids on solids have been well investigated and reviewed in many papers [38, 69-75].

2.1.1 Static Wetting

When a liquid drop is deposited on a solid, the drop spreads over the solid to minimize the free energy of the system and equilibrates at a final state. One of the most frequently used parameters to characterize wetting is the contact angle, θ, which is geometrically defined as the angle formed by the liquid drop at the three phase boundary where liquid, air, and solid meet (Figure 2-1). The liquid, air and solid phases are designated by l, a and s, respectively. The contact angle quantitatively measures the wetting ability of a liquid on a solid. The contact perimeter between the

three phases is commonly referred to as the triple phase contact line (TPCL). r is the contact radius of the drop and R is radius of the curvature.

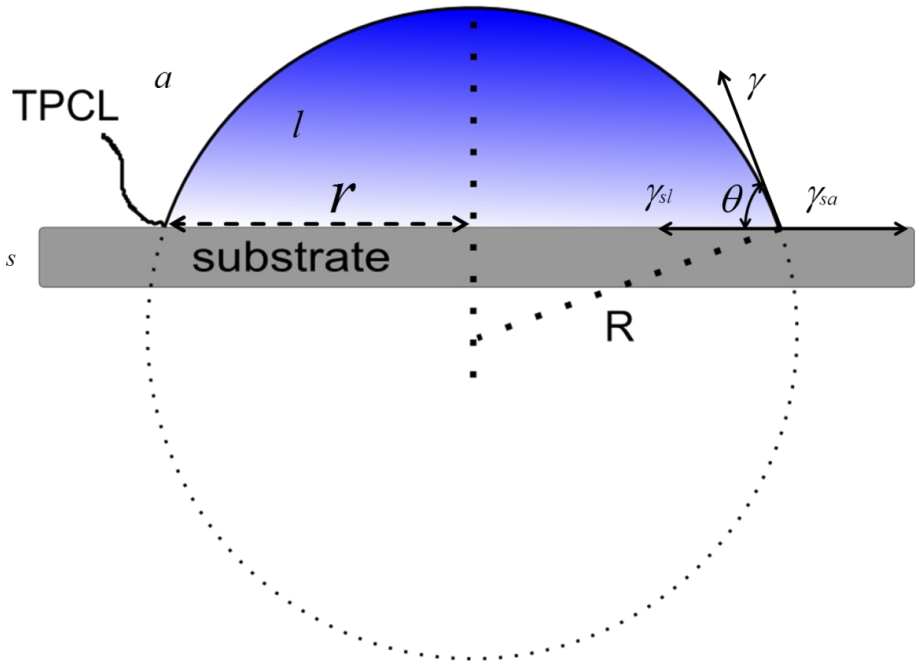

Figure 2-1 Graphical representation of a sessile drop forming a spherical cap on a solid.

By balancing the forces acting at the TPCL, Young [68] firstly quantified wetting with the equilibrium contact angle, θ_{eq}, which is determined by the interfacial tensions of solid/air (γ_{sa}), solid/liquid (γ_{sl}) and air/liquid (γ).

$$\cos\theta_{eq} = \frac{\gamma_{sa} - \gamma_{sl}}{\gamma} \tag{2.1}$$

In general, two distinct equilibria are defined based on the equilibrium contact angle: complete wetting and partial wetting [76]. The complete wetting case is shown in Figure 2-2a, where the drop wets the solid completely with θ_{eq} close to 0°. In case of partial wetting (Figs. 2-2b & c), the drop at equilibrium forms a spherical cap resting on the solid with θ_{eq} between 0° and 180°. If θ_{eq} is smaller than 90°, a liquid is said to be “mostly wetting”. Similarly, if θ_{eq} is larger than 90°, a liquid is said to be “mostly non-wetting”.

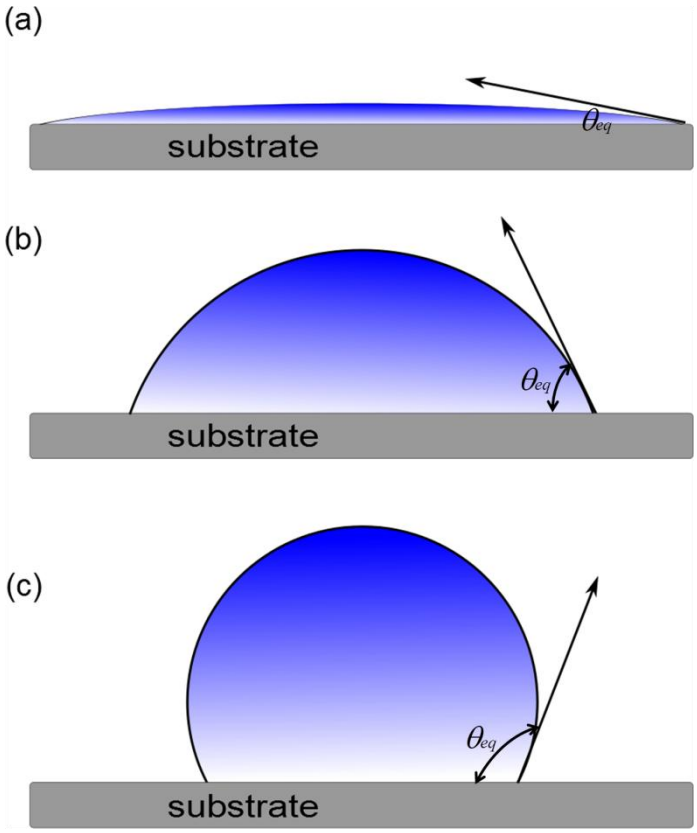

Figure 2-2 A liquid drop in thermodynamic equilibrium on a solid. (a) complete wetting, (b) and (c) partial wetting, where drops have a finite contact radius at the wetted portion of the solid.

Note that the liquid drops discussed in this thesis are restricted to drops with initial radius r_0 smaller than the capillary length $L_C = \sqrt{\gamma/\rho g}$. ρ denotes the density of the liquid and g is the acceleration due to gravity. At the air/water interface, L_C is approx. 2.7 mm. When $r_0 < L_C$ is satisfied, surface tension effects dominate over gravitational effects. Such drops deposited on solids take shapes of spherical caps (Figure 2-1). For large drops with radii larger than L_C, gravitational effects dominate. Such sessile drops are flattened by gravity and take the shape of a liquid puddle. The latter case is out of the scope of the present work.

The Spreading Coefficient

While Young's equation provides a thermodynamic definition of contact angle, it is only valid for ideal solids, which are chemically homogeneous and smooth even at atomic scale. Moreover, the experimental verification is complicated by the fact that

the values of γ_{sa} and γ_{sl} cannot be directly determined experimentally. Despite the limitations, Young's equation has nevertheless been demonstrated to be an adequate method of describing wetting equilibrium in most circumstances. It also provides a simple way to define the spreading coefficient, S.

$$S = \gamma_{sa} - \gamma_{sl} - \gamma \tag{2.2}$$

If the spreading coefficient is positive, the liquid drop will spread completely over the solid in order to lower its free energy. Otherwise, the liquid drop remains as a spherical cap on the solid. Therefore, the parameter S can be used to distinguish the wetting scenarios shown in Figure 2-2.

For a drop in equilibrium, substituting Eq. (2.1) into Eq. (2.2) yields:

$$S = \gamma(cos\,\theta_{eq} - 1) \tag{2.3}$$

It is evident that θ_{eq} can be defined only if the spreading coefficient is zero or negative.

Wetting Criterion: Zisman's Rule

Solids can be divided into two categories with regard to their surface energy [38]. High-energy solids are made of materials that are ionic, covalent, or metallic. In this category, the surface energy ranges from $500\,mN/m$ to $5{,}000\,mN/m$. Low-energy solids, like crystals and plastics, are made of materials that are held together by van der Waals forces, or in some special cases, by hydrogen bonds. In this case, the surface energy is between $10\,mN/m$ to $50\,mN/m$.

The question arises if it is possible to predict whether a solid is wetted by a liquid. Zisman [77, 78] worked out an empirical criterion to classify solids and to predict the wetting states of liquids on them. Each solid has a characteristic critical surface tension γ_C, which can be determined by studying the wetting properties of a series of liquids with known surface tensions γ on it. Partial wetting occurs when $\gamma > \gamma_C$, and complete wetting occurs when $\gamma < \gamma_C$. With this criterion, it is possible to understand why most simple liquids spread on high-energy solids like glass and metals, and not on plastics. Therefore, γ_C is an essential parameter that characterizes solids.

Contact Angle Hysteresis

The equilibrium contact angle θ_{eq} yielded by Young's equation is only valid for ideal solids. However, a real solid always has a certain degree of contamination and inhomogeneity (e.g. surface roughness, chemical heterogeneity, dust). This may cause Young's equation and the spreading coefficient to depend on the position of the drop on the solid. In many practical situations, one almost never measures the equilibrium contact angle, since even a small surface inhomogeneity may lead to a significant contact angle deviation. Furthermore, the contact angle varies depending on whether the liquid is advancing on the dry solid with an advancing contact angle, θ_A, or receding from the already wetted solid with a receding contact angle, θ_R. The equilibrium contact angle θ_{eq} is between those values, $\theta_A \geq \theta_{eq} \geq \theta_R$. The advancing and receding contact angles (called dynamic contact angles for distinguishing them from the equilibrium contact angle) depend on the velocity of the TPCL. The dependence of measured dynamic contact angle on the TPCL velocity is shown schematically in Figure 2-3.

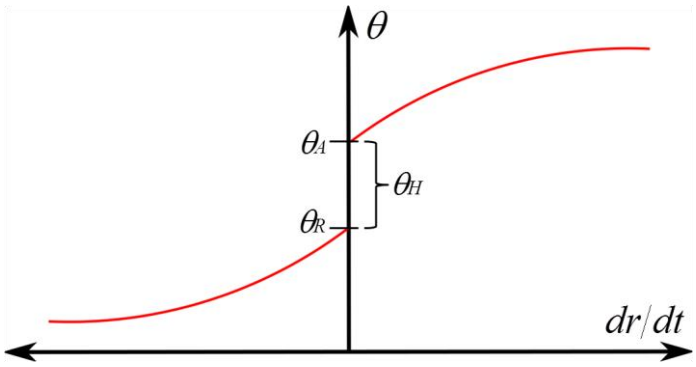

Figure 2-3 Schematic of the dynamic contact angle dependence on the TPCL velocity.

The contact angle hysteresis, θ_H, is defined as the difference between the advancing and receding contact angles when the velocity is zero [38]:

$$\theta_H = \theta_A - \theta_R \tag{2.4}$$

The contact angle hysteresis characterizes the surface homogeneity. A surface is considered to be clean and smooth if θ_H is smaller than 5°. In practice, θ_H is often of

the order of several tens of degrees [73]. Therefore, θ_H is useful as spot test of the cleanness of sensitive solids such as glass or silicon wafers for microelectronic fabrications. It is also used as a test in the automobile industry to ensure that solids are perfectly clean before applying paint.

Even on a perfectly smooth solid as assumed by Young's equation, liquids still exhibit contact angle hysteresis. The equilibrium contact angle, θ_{eq}, can be calculated from θ_A and θ_R, according to [79, 80]:

$$\theta_{eq} = arccos\left(\frac{r_A cos\,\theta_A + r_R cos\,\theta_R}{r_A + r_R}\right) \tag{2.5}$$

where

$$r_A = \left(\frac{sin^3\,\theta_A}{2 - 3cos\,\theta_A + cos^3\,\theta_A}\right)^{1/3} \tag{2.6}$$

$$r_R = \left(\frac{sin^3\,\theta_R}{2 - 3cos\,\theta_R + cos^3\,\theta_R}\right)^{1/3} \tag{2.7}$$

2.1.2 Dynamic Wetting

Whenever a liquid drop is deposited on a solid, the drop is expected to spread until equilibrium is reached. This may require the drop to either spread over the solid or remain as a spherical cap, or even try to escape from the solid in some cases. The net horizontal force resulting from out-of-balance interfacial tensions at the TPCL drives the drop to spread in the direction of equilibrium:

$$F = \gamma_{sa} - \gamma\cos\theta - \gamma_{sl} = \gamma(\cos\theta_0 - \cos\theta) \tag{2.8}$$

Here static contact angle θ_0 is used to characterize the equilibrium state. This is because the angle θ_{eq} from Young's equation represents equilibrium on an ideal solid, and is not measurable in experiments. The inertia of the drop, the friction at the TPCL and the viscous dissipation within the drop oppose the wetting process. When the capillary driving force is balanced by inertial or viscous forces, the drop reaches an equilibrium state.

Investigation of the first moments of drop spreading is crucial to understand rapid adhesion phenomena that occur in nature and in technology. With the advent of high-

speed video cameras, wetting dynamics of drops spreading within several milliseconds has become accessible. An early inertia-dominated stage of low-viscosity drops has been reported in a number of experimental and theoretical studies [58-61, 81, 82]. Following the inertial stage, a viscosity-dominated stage can be observed in partial and complete wetting systems [38, 63, 64, 83]. In the inertial and in the viscous stages, the wetting radius r versus (vs.) time t follow power laws, $r \propto Ct^{\alpha}$. Here coefficient C and exponent α depend on the type of forces resisting drop spreading [83]. The following section will introduce dynamic wetting in detail.

Inertial Wetting Dynamics

Figure 2-4 shows snapshots of liquid drops with different surface tensions spreading on the same solids. Just after a spherical drop is brought into contact with a solid ($t = 0\ ms$), the contact generates a mechanical "shock" that initiates capillary waves (red arrow in Figure 2-4) travelling along the surface of the drop. The capillary waves were observed in several studies [58, 59, 81]. The capillary driving force, $\gamma(\cos\theta_0 - \cos\theta)$, is concentrated into a singular point of contact and drives the drop to spread at a velocity of U. A recent study using experiments and molecular dynamics simulations

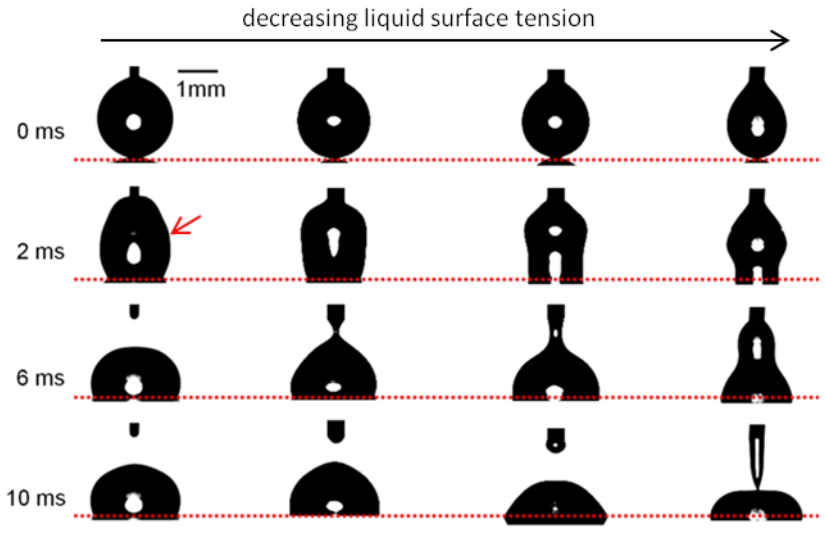

Figure 2-4 Snapshots of liquid drops with different surface tensions (from left to right: 72.8 mN/m, 55.4 mN/m, 33.5 mN/m, 23.2 mN/m) on polypropylene substrates represented by dotted red lines. 0 ms corresponds to the moment when the drop is initially deposited on the substrate.

has shown that the early wetting stage ($t \lesssim 0.1\ ms$) of low-viscosity drops on a partially wetting substrate is independent of substrate wettability [62]. However, about 0.1 ms after contact, the wetting dynamics begins to show a dependence on substrate wettability. Two main forces resist the wetting process of the drop: the inertia of the spreading drop and viscous dissipation in the liquid. The Reynolds number, $Re = \rho U r_0/\mu$, which compares inertial and viscous effects, is much larger than unity. μ is the dynamic viscosity of the liquid drop. Therefore, it is reasonable to neglect viscosity and assume that the wetting process is dominated only by inertia.

Based on Newton's second law, Biance *et al.* [58] proposed a scaling relation of the wetting radius with time, $r \propto t^{1/2}$, to describe the early stage ($t < 10\ ms$) of complete wetting. Bird and co-workers [59] theoretically derived a power law for the wetting radius vs. time, with the exponent depending continuously on substrate wettability. By considering the energy conservation between surface energy and kinetic energy, they obtained the governing equation:

$$\int_V \frac{1}{2}\rho|U|^2 dV = \gamma[A(0) - A(t) + \pi r^2 \cos\theta_0] \tag{2.9}$$

Here V is the "effective" volume of the spreading drop. $U(r,t)$, with the magnitude described as $U(r,t) \propto dr/dt$, is the velocity field as a function of drop position r and time t, which is assumed to vary over the length $l_v \propto (\gamma t^2/\rho)^{1/3}$ near the TPCL [84]. $A(t)$ is the surface area of the air/liquid interface. The change in the surface area is expected to scale as r^2, i.e. $A(0) - A(t) = \pi r^2 F(\theta_0)$, where $F(\theta_0)$ is an unknown function.

With these simplifications, Eq. (2.9) is reduced to:

$$\frac{t}{r}\frac{dr}{dt} \propto \sqrt{F(\theta_0) + \cos\theta_0} \tag{2.10}$$

The nondimensional solution to Eq. (2.10) is a power law:

$$r \propto Ct^{\alpha}, \text{ with } \alpha \propto \sqrt{F(\theta_0) + \cos\theta_0} \tag{2.11}$$

The exponent α depends only on the static contact angle θ_0, but not on any other physical properties of liquids. This scaling model was confirmed by experimental

results on the effect of substrate wettability on the early wetting dynamics [59]. With a modification of existing works [58, 59], Chen *et al.* [60] derived the same scaling law with $1/5 \lesssim \alpha \lesssim 1/2$ for solids with different wettability.

The inertial wetting stage lasts for a characteristic inertial time $\tau_c = (\rho r_0^3/\gamma)^{1/2}$ [58]. However, it was found that the actual inertial time τ, increasing with the size of drop, is always larger than τ_c [58, 59, 81]. One possible rationale is that the inertial wetting lasts as long as the capillary waves generated upon contact between drop and substrate propagates along the drop [59]. Following the vibration model of suspended drops proposed by Lamb [85], a linear relationship between τ and τ_c, $\tau \approx 2.2\tau_c$, was obtained [81]. The authors experimentally proved that the actual duration of the inertial wetting was longer than the characteristic inertial time, because the constantly growing wetting radius would slow the propagation of the capillary waves.

Viscous Wetting Dynamics

For hydrophilic ($\theta_0 \lesssim 57.3°$) and complete wetting ($\theta_0 \sim 0°$) systems, a second wetting stage is observed after the early inertial wetting stage. The unbalanced horizontal capillary driving force is counteracted by viscous dissipation in the bulk drop and dissipation by friction of the TPCL of the drop. The hydrodynamic theory (HDT) assumes that the capillarity-driven wetting is opposed by viscous dissipation in the bulk drop [38, 86, 87], while the molecular kinetic theory (MKT) suggests a molecular dissipation process happening in the close vicinity of the TPCL [88, 89].

Figure 2-5 shows a liquid drop spreading on a partially wettable solid. The parameters for HDT and MKT are illustrated on the left and right side of the liquid drop, respectively. In the HDT, Voinov [86] established a relation between dynamic contact angle θ and microscopic contact angle θ_m, which is determined at a microscopic height h_m. The HDT assumes dissipation due to viscous flow within the wedge of liquid near the TPCL, without considering any dissipation due to friction between liquid and solid. Because of the conflict between a moving TPCL and the no-slip boundary condition at the solid/liquid interface, stresses are unbounded near the TPCL, and the force exerted by the liquid on the solid becomes infinite [64]. One way to deal with the viscous stress singularity arising from the no-slip condition is to

assume that the liquid slips in a region of length L_s near the TPCL. θ_m is independent of the TPCL velocity U, when the Reynolds number Re and Capillary number $Ca = \mu U/\gamma$, are much smaller than one. The Capillary number represents the relative effect of viscous forces vs. surface tension forces of a spreading drop; $Ca \approx 10^{-5} - 10^{-3}$ in most wetting experiments. With these assumptions, the dependence of the dynamic contact angle on the contact line velocity was obtained by Cox [87]:

$$g(\theta) = g(\theta_0) + Ca\, ln(L/L_s) \tag{2.12}$$

where

$$g(\theta) = \int_0^{\theta} \frac{x - sin\, x\, cos x}{2\, sin\, x} dx \tag{2.13}$$

L characterizes a macroscopic length scale (of the order of the drop size), and L_s denotes a microscopic slip length, which is of the order of a molecular size [90]. The free parameters in Eq. (2.12) are the static contact angle θ_0 and $ln(L/L_s)$, and the latter is expected to be $10 - 15$ as L is of micrometer scale and L_s of nanometer scale.

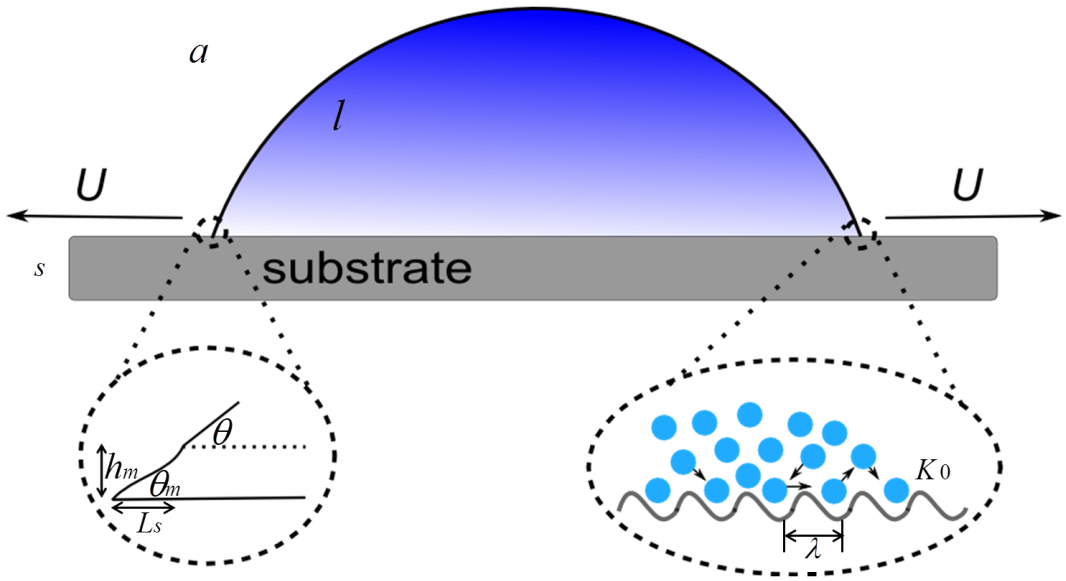

Figure 2-5 A liquid drop on a partially wettable solid. The parameters of the hydrodynamic theory (HDT) and the molecular kinetic theory (MKT) are schematically shown on the left side and right side of the drop, respectively. (adapted from Ref. [91])

For contact angles smaller than 135°, the integrand $g(\theta)$ can be reduced to $\theta^3/9$ with proximity smaller than 1%. Equation (2.12) can then be simplified to [86]:

$$\theta^3 = \theta_0^3 + 9Ca\ ln\ (L/L_s) \tag{2.14}$$

Under the assumption that the drop shape is a spherical cap at all times during wetting, θ and r are coupled due to the constraint of fixed drop volume $V \approx \pi r^3 \theta$. For complete wetting, i.e. $\theta_0 \sim 0°$, one can find the relationships between dynamic contact angle θ, wetting radius r and wetting time t [86]:

$$\theta\ (t) \propto t^{-3/10} \tag{2.15}$$

$$r\ (t) \propto t^{1/10} \tag{2.16}$$

These power laws have been verified experimentally [92-94]. Equation (2.16) is mostly referred to as Tanner's law [64] which was developed in the pioneering investigation of spreading drops on completely wettable solids.

Blake [88] was the first to account for a microscopic dissipation process happening in the close vicinity of the TPCL and developed the MKT. In the MKT, thermally activated displacements of liquid molecules control the TPCL motion. As shown schematically in Figure 2-5, during drop spreading individual liquid molecules jump forward or backward from one adsorption site to another with a certain frequency. Based on the application of Eyring's model of activated rate theory [95], the frequency of molecular displacements in the forward direction K_+ and that in the backward direction K_- can be expressed as

$$K_+ = K_0 exp\ (\frac{W}{2nkT}) \tag{2.17}$$

$$K_- = K_0 exp\ (\frac{-W}{2nkT}) \tag{2.18}$$

Here, K_0 is the equilibrium frequency of molecular displacements, with a value of ~ 1 MHz. W is the work done by the shear stress per unit length displacement of the TPCL, $W = \gamma(cos\theta_0 - cos\theta)$. n represents the adsorption sites per unit area. k is the Boltzmann constant and T is the absolute temperature.

The TPCL moves outward only when the molecular displacement in the forward direction is more frequent than that in the backward direction. The TPCL velocity can be expressed as:

$$U = (K_+ - K_-)\lambda = 2K_0\lambda\, sinh(\frac{W}{2nkT}) \tag{2.19}$$

Here, λ is the displacement distance of individual molecules (typically $\sim 1\ nm$), and λ^2 is taken as $1/n$. Then the relationship between dynamic contact angle and TPCL velocity is given by:

$$U = 2K_0\lambda sinh\left[\frac{\gamma\lambda^2}{2kT}(cos\theta_0 - cos\theta)\right] \tag{2.20}$$

If the argument of $sinh$ is small, equation (2.20) simplifies to:

$$U = \frac{K_0\lambda^3}{kT}\gamma(cos\theta_0 - cos\theta) \tag{2.21}$$

Again, if $\theta_0 \sim 0°$ and θ is relatively small, equation (2.21) yields the dependence of the dynamic contact angle θ and wetting radius r with time:

$$\theta\,(t) \propto t^{-3/7} \tag{2.22}$$

$$r\,(t) \propto t^{1/7} \tag{2.23}$$

The above equations have also been validated experimentally and theoretically [94, 96].

The power laws derived from HDT (Eq. 2.16) and MKT (Eq. 2.23) are different. This is due to the different dependence of TPCL velocity on the dynamic contact angle: HDT predicts that for small angles $U \propto \theta^3$ (2.14), while MKT predicts that $U \propto \theta^2$ (2.21).

2.1.3 Drop Impact

Wetting of liquid drops due to impact on solids is a phenomenon encountered in a number of industrial and environmental processes. Examples include cooling of solids by sprays [97], raindrop dynamics [98], ink-jet printing [99] and deposition of

pesticides or nutrients on plant leaves [2]. In these applications, the maximum coverage of the solids with the minimum amount of spray is favorable. Understanding the impact process of liquid drops on solids is therefore important, and the topic has been extensively studied [100-105]. Drop impact on solids results in many phenomena, from splashes to spreading, and from large deformation of drop surface to drop rebound [106, 107]. Upon contact with the solid, the drop expands rapidly to a maximum extent, and then recoils with an oscillating movement. Eventually, the drop reaches a final equilibrium, characterized by a static contact angle and an equilibrium contact area. On a hydrophobic solid, the drop may retract so violently that the recoiling process ends by partial or complete rebound of the drop from the solid, while on a hydrophilic solid the drop remains stuck to it. Numerical predictions in Ref. [104] showed that the early wetting stage was solely controlled by inertial force, which was confirmed later experimentally [103, 108, 109]. Normalizing the spreading diameter (d^*) by the initial diameter (d_0) of a drop yields the so-called dimensionless spreading factor β. The experimental observations of drops impacting on solids indicated that β grew according to a power law with time, with an exponent lying between 0.45 and 0.57 [109]. Several studies on drop impact have focused on determining the maximum spreading factor β_{max}, defined as the ratio of maximum spreading diameter d^*_{max} to initial drop diameter d_0 [102, 110, 111]. For low-viscosity liquids on superhydrophobic or partially wettable solids, Clanet *et al.* [110] proposed that β_{max} can be determined by a balance between inertia and surface tension. When the velocity of a drop impacting on a solid decreases from the initial impact velocity u_0 to 0, the impact time is of the order of d_0/u_0. The acceleration experienced by the drop scales as u_0^2/d_0. Using volume conservation, the authors [110] deduced a scaling relation for flattened drops on partially wettable solids:

$$\beta \propto We^{1/4} \tag{2.24}$$

The dimensionless Weber number, $We = \rho u_0^2 d_0/\gamma$, compares inertial to capillary forces.

2.2 Wetting of Aqueous Surfactant Solutions

This section concentrates on wetting of aqueous surfactant solutions. The wetting dynamics of surfactant solutions is more complex than that of simple liquids, because the time-dependent surfactant adsorption at an interface between two phases generates a dynamic interfacial tension. Zisman's rule works well for simple liquids, however, it is not a universal law for surfactant solutions, since in some cases low surface tension does not guarantee complete wetting [10, 16]. The structure of surfactant aggregates in bulk solutions and the adsorption of surfactant molecules at interfaces are factors that influence the wetting dynamics of surfactant solutions. The question that arises is: under what conditions can surfactants become effective in wetting processes on plant leaves, printing papers or other solids? Understanding the physicochemical properties of surfactants is useful in selecting them for desired applications and predicting their wetting dynamics.

2.2.1 Fundamentals about Surfactants

Figure 2-6 shows the schematic of a surfactant molecule with two parts: a polar hydrophilic head group that has strong interaction with water, and a non-polar hydrophobic tail group that has little interaction with water. Their chemical structure is responsible for their tendency to reduce the free energy of a system by adsorption at the liquid/liquid interface or air/liquid interface. Materials that possess chemical groups leading to surface activity are generally referred to as being amphiphilic, indicating that they have some affinity for two essentially immiscible phases.

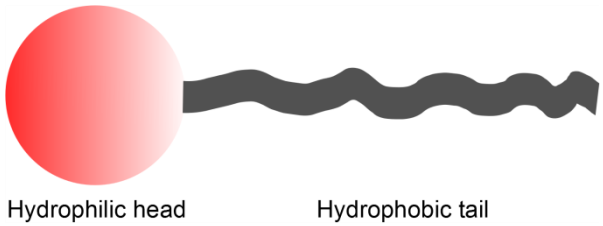

Figure 2-6 The representation of a surfactant molecule includes a hydrophilic head group having strong interactions with water and a hydrophobic tail group having little interactions with water.

Figure 2-7 shows that when surfactants are dissolved in water, they orientate at the free air/water interface with hydrophobic tails exposed to air. Some of the water molecules at the interface are replaced by surfactant molecules. The attraction forces between surfactant and water molecules are less than those between two water molecules; hence the "surface tension" is reduced. According to Zisman's criterion, a liquid with surface tension less than the critical surface tension of a solid tends to spread completely. Since water has a high surface tension (72.8 mN/m), it does not spontaneously spread over solids with surface energy lower than 72.8 mN/m. Therefore, surfactants are used as aids to enhance wetting by reducing the surface tensions of liquids.

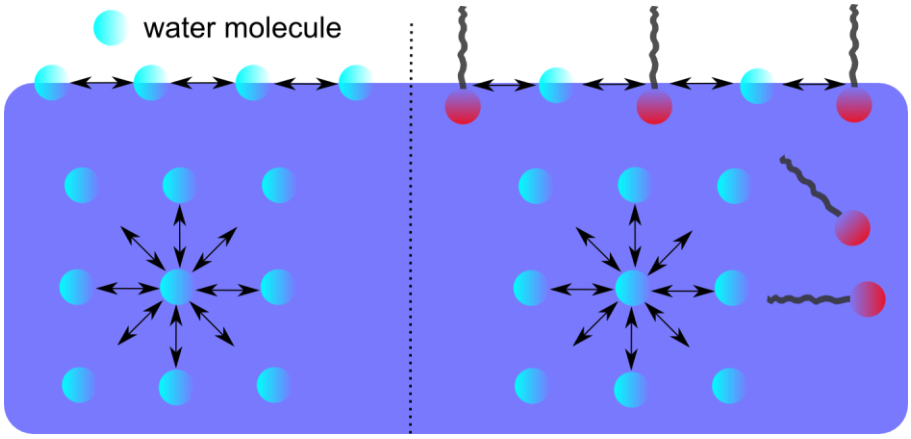

Figure 2-7 Surfactant molecules reside at the air/water interface with hydrophobic tails sticking out of water.

The Classification of Surfactants

The classification of surfactants depends on their applications and users' preferences. Surfactants may be classified as detergents, wetting agents, emulsifiers, foaming agents, and dispersants. This classification does not tell us the specific chemical property of a surfactant, nor does it give guidance to other possible applications. The most commonly used way to classify surfactants is based on their polar head groups. Accordingly, surfactants are divided into the following four general groups that are schematically shown in Figure 2-8.

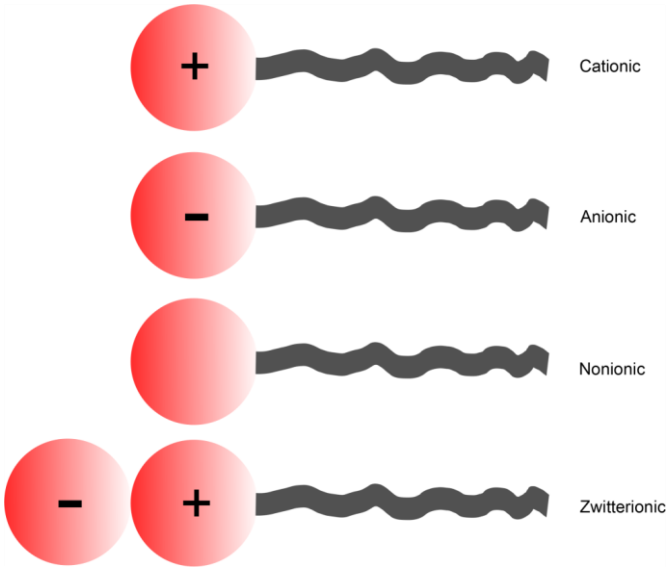

Figure 2-8 Classification of surfactants into four classes, based on the properties of their head groups.

- Cationic surfactants, with the hydrophilic head group carrying a positive charge, such as the quaternary ammonium halides.
  e.g. cetyl trimethylammonium bromide (CTAB)

Cationic surfactants exhibit two important features. First, their positive charge allows them to adsorb on negatively charged sites that occur on the surfaces of most inorganic natural and man-made materials, e.g. fabrics. They can bind to these sites and provide the fabrics with a soft feel. For this reason, cationic surfactants are used as fabric softeners. They can make fabrics water-repellent by exposing their hydrophobic tails to air. They are also used in vehicle care products as a wax additive for improved shine and surface protection. Second, some cationic surfactants (e.g. chlorhexidine) are bactericides. They are useful in cleaning surgery hardware and sterilizing food containers.

- Anionic surfactants, with the hydrophilic head group carrying a negative charge such as sulfate, sulfonate, phosphate, or carboxylate.
  e.g. sodium dodecyl sulfate (SDS), Dioctyl sodium sulfosuccinate (AOT)

Oil does not mix with water because the main interactions between water molecules are hydrogen bonding and those between molecules of oil are van der Waals forces.

Therefore, water by itself cannot effectively remove oil or grease from the surface of dishes. However, if a few drops of dishwasher detergent are added to the water, the oil or grease is dispersed in water. This is because the detergents, which are adsorbed at the water surface, act as an emulsifier, holding the water and oil together. Anionic surfactants are used in food processing as emulsifiers to change the structure and texture of food by mixing two immiscible liquids.

- Nonionic surfactants, in which the hydrophilic head has no charge but derives its water solubility from highly polar groups such as polyoxyethylen or sugars.
  e.g. polyoxyethylene octyl phenyl ether, trisiloxanes

Nonionic surfactants are preferable in practical applications because of their biocompatibility and lower surface tension compared to ionic surfactants. Trisiloxane surfactants are excellent wetting agents in formulations of herbicides, pesticides, upholstery and floor care products.

- Zwitterionic surfactants, where the hydrophilic head group contains a positive and a negative charge in the principal chain.
  e.g. cocamidopropyl betaine, imino diacid

The presence of both a positive and a negative charge renders the net charge zero at neutral pH. Zwitterionic surfactants are biocompatible, and used in pharmaceuticals, cosmetics and hair care formulations. They can reduce static in hair by reducing its surface charge density.

Critical Micelle Concentration of Surfactants

In aqueous solutions with little surfactants, dispersed surfactants act as normal electrolytes. The surface tension of liquids decreases with increasing surfactant concentration. However, at a certain concentration - Critical Micelle Concentration (CMC) - increasing the surfactant concentration does not decrease the surface tension, but stimulates the spontaneous aggregation process of surfactant molecules [112]. Below the CMC the aggregation of the surfactants is negligible and most of surfactant molecules are in a free state. Above the CMC all additional surfactant molecules form aggregates. The methods for CMC determination involve the characterization of conductivity, solubility, viscosity, light scattering, surface tension, and osmotic

pressure of the solution [113-115]. In practice, the CMC is a (narrow) range of surfactant concentration instead of a fixed value. Figure 2-9 schematically shows the evolution of various properties of surfactant solutions vs. surfactant concentration. An abrupt change in the slope of the plots occurs when the surfactant concentration is around CMC. Therefore, measuring CMC is probably the simplest method to characterize surfactants due to the sharp change in the properties of the solutions.

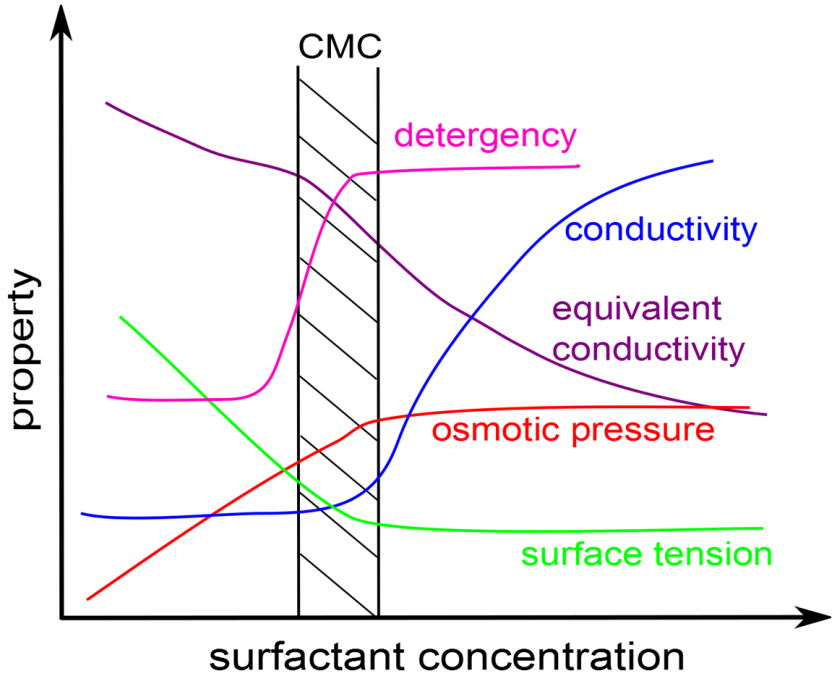

Figure 2-9 Schematic dependence of various properties of surfactant solutions on surfactant concentration. (adapted from Ref. [116])

Structure of Surfactant Aggregates

The simplest structures of surfactant aggregates in water are micelles, with hydrophilic head groups in contact with water and hydrophobic tail groups associating in the micelle center. The structures shown in Figs. 2-10a-b are known as normal micelles. Inverse micelles (Figure 2-10c) have the head groups at the micelle center with the tail groups exposed to surrounding non-polar solvent, e.g. oil. Most surfactant molecules in aqueous solution can aggregate to form micellar structures with 30-200 molecules on average [117]. In this way the hydrophobic portions of the molecules are associated and mutually protected from extensive contact with the

water phase [118]. Typically outer diameters of micelles are $3-6\,nm$ as determined by dynamic light scattering (DLS), small-angle X-ray scattering (SAXS) and small-angle neutron scattering (SANS) [117].

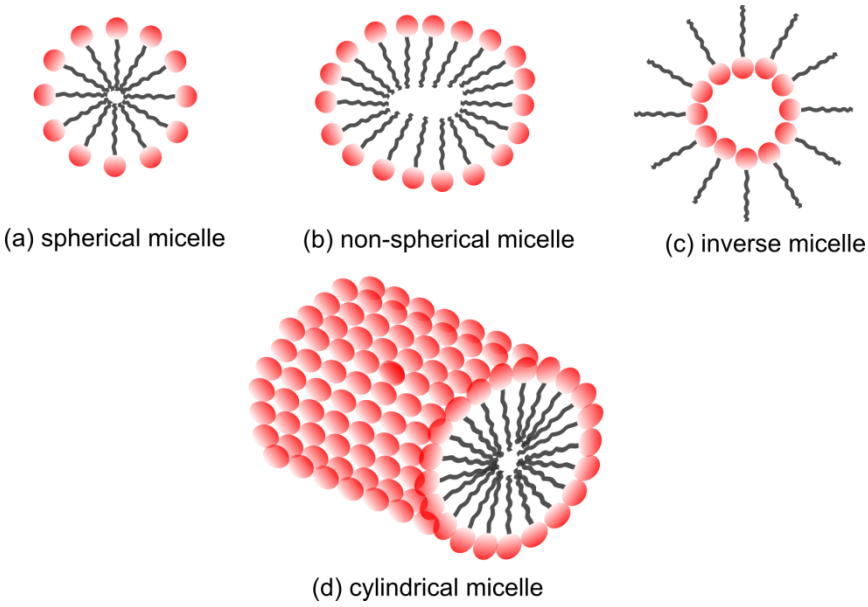

Figure 2-10 Different aggregates formed by surfactant molecules. Normal micelles in water include spherical micelles (a) and non-spherical micelles (b). Inverse micelles in oil with the head groups at the micelle center (c) and cylindrical micelle aggregates in water (d).

Depending on the chemical structure of the surfactant molecules and solution conditions such as surfactant concentration, temperature and pH, the shape and size of a micelle can vary [119, 120]. Based on the spatial occupation of the hydrophilic and hydrophobic groups, Israelachvili *et al.* [121] developed a model for aggregation structures. In this model, the volume occupied by the hydrophobic group in the micellar core V_H, the length of the hydrophobic group in the core l_b, and the cross-sectional area occupied by the hydrophilic group a_0, are taken into account to define a critical packing parameter P:

$$P = \frac{V_H}{a_0 l_b} \tag{2.25}$$

Due to variations in the relative size of head and tail groups of surfactants, the parameter governs the optimal way in which surfactant molecules aggregate into different geometries. According to this concept, surfactant molecules with $P < 1/3$ form spherical micelles in aqueous solutions. An increase in surfactant concentration causes these spherical micelles to assemble themselves into cylindrical micelles or rod-like micelles (Figure 2-10d). If the surfactant concentration is sufficiently high, these rod-shaped micelles assemble into a hexagonal array, thereby creating a hexagonal liquid crystal. When the parameter reaches a value of approx. 1, a balance between size of the head and tail groups is reached. In this case, surfactant molecules form aggregates with a bilayer structure, as schematically shown in Figure 2-11. These can be flat lamellae (lamellar or L_α phase, Figure 2-11a), spherically closed bilayers (vesicles, Figure 2-11b), or the so-called sponge (L_3 phase, Figure 2-11c) [122]. L_3 phase is a stable isotropic phase, which consists of a sponge-like "random surface" of bilayer that divides space into two interpenetrating solvent labyrinths. If the parameter is above 1, surfactant molecules form reversed "water-in-oil" systems.

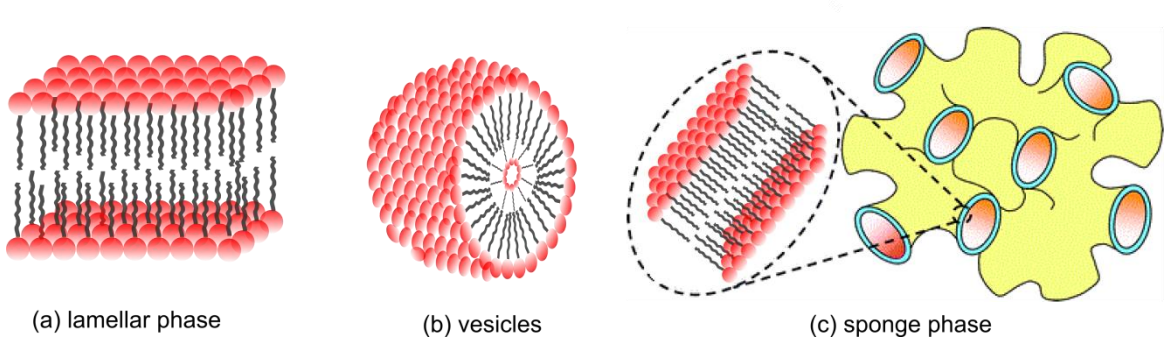

Figure 2-11 Different bilayer aggregates formed by surfactant molecules.

2.2.2 Surfactant-enhanced Wetting and Superspreading

Surfactant-enhanced Wetting on Solids

Wetting of solids by aqueous surfactant solutions is common in many industrial and daily life processes. For many applications, e.g. wetting of textile fibers, printing with water-borne inks, the major problem is to increase the velocity and uniformity of wetting. The dynamic wetting of surfactant solutions is more complicated than that of simple liquids. The complexity of the problem results from an interplay between

wetting, surfactant diffusion and time-dependent adsorption at the three interfaces [123-125]. Much effort has been put on studying the wetting dynamics of surfactant solutions on solids, in terms of the wetting area or radius between solid and liquid vs. time [33, 34, 126]. The wetting experiments on clean hydrophilic glasses was conducted by gently contacting the glasses with pendent surfactant-laden drops that were generated with a syringe pump [34]. The authors for the first time demonstrated that drops of aqueous anionic, cationic and nonionic surfactant solutions spread to a maximum area and then finally contracted to a smaller area [34]. It was found that the time scale of wetting and contraction is shorter for cationic surfactants than other surfactants. This observation was explained by the tendency of the positively charged heads of cationic surfactants to absorb more rapidly to the negatively charged glass surface than negative and uncharged heads of anionic and nonionic surfactants. The initially hydrophilic glass surface gradually became more hydrophobic, which led to the contraction of the drop. More attention has been paid to surfactant-enhanced wetting on hydrophobic solids, which are not wettable by water. By performing wetting experiments of polyoxyethylene glycol alkyl ethers ($C_{14}E_6$ and $C_{10}E_6$) on thiolate-modified gold solids, von Bahr *et al.* [32] systematically studied the influential factors on surfactant-enhanced wetting, such as substrate wettability and surfactant concentrations. The wetting velocity was found to decrease with decreasing substrate wettability, and to increase with increasing surfactant concentrations. Dutschk *et al.* [126] confirmed these observations by investigating the wetting dynamics of aqueous ionic and nonionic surfactant solutions on hydrophobic polymer solids of different wettability. It was found that the wetting process could be divided into two stages with different time dependence of wetting radius [126]. In the short time stage ($t < 1\,s$), the experimental results followed $r \propto t$. In the long time stage ($t \gtrsim 1\,s$), exponent values of power laws were lower than 0.1. The authors [126] concluded that the wetting is not only controlled by surfactant diffusion to the expanding air/liquid interface, but surfactant adsorption at the solid/liquid interface played a role as well. Starov *et al.* [124] assumed that three transfer processes take place from the spreading drop onto all three interfaces. Surfactant adsorption at both the solid/liquid interface and the air/liquid interface decreases the corresponding interfacial tensions, γ_{sl} and γ. The transfer of surfactant molecules onto the solid/air

interface ahead of the TPCL increases the interfacial tension γ_{sa} and hydrophilizes the solid. All three surfactant transfer processes are favorable to a positive spreading coefficient, and hence enhance drop spreading. The experimental results of SDS solutions on hydrophobic solids agreed with their assumption [124].

Surfactant-enhanced Wetting on Liquid Subphases

Wetting of liquid subphases by other liquids has a number of applications including liquid fuel fire extinguishers, anti-foaming agents, coating flows and drug delivery [52, 127-130]. In the 1970s and 1980s, the spreading of oil on water attracted much interest in the context of oil spills on the sea [131-133]. Theoretical analysis of wetting on liquid subphases is more complicated than that on solids. This is due to the fact that complex fluid mechanics is involved on liquid subphases. A surface tension gradient arises from an inhomogeneous distribution in the surfacial surfactant concentration, which distributes a liquid flow in the direction of higher surface tension. The solubility of the surfactant in the liquid subphases and the miscibility of the solvent drops with the liquid subphases also complicate the case. In wetting experiments conducted at the air/liquid interface, the contact line of drops cannot be well defined. One of the parameters to characterize surfactant-enhanced wetting on liquid subphases is spreading front, which is termed surfactant leading edge [45, 134]. The contact line is behind the experimentally determined surfactant leading edge, as was theoretically predicted [45, 135] and experimentally confirmed [52, 136, 137]. The deposition of a drop on a liquid subphase generates capillary waves propagating ahead of the drop and surfactant leading edge [48, 134, 138]. Since the wave amplitude decreases as the wave propagates, the observation of the waves becomes more difficult as time elapses. Therefore, qualitative data of the propagating distance vs. time of capillary waves is limited.

When a drop of pure surfactant is deposited on a flat liquid subphase, the surfactant escapes from the bulk of the drop and moves along the air/liquid interface [41, 43, 45, 54, 139]. For insoluble pure surfactants (e.g. organic oleic acid), a thin precursor film spreading along the liquid is referred to as a surfactant monolayer [43, 140, 141]. At the leading edge of the advancing monolayer, there is an abrupt change in the tangential stress boundary where the liquid subphase is deformed with height

variations. A ridge of liquid with height almost twice the thickness of the undisturbed liquid region moves along the air/liquid interface [40, 43, 142]. Joos *et al.* [141] assumed that a linear surface tension gradient is the driving force for the spreading of insoluble surfactant (e.g. oleic acid) on water subphases. The distance ξ traveled by the surfactant leading edge at time t is described with [141]:

$$\xi = \left(\frac{4}{3}\right)^{1/2} \frac{(\gamma_w - \gamma_s)^{1/2}}{(\mu\rho)^{1/4}} t^{3/4} \tag{2.26}$$

γ_w and γ_s are the surface tension of the water subphase and the surfactant drop, respectively.

The time required to spread over the distance ξ is given by:

$$t = \left[\xi(\mu\rho)^{1/4} \left(\frac{3}{4(\gamma_w - \gamma_s)}\right)^{1/2}\right]^{4/3} \tag{2.27}$$

The spreading velocity u of the surfactant leading edge over the spreading distance can be obtained from $d\xi/dt$:

$$u = \left(\frac{3}{4}\right)^{1/2} \frac{(\gamma_w - \gamma_s)^{1/2}}{(\mu\rho)^{1/4}} t^{-1/4} \tag{2.28}$$

The spreading velocity may also be expressed as a function of ξ:

$$u = \left(\frac{3}{4}\right)^{1/3} \frac{(\gamma_w - \gamma_s)^{2/3}}{(\mu\rho)^{1/3}} \xi^{-1/3} \tag{2.29}$$

Other theoretical studies also predicted that the advancement of the surfactant leading edge scales with time as $t^{3/4}$ [140, 143]. This scaling law has been confirmed by a number of experimental studies [54, 131, 132, 134, 140, 144].

Taking surfactant solubility into consideration, Lee *et al.* [145] showed by scaling analysis that the evolution of surfactant leading edge vs. time follows $t^{3/4}$ and $t^{1/2}$ for insoluble and soluble surfactants, respectively. This can be explained by the fact that the radial wetting of soluble surfactants is accompanied by surfactant dissolution into the liquid subphases in the normal direction, which causes a lower surfacial surfactant concentration and a less strong surface tension gradient at the air/liquid interface. Their experimental results for surfactants with different solubility on water subphases

agreed with the theoretical predictions [46, 145]. Other experimental studies examined the surfactant leading edge of surfactant-laden drops on liquid subphases and confirmed the scaling analysis [53, 138]. Studies have shown that during the wetting, the liquid in the drop and that in the subphase do not advectively or diffusively mix even if they are completely miscible [137, 145]. In one study of wetting on an entangled solution of aqueous polymer, the drop of aqueous surfactant solutions remained at the air/liquid interface for minutes despite the complete miscibility of the drop and the subphase [137]. This showed that advective mixing did not occur in those systems. The wetting of surfactant solutions on immiscible organic liquid subphases has also been investigated [146-149]. It was observed that the subphase viscosity had only a minor effect on the wetting velocity of surfactant solutions.

Superspreading on Hydrophobic Solids

Silicone surfactants, especially trisiloxane surfactants, have attracted much attention from science and industry since the early 1960s. Figure 2-12 shows the chemical structure of the trisiloxane surfactant, which is denoted as M(D'EO_pPO_qR)M. Here, M represents the trimethylsiloxy group $(CH_3)_3SiO_{1/2}$–. The term D' stands for the –$O_{1/2}Si(CH_3)(R')O_{1/2}$–, where R' is obtained from a mixture of ethylene oxide (EO) and

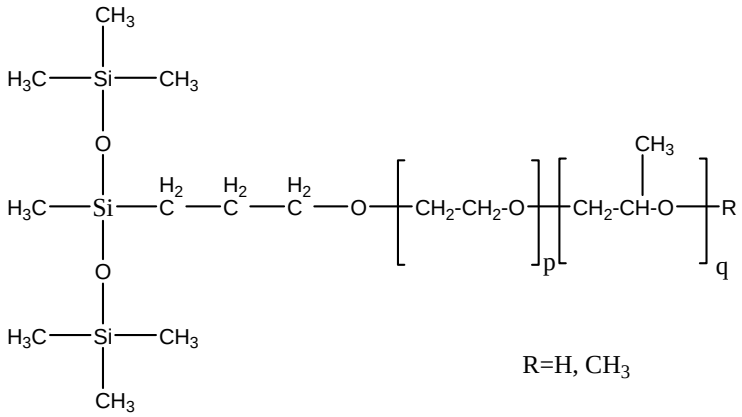

Figure 2-12 Chemical structure of the trisiloxane surfactant molecule.

propylene oxide (PO) (R'=–$(CH_2)_3$–O–$(EO)_p$–$(PO)_q$, with EO=CH_2–CH_2–O– and PO=CH_2–$CH(CH_3)$–O–). R represents the end group –H or –CH_3. Under appropriate

conditions, certain trisiloxanes possess an unusual ability to promote the spreading of a spherical drop on hydrophobic solids into an ultra-thin liquid film within tens of seconds. This phenomenon was referred to as superspreading [8-13]. Because of the capability to promote fast spreading on plant leaves, trisiloxane surfactants are widely used as herbicide wetting agents [2]. Among numerous commercial trisiloxane surfactants, trisiloxanes like Silwet® L-77 and Silwet® Gold promote superspreading of water drops on hydrophobic solids [13, 14]. The application of superspreader TEGOPREN® 5840 (with p=6, q=3) as adjuvants is shown in Figure 2-13. Water alone on the plant leaf exhibits a relatively poor wetting ability with a high static contact angle, while the drop of aqueous TEGORPEN® 5840 solutions wets the plant leaf with a much larger covered area and a much smaller contact angle.

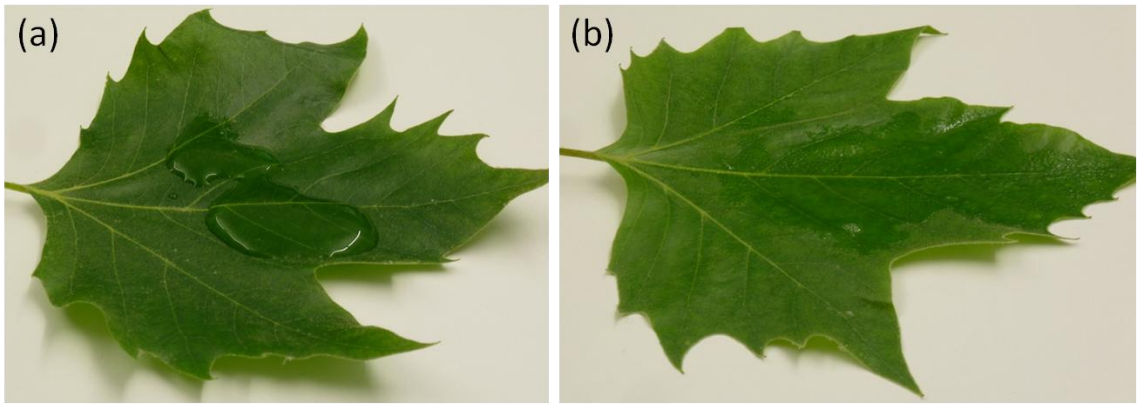

Figure 2-13 Photographs depicting the spreading of a water drop (a), and aqueous superspreader TEGOPREN® 5840 solution at 0.1 wt% (b), on plant leaves.

Due to their unique characteristics and practical applications, the superspreading trisiloxane surfactants have been intensively investigated from both experimental and theoretical points of view [8, 13-29, 66, 150]. An overview on superspreading by Hill [10] describes four main features of superspreading.

- Initially the wetting area increases linearly with time. This process can last for a few seconds.
- During the linear-dependence period, the wetting area is proportional to surfactant concentration.

- Maxima in wetting velocity vs. surfactant concentration and substrate wettability are observed.
- Surfactant solutions with vesicle aggregates spread faster than solutions with micelle aggregates on the same solids.

Earlier experiments were conducted on Parafilm® [8, 10, 16, 150], followed by experiments on different polymers with varying wettability [13, 24, 151-155]. Plant leaves, like cabbage (Brassica oleracea) and wheat (Triticum aestivum L.) [15], lotus [156] and velvetleaf (Abutilon theophrasti) [13] were also used as substrates for wetting experiments with aqueous drops with superspreaders. The experimental studies were mainly carried out by measuring the dynamic contact angle and wetting radius of drops spreading on solids. One of the commonly used methods for data analysis is fitting the curves of the wetting radius vs. time with a power law, $r \sim t^{\alpha}$ [13, 24, 25, 46, 66, 153, 157]. Different exponents α were obtained for aqueous trisiloxane solutions, ranging from 0.036 to 0.8 [13, 24, 65]. The incompatibility of results may stem from several reasons. For example, most commercial surfactants are not single species but mixtures of different homologues. Aqueous trisiloxane solutions are not stable and slowly hydrolyze over time, depending on pH, concentration and temperature [158]. In addition, hydrophobic solids with different wettability have been used in the experiments, which makes it difficult to compare results. The appearance of a maximum in the wetting velocity vs. surfactant concentration on different solids was revealed in Refs. [10, 13]. The value of surfactant concentration corresponding to the maximum wetting velocity does not depend on the substrate wettability. For aqueous Silwet® L-77 solutions, a well-pronounced maximum in wetting velocity at concentration of 0.1 wt% was observed on polystyrene solids [13] and on decalin layers [159]. However, up to now the reasons for the maximum appearing in wetting velocity vs. surfactant concentration still remains unclear.

In the pioneering work about superspreading, Ananthapadmanabhan *et al.* [16] suggested that the compact structure of trisiloxane superspreader determines its unique superspreading ability on polyethylene. Superspreader molecules at the air/liquid interface are readily transferred to the solid/air interface. This facilitates progressive advance of the liquid in a process which can be compared to “molecular

unzippering" at the solid/liquid interface. The efficient adsorption and packing of superspreader molecules reduces interfacial tensions at the TPCL and creates a positive spreading coefficient. In contrast, the orientation of "conventional" surfactants is not favorable for the molecular transfer; hence the wetting process is impeded. Hill *et al.* [12] studied the wetting dynamics of various superspreaders including analogous linear trisiloxane surfactants. They contested that the compact structure of trisiloxane surfactants was crucial for superspreading, as suggested in Ref. [16]. Instead, Hill *et al.* [12] proposed that one common feature of superspreaders is to form bilayer aggregates in aqueous solutions, such as vesicles and lamellae. A possible link between the formation of bilayer aggregates and superspreading was postulated as well by other researchers [8-11, 16, 22, 26, 150, 160]. The reason lies in the possibility that the bilayer aggregates enable an efficient and rapid transfer of surfactant molecules to the air/liquid and solid/liquid interfaces. Kumar *et al.* [22] suggested that bilayer adsorption may account for the ability of superspreaders to maintain a high surfactant concentration at the TPCL to promote a positive spreading coefficient. A similar argument was proposed in Ref. [30], where the authors suggested that the way in which surfactants interacted with hydrophobic solids could be crucial to superspreading. Figure 2-14 shows the possible situation when a surfactant-laden drop spreads on a hydrophobic solid. When micelle-forming surfactants adsorb on the substrate, hemimicelles are formed the orientation of which is less ideal for lowering the interfacial tension of solid/liquid. In contrast, for superspreading surfactants, a transfer of surfactant molecules to both the substrate and the air/liquid interface is especially efficient in case of the "molecular unzippering" bilayer aggregates. The orientation of surfactant molecules on the substrate is optimal for reducing the interfacial tension of solid/liquid and allows for keeping up over a longer time a positive spreading coefficient responsible for further spreading.

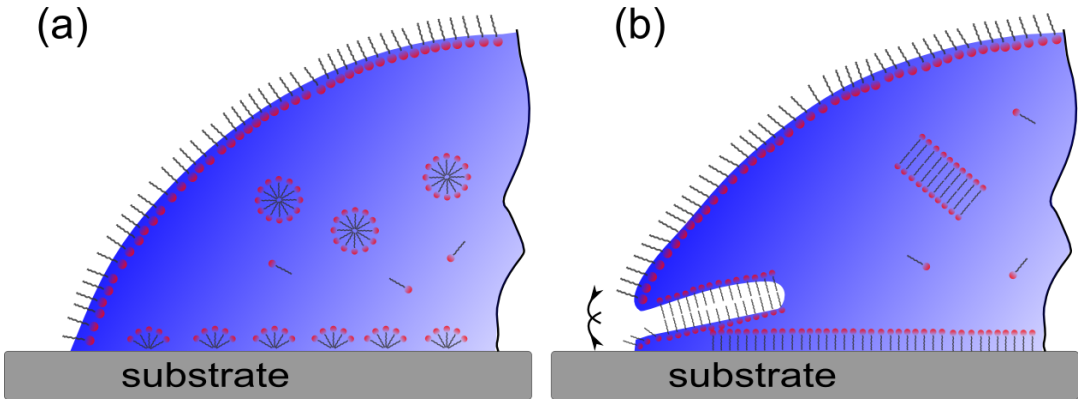

Figure 2-14 Possible situation at the leading edge of a surfactant-laden drop on a hydrophobic substrate. (a) micelle-forming non-superspreading surfactant, (b) bilayer-forming superspreading surfactant. (adapted from Ref. [9])

The hydrophilic chain length of trisiloxane surfactants has also been postulated to influence drop spreading, because micelles rather than bilayers are formed in aqueous solutions for trisiloxane surfactants with long hydrophilic chain [9, 26]. The experimental work found that surfactants with moderately long hydrophilic chains (7-8 EO groups) show fast spreading on hydrophobic solids [150, 161]. Later Ruckenstein [26] theoretically argued that only surfactants with intermediate hydrophilic chain length are able to induce superspreading on hydrophobic solids, whereas longer hydrophilic chains prefer to interact with water and decrease the adsorbability of the surfactant to the interfaces, thus reducing the spreading efficiency. Some work proved that wetting of trisiloxane surfactant solutions is sensitive to RH and the wetting velocity increases with increasing RH [8, 30, 152, 162]. Superspreading of trisiloxane solutions on Parafilm® was not observed in dry air [8, 152], which implies that a precursor water film formed at high RH is probably required for superspreading [8, 21, 162, 163]. The concept of precursor film was proposed almost one century ago when Hardy [164] first demonstrated that due to vapor condensation a microscopically precursor water film precedes a spreading drop on a solid. The thickness of such a film is a few nanometers and the extension ahead of the drop rim can reach up to few hundred micrometers on solids [31, 165, 166]. The presence of precursor films ahead of surfactant-laden drops spreading on solids was experimentally investigated and verified by researchers with quartz crystal

microbalance [162], ellipsometry [31] and interferometry methods [21]. In contrast, Rafai *et al.* [24] did not find difference in the wetting dynamics of trisiloxane solutions when changing the RH from 30 % to 80 %. It was also observed that the RH effect on the wetting velocity was weaker for smoother hydrophobic solids [10, 150, 162, 163, 167]. Venzmer *et al.* [30] argued that evaporation in dry air should be considered during drop spreading process and put forward a plausible explanation about the secondary effect of evaporation. Evaporation mostly occurs at the leading edge of the drops [168]. The evaporation rate of spreading drops depends on the atmospheric RH; hence the contact angle dynamics is in turn affected. Due to the strong evaporation in dry air, the surfactant concentration at the leading edge of the drop increases. A lamellar phase formed locally via evaporation may inhibit further spreading of the drop because of its high viscosity [30].

Nikolov *et al.* [13] built a simple model to predict the wetting radius as a function of time under the action of the surface tension gradient that develops at the expanding air/liquid interface. According to this model, the depletion of surfactant from the interfacial region near the TPCL is greater than that from the region near the drop apex, as schematically shown in Figure 2-15. Therefore, the surface tension gradient along the drop surface drags the adjacent bulk liquid in the direction of increasing surface tension towards the drop rim.

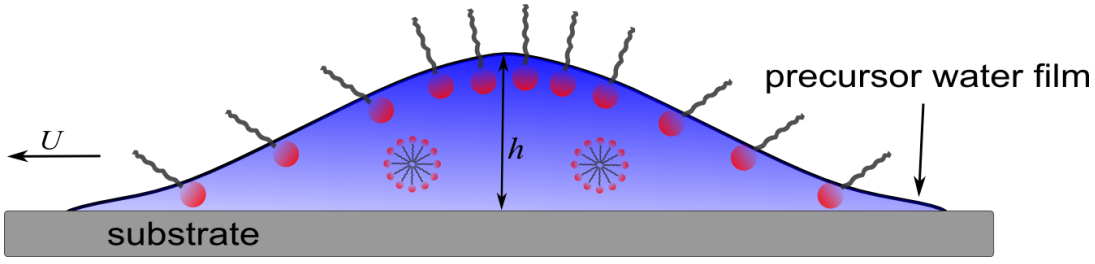

Figure 2-15 Schematic of the drop spreading driven by surface tension gradient.

Considering the surface tension gradient as the driving force, Nikolov *et al.* [13] derived the average spreading velocity U as

$$U \approx \frac{h(t)}{2\mu}\nabla\gamma(t) \tag{2.30}$$

$h(t)$ is the height of spreading drop, and the relation $h(t) \propto 1/r^2(t)$ can be derived from mass conservation. $\nabla\gamma(t)$ is the surface tension gradient over the drop surface, which is approximated as

$$\nabla\gamma(t) \approx \frac{\Delta\gamma(t)}{r(t)} \tag{2.31}$$

Here $\Delta\gamma(t)$ is the difference between the surface tension near the TPCL and the drop apex. Based on Eq. (2.30) and Eq. (2.31), the authors [13] predicted the wetting radius vs. time as $r \propto t^{1/2}$, if $\Delta\gamma(t)$ increased linearly with time. On the other hand, if $\Delta\gamma(t)$ was assumed to remain constant with time, they obtained $r \propto t^{1/4}$. This result was also reported by Rafai *et al.* [24] using similar arguments. However, it is still not known over what distance the surface tension gradient is active in this spreading geometry. Zhu *et al.* [8] suggested that the surface tension gradient was established between the spreading drop and a precursor water film (Figure 2-15) formed at a humid atmosphere (i.e. 100% RH). As reported in Ref. [24], different options lead to power laws with different exponents. If the surface tension gradient is established over the precursor film ahead of the drop rim, the time dependence of wetting radius follows $r \propto t^{1/3}$ [24]. If, as might also be possible, the surface tension gradient acts over the drop height, $\nabla\gamma(t) \approx \Delta\gamma/h(t)$ applies. In this case, a simple dimensional analysis of Eq. (2.30) results in a linear relationship between the drop radius and time, $r \propto t$ [24].

3 Experimental Methods and Data Analysis

This chapter is devoted to a description of experimental materials, experimental setups, working principles of measuring techniques, image processing and data analysis methods.

3.1 Preparation of Aqueous Surfactant Solutions

In the present work, the studied surfactants are cationic cetyltrimethyl ammonium bromide (CTAB, purity ≥95%, Sigma-Aldrich), anionic sodium dodecyl sulfate (SDS, purity ≥98%, Acros Organics) and two nonionic trisiloxane surfactants TEGOPREN® 5847 and TEGOPREN® 5840 (Evonik Industries AG, Essen, Germany, 100% undiluted). These surfactants are used as received without further purification. For brevity, TEGOPREN® 5847 and TEGOPREN® 5840 are named as TSS10/2 and TSS6/3, respectively. Their chemical structures can be written as M(D'EO_pPO_qOH)M, with p=10, 6 and q=2, 3 on average. The physicochemical properties of these surfactants are listed in Table 3-1.

Table 3-1 Physicochemical properties of various surfactants. The standard deviation in the surface tension measurement is ~ 1 mN/m.

Surfactant	Molecular Formula	Molecular Weight (g/mol)	Concentration Ranges Used	γ (mN/m)
CTAB	$CH_3(CH_2)_{15}N(CH_3)_3Br$	364	0.1 CMC	55
			1-3 CMC	32
SDS	$CH_3(CH_2)_{11}OSO_3Na$	288	0.1 CMC	55
			1-6 CMC	32
TSS10/2	M(D'$EO_{10}PO_2$OH)M	850	0.05-10 wt%	22
TSS6/3	M(D'EO_6PO_3OH)M	700	0.05-10 wt%	22

Aqueous surfactant solutions are prepared using ultra-pure water (18.2 MΩcm, Merck Millipore, Germany). The concentrations of CTAB and SDS solutions are 0.1-6 CMC.

The CMC values are 9.6×10^{-4} mol/L (~ 0.035 wt%) and 8.3×10^{-3} mol/L (~ 0.25 wt%) for CTAB and SDS, respectively [169, 170]. Aqueous TSS10/2 and TSS6/3 surfactant solutions have concentrations from 0.05-10 wt%, which are well above CMC (~ 0.005 wt%). The water/surfactant mixtures are shaken vigorously by hand in order to disperse the surfactants completely in the solutions. Afterwards they are kept at rest for 3 hours in order to allow any foam generated during shaking to disappear. Aqueous surfactant solutions are used within 24 hours after preparation. Thus, the influence of hydrolytic degradation of such aqueous solutions can be neglected.

3.1.1 Interfacial Tension Measurements

The static surface tensions of all aqueous surfactant solutions are measured by the pendent drop technique with a Profile Analysis Tensiometer (PAT 1, SINTERFACE Technologies, Berlin, Germany). The details of the PAT 1 instrument can be found in Ref. [171]. The main principle of this technique is to determine the liquid surface tension from the shape of a pendent drop (Figure 3-1) with the Gauss-Laplace equation:

$$\gamma\left(\frac{1}{R_1}+\frac{1}{R_2}\right)=\Delta P_0+\Delta\rho g z \tag{3.1}$$

Here R_1 and R_2 are the main radii of curvature. ΔP_0 is the pressure difference at any arbitrary reference plane, depending on where the origin of the coordinate system is placed. $\Delta\rho$ is the density difference between air and liquid, and z is the vertical height of the drop measured from the reference plane. By changing the fitting parameter γ, a group of theoretical curves can be obtained. The curve that fits best to the experimental points (Figure 3-1, red points obtained from the video image of a pendent drop) corresponds to the optimum value of the surface tension.

All static surface tension values of aqueous surfactant solutions measured with PAT 1 are summarized in Table 3-1. For aqueous ionic surfactants solutions, the surface tension is 55 mN/m with concentration 0.1 CMC, and it decreases to 32 mN/m at/above the CMC. For both aqueous trisiloxane surfactant solutions, the surface tensions above CMC are identical (22 mN/m) in the entire range of concentrations studied (0.05-10 wt%).

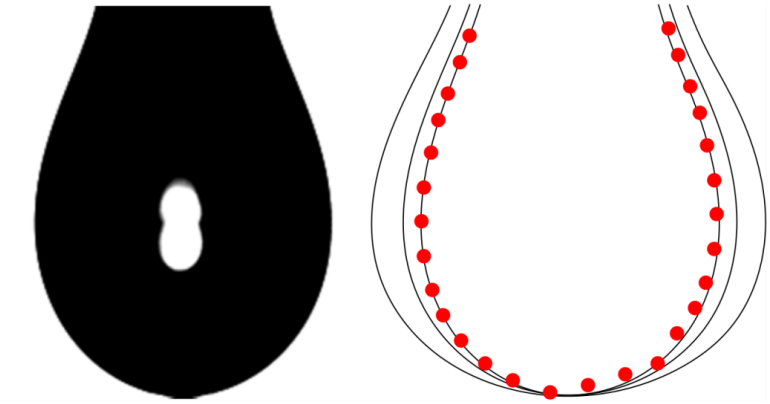

Figure 3-1 Image of a pendent drop and the principle of fitting the Gauss-Laplace equation to the drop profile (red points are coordinates of the drop profile).

Note that the static surface tension of a surfactant solution is not achieved instantaneously. When a fresh air/liquid interface is formed, it has a surface tension close to that of water. Surfactants reduce the liquid surface tension by diffusing to the air/liquid interface. This process can last from milliseconds to days, depending on surfactant types and concentrations. This time-dependent surfactant diffusion results in a dynamic surface tension (DST) of one surfactant solution, which characterizes the evolution of liquid surface tension. DST is usually measured with a maximum bubble pressure technique. The main principle is to generate continuously air bubbles at the tip of a capillary and to determine the pressure in the bubble. Figure 3-2 schematically shows the formation process of a bubble at the tip of a capillary. When a bubble is produced in a liquid phase, the curvature initially increases and then decreases, resulting in a maximum of bubble pressure at the hemispherical size (Figure 3-2c). The surface tension γ can be calculated according to the Gauss-Laplace equation (3.1), when the capillary radius is known. The time interval from initial bubble generation to the hemispherical size is called bubble lifetime. The dependence of dynamic surface tension on bubble lifetime can be measured by varying the speed at which the bubbles are generated.

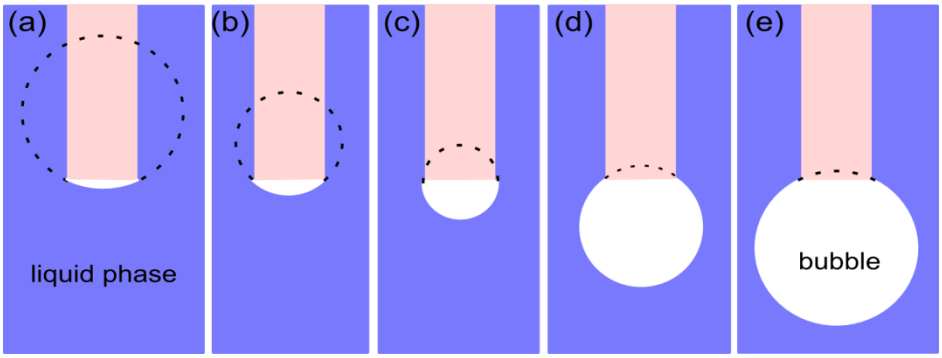

Figure 3-2 The radius of curvature of the bubble is large at first (a), then decreases to a minimum when the radius is the same as that of the capillary (c) and then increases again (e).

The DST measurements of trisiloxane surfactant solutions are conducted by Zorana Drljaca (Research Interfacial Technology, Evonik Industries AG, Essen, Germany) with a bubble pressure tensiometer (SITA science line t60, SITA Messtechnik GmbH). The data in Figure 3-3 shows that for surfactant solutions at low concentrations (e.g. 0.05 wt%) the initial surface tension values are larger than that of solutions at higher concentrations. The time required to reach static surface tension is also shorter for solutions at higher concentrations. This is simply because with more surfactants inside of the drop, the formed fresh air/liquid interface is covered by surfactants more quickly.

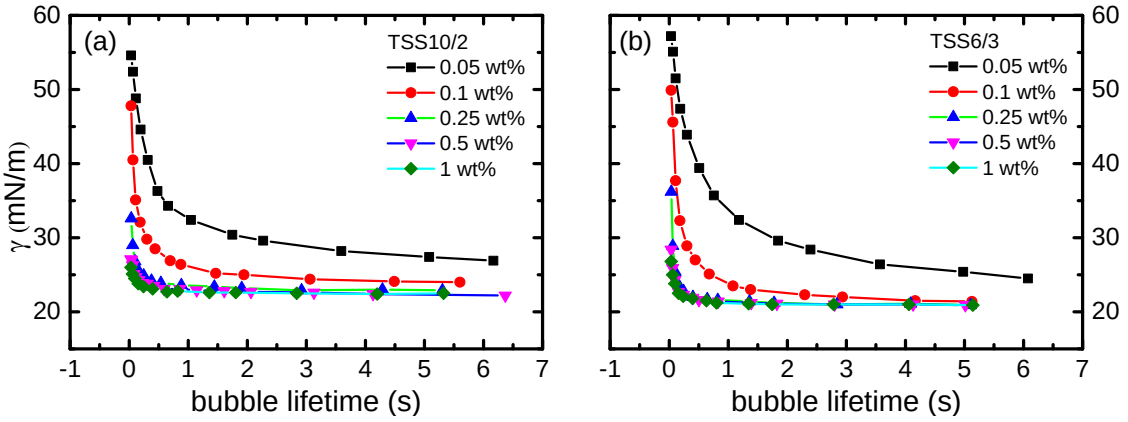

Figure 3-3 The dynamic surface tension of aqueous TSS10/2 solutions (a) and TSS6/3 solutions (b) at different concentrations.

3.2 Preparation of Substrates

The hydrophobic solids used in experiments are polypropylene (PP, FORCO OPPB AT-OPAL, 4P Folie Forchheim, Germany), polystyrene (PS, Greiner Bio-One GmbH, Germany), polymethyl methacrylate (PMMA, Folie Farblos, Evonik, Essen, Germany), polycarbonate (PC, Bayer MaterialScience, Germany), Parafilm® (Bemis Company, Inc., USA), polydimethylsiloxane (PDMS, Sylgard 184, Dow Corning, Wiesbaden, Germany) elastomer, and hydrophobized glass slides. The PDMS substrates are prepared in the following way. The first step is to mix the base (monomer) and cross-linker (curing agent) at a weight ratio of 10:1. The mixture is degassed in a vacuum chamber for 20 minutes and then poured into a mold with thickness approx. 5 mm. After curing at 60 °C in an oven for overnight, the mixture becomes solid. Glass slides (Carl Roth GmbH, Karlsruhe, Germany) with dimension of $22 \times 22\, mm^2$ and a thickness of $0.5\, mm$ are hydrophobized in a standardized silanization procedure. Firstly, they are cleaned with isopropyl alcohol (Sigma-Aldrich), acetone (Sigma-Aldrich), ethanol (Sigma-Aldrich) and then with ultra-pure water in an ultrasonic bath (Elma, Singen, Germany) for 15 minutes in each step. The next step is to further clean the slides with a plasma cleaner (Diener electronic GmbH + Co. KG, Jettingen, Germany) for 3 minutes. After the cleaning treatment, the slides are silanized with 1,1,1,3,3,3-hexamethyldisilazane (Carl Roth GmbH, Germany) in a desiccator at room temperature for 12 hours. Prior to experiments, all the polymers are cut into $60 \times 60\, mm^2$ squares and cleaned with an air gun. In order to get a flat polymer substrate, the polymer film is firstly adhered to a glass slide by sandwiching a thin layer of ethanol between them. After the ethanol evaporates, the polymer film is flatly fixed onto the glass glide. Among these solid substrates, PP has an intermediate wettability (see Table 3-2) and superspreading can occur on such polymers. Therefore, it is chosen as the most appropriate solid substrate in the work.

In Chapter 5, wetting experiments of aqueous surfactant solutions on flat water subphases (deep pool of water) are shown. The subphase is formed by filling $50\, ml$ of ultra-pure water into a plastic Petri dish (Greiner Bio-One GmbH, Germany) with a mean diameter $D_0 \sim 145\, mm$. The water distributes evenly across the bottom of the Petri dish and the so-formed uniform subphase has a thickness of $H_0 \sim 3\, mm$. A small

amount of PMMA microparticles (Bangs Laboratories, Inc.) with a mean diameter of ~108 μm is dispersed at the air/water interface to track the spreading of surfactant. The transient surface tension of the subphase is measured by the Wilhelmy pin technique（Nima Technology Ltd., Coventry, England）as a function of time before and after drop deposition in a region well outside the final area covered by the drop. The measurements are conducted by Ramankur Sharma (The Interfacial Physics Group, Department of Physics, Carnegie Mellon University). The pin is positioned 20 mm away from the wall of the dish. For the surfactant concentrations and deposited drop volumes used here, the Petri dishes are sufficiently large that neither the contact line of the spreading drops nor the PMMA microparticles ever reach the dish edge or the Wilhelmy pin. Drops with a volume of approx. 4 μl are placed on the water subphase with a minimum of kinetic energy by gently contacting the drop formed at the end of the micropipette tip to the subphase. Details of this method were described in Ref. [137].

3.2.1 Contact Angle Measurements

The hydrophobic solids are characterized by advancing, receding and static contact angles. Figure 3-4a depicts the measurement method to determine the advancing contact angle and the receding contact angle by inflating or deflating water drops. The liquid dispensing unit is software-controlled, which enables the drop volume and the dispensing rate to be precisely adjusted. Therefore, the dynamic contact angle measurements can be repeated with high reproducibility. If a small enough amount of liquid is added to the drop, the contact line will still be pinned until the contact angle increases to maximum θ_A. On the other hand, if a small enough amount of liquid is removed from the drop, the contact line will not move until the contact angle decreases to minimum θ_R. Note that in this work the static contact angle θ_0 is not defined as the arithmetic mean of the advancing and receding angles, but as the angle at which the TPCL of a spreading drop with a volume of approx. 4 μl comes at rest. This angle is used because it is the only measurable angle with water and with surfactant-laden drops, since the receding contact angles of nearly all surfactant solutions used will be zero. These contact angles are measured by the sessile drop

technique with the PAT 1. All measurement results of hydrophobic substrates with different surface energies are summarized in Table 3-2.

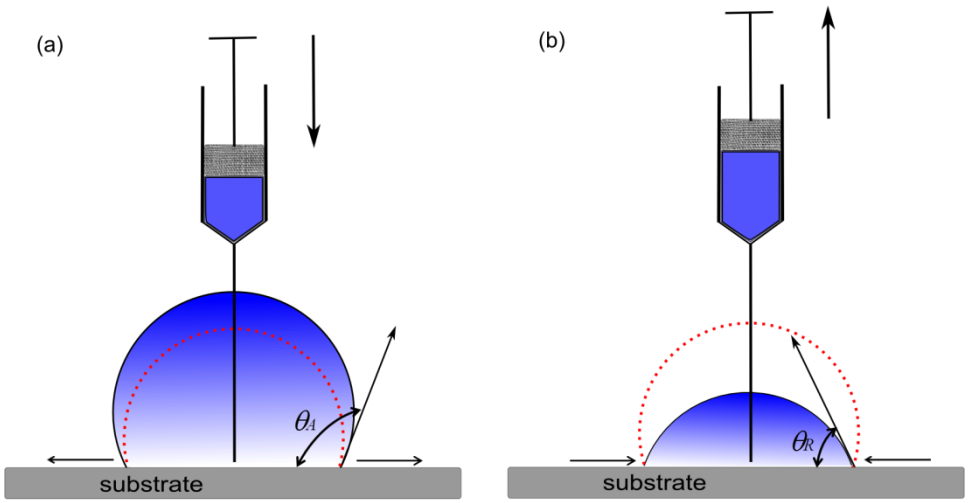

Figure 3-4 Schematic drawing of advancing contact angle (a) and receding contact angle (b). The red dotted lines indicate the initial shapes of sessile drops.

Table 3-2 Surface tension of different solids and advancing, receding and static contact angles of water on them. The standard deviation in the contact angle measurement is ~ 1°.

Substrate	Surface tension [172] (mN/m)	θ_A (°)	θ_R (°)	θ_0 (°)
Polypropylene (PP)	30	114	88	97
Polystyrene (PS)	34	85	65	73
Polycarbonate (PC)	44	105	46	86
Polymethylmethacrylate (PMMA)	38	97	54	72
Parafilm®	25	119	98	105
Polydimethylsiloxane (PDMS)	20	115	68	104
Hydrophobized glass	-	120	99	107

3.2.2 Roughness Measurements

Roughness measurements of PP substrates at various points are performed by Dr. Lars-Oliver Heim (Experimental Interface Physics, Center of Smart Interfaces, Technische Universität Darmstadt) with an atomic force microscope (AFM, MFP-3D, Asylum Research, Santa Barbara, USA). PP substrates with examined area of $50 \times 50\ \mu m^2$ are imaged with AC mode, and an exemplary 3D topography image is shown in Figure 3-5. The average deviation R_a of surface roughness is $200 \pm 15\ nm$ for all examined PP substrates.

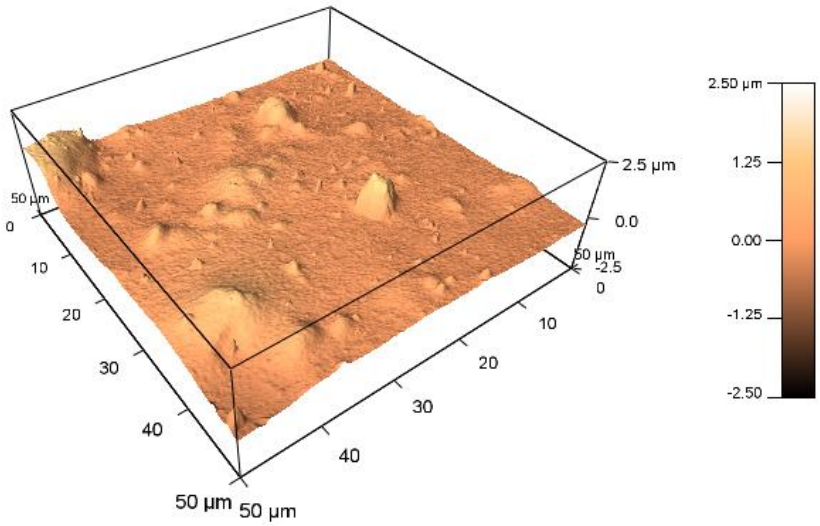

Figure 3-5 3D AFM topography image of an exemplary PP substrate over an area of $50 \times 50\ \mu m^2$.

3.3 Experimental Setups

Figure 3-6 shows the setup to record the early spontaneous wetting process ($t \leq 1$ s) of aqueous surfactant solutions on solids from the side. The solid used in the experiment is put into a closed chamber on an adjustable stage controlled by a micrometer screw. Through the chamber possible dust contamination is avoided. A steel needle with an outer diameter of 400 μm is placed above the solid at a certain distance for drop generation. The needle is hydrophobized with 1,1,1,3,3,3-hexamethyldisilazane in a desiccator at room temperature for 12 hours beforehand. This prevents the generated drop from wetting the needle. Drops with radii

$0.7 - 1.5\,mm$ are produced with a syringe pump (Landgraf HLL, Germany) and brought to the solids at a speed of few micrometers per second to minimize the kinetic energy. A cold light source (KL 2500 LCD, Schott, Germany) with a diffuser, which allows uniform lighting and good contrast, is used for illumination. The wetting process is captured with a high-speed video camera (FASTACAM SA-1, Photron Inc., USA) at a rate of 54,000 frames per second (fps) with image size of 384 × 240 pixels. The setup is also used to study surfactant-enhanced wetting of sessile water drops on PP substrates, which is achieved by local addition of a small surfactant-laden drop on the apex of sessile drops (Chapter 5). A $10\,\mu l$ pipette with a dispensing accuracy of $0.01\,\mu l$ is used to deposit a water drop with a defined volume of $5\,\mu l$ on the PP substrate. Then, a small surfactant-laden drop ($0.2 - 0.5\,\mu l$) is gently dispensed on the apex of the sessile drop. The release of small surfactant-laden drops is controlled with a syringe connected with a home-made mechanical manipulator. The surfactant-laden drop is approached to the sessile drop in a quasi-static way ($\sim 10\,\mu m/s$) to minimize the impact effects. The spreading of surfactant on the curved water surface as well as the wetting process of sessile drops on PP substrates are captured at a rate of 45,000 fps with image size of 424 × 137 pixels.

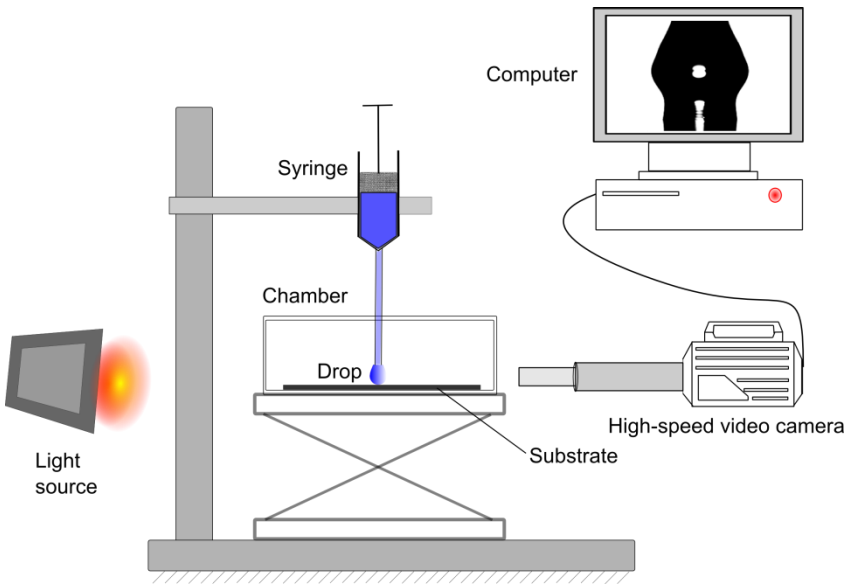

Figure 3-6 Setup for the early wetting process of surfactant-laden drops on solids.

Impact experiments in Chapter 6 are also performed with this setup. Drops of different aqueous surfactant solutions are released from various heights by adjusting the position of syringe holder. The impact velocities range from 0.6 m/s to 3 m/s, which are determined from two consecutive images prior to impact. The impact process is recorded at 30,000 fps with image size of 552 × 287 pixels.

The side view of spreading drops suffers from the limitation of spatial resolution in the case of superspreading, as a very thin liquid film will be formed with non-detectable wetting radius and contact angle (below 8°) due to complete loss of the spherical shape of the drop and its subsequent distortion. Therefore, for the late stage of spontaneous wetting ($1 < t < 10\ s$), the top view is monitored with another high-speed camera (Mikrotron GmBH, Germany) at a rate of 150 fps with image size of 1,040 × 916 pixels. Figure 3-7 shows the experimental setup. A tungsten light source (DEDOCOOL, Munich, Germany) is used to illuminate the substrates with a high intensity over a large area. The steel needle is bent so that the generated drops can approach the substrates gently (Figure 3-7). In this setup, the substrates are enclosed in a home-made chamber where the relative humidity is controlled by means of two mass flow controllers (MFC 358, Analyt-MTC GmbH, Müllheim, Germany) and is monitored with a sensor reader (SHT75, Sensirion AG, Staefa, Switzerland). The sensor is embedded beneath the top window of the experimental chamber. Dry nitrogen gas stream introduced from the inlet is firstly separated into two channels, one “dry” channel with RH~0 % and the other “wet” channel with RH~100 %. The RH in the experimental chamber is controlled between 10 % and 90 % with accuracy ±1.5 % by adjusting the flow rate of each MFC. The ambient temperature in the chamber is also monitored by the sensor. Prior to each experiment, the temperature and RH are maintained constant.

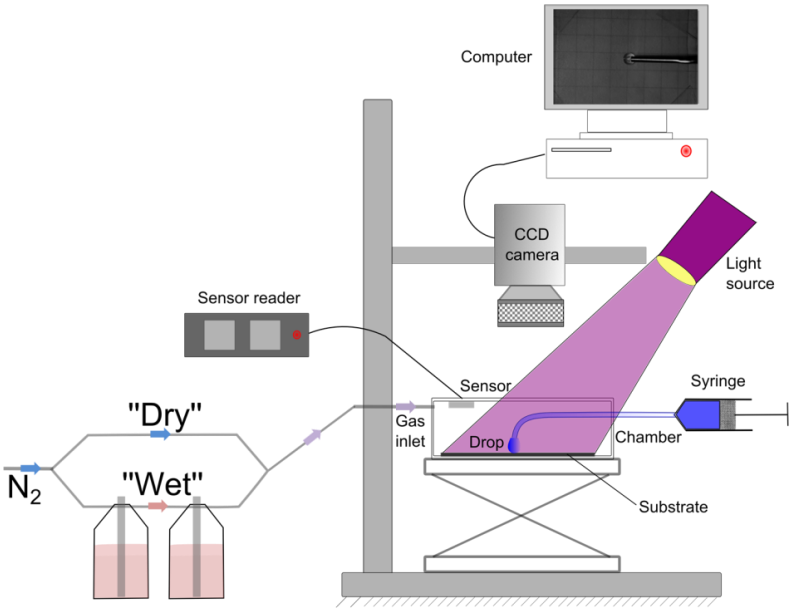

Figure 3-7 Setup for late wetting process of aqueous surfactant solutions.

The setup is also used to study the early wetting process of aqueous surfactant solutions on flat water subphases (Chapter 5). The advancing distance of the surfactant leading edge, the marker microparticles as well as capillary waves triggered by the deposition of surfactant-laden drops on water subphases, are monitored simultaneously at 1,000 fps with image size of 1,280 × 1,066 pixels.

All experiments are performed on a vibration-free table at room temperature (22 ± 1 °C) and relative humidity of 40 ± 5 %, if not otherwise stated. To ensure reproducibility, each set of experiments is repeated at least six times with fresh solid substrates and water subphases.

3.4 Data Analysis Methods

The data analysis process consists of two steps: extracting relevant parameters out of recorded images, and data fitting.

3.4.1 Extracting Contact Radius and Contact Angle from Videos

The wetting radius and contact angle of drops on solids are extracted from recorded images with self-programmed MATLAB® (R2010a, MathWorks Inc., USA) algorithm and C++ (Visual Studio 6.0) algorithm. In the MATLAB® code, each recorded

sequence is firstly transformed into a black and white image. A threshold value is set to differentiate between drop profile and background. Then, the information of contact radius and contact angle of drops on solids is extracted by zooming in the vicinity of the contact area. The profiles of spreading drops triggered by addition of surfactants (Chapter 5) is extracted with a MATLAB® code. In the C++ code, the contact contour between the drop and substrate is obtained by subtracting the image background of the first recorded sequence.

3.4.2 Data Fitting

Fitting the curves of wetting radius vs. time with power laws, $r \propto t^{\alpha}$, is a commonly used method for wetting of simple liquids [38, 58, 59, 87, 88] as well as wetting of aqueous surfactant solutions [13, 24, 25, 66]. Therefore, in this work power law fitting with a least square method (LSM) is used to determine the wetting dynamics of surfactant solutions. The Pearson's correlation coefficient ϵ is used to check the linear dependence of two variables log$r$ and log$t$.

$$\epsilon = \frac{\sum_{i=1}^{m}(logr_i - \bar{r})(logt_i - \bar{t})}{\sqrt{\sum_{i=1}^{m}(logr_i - \bar{r})^2}\ \sqrt{\sum_{i=1}^{m}(logt_i - \bar{t})^2}} \tag{3.2}$$

With

$$\bar{r} = \frac{1}{m}\sum_{i=1}^{m} \log r_i \tag{3.3}$$

$$\bar{t} = \frac{1}{m}\sum_{i=1}^{m} \log t_i \tag{3.4}$$

The correlation coefficient has a value of $-1 \leq \epsilon \leq 1$. Here -1 and 1 mean total negative linear dependence and total positive linear dependence, respectively, between log$r$ and log$t$. 0 means no correlation of the two variables.

In Chapter 4, the experimental data in the viscosity-dominated wetting stage is analyzed with G-dyna software, which was described in detail by Seveno *et al.* [91]. To determine the velocity of the TPCL, the time dependence of the wetting radius is fitted by a polynomial function of maximum order 10.

$$\sum r_{fit}(t) = \frac{\sum_{i=0}^{m} a_i t^i}{1 + \sum_{i=1}^{m} b_i t^i} \tag{3.5}$$

The function used can accurately reproduce the observed evolution of the wetting radius with time. The velocity of the TPCL vs. time, $U(t)$, is calculated by differentiating $r_{fit}(t)$ numerically.

With the G-dyna software, the wetting radius vs. time curves in my work can be accurately fitted in the range of interest with polynomials of order 2. The experimental dependence of $\theta = f(U)$ can be determined from continuous functions for $\theta(t)$ and $U(t)$. Both HDT and MKT, embedded in the G-dyna software, are chosen for data fitting of $\theta = f(U)$.

4 Spontaneous Wetting of Surfactant-laden Drops on Solids[1]

In this chapter, the wetting performances of different aqueous surfactant solutions on various hydrophobic solids are comparatively investigated. Depending on the surfactants or solids, one, two or three stages of dynamic wetting occur, and each stage can be described by power law dynamics. An early wetting stage ($t < 12\,ms$) is observed for all surfactant solutions on all solids. Scaling analysis of the experimental data shows that the early stage is dominated by inertia and that the duration of this stage is not influenced by surfactants. After the inertial stage, a viscosity-dominated wetting stage is observed for aqueous trisiloxane surfactant solutions. It is found that superspreader-laden drops do not superspread on solids with wettability lower than that of PP. For superspreader solutions, a strong dependence of the wetting dynamics on surfactant concentration and RH is found in a superspreading stage on PP. The findings suggest that the superspreading properties of superspreaders begin to take effect after a certain time, before which the superspreader and the non-superspreader solutions behave similarly. The results also imply that there is interplay between several factors (e.g. surfactant adsorption, evaporation, surfactant aggregates) that influence superspreading.

4.1 Motivation

Although the superspreading phenomenon on hydrophobic solids has attracted much attention from industrial and scientific fields, researchers still disagree about the interpretation about the observed superspreading dynamics. Svitova *et al.* [173] reported two wetting stages of trisiloxane surfactant solutions on graphite: the first stage has the wetting exponent α in the range of $0.12 - 0.22$; during the second stage α increases to $0.38 - 0.58$. Rafai *et al.* [24, 157] found the wetting exponent is larger than 0.1 for superspreader solutions at concentrations both above and below CMC on polyethylene terephthalate (PET) solids. A linear relation $r \sim t$ was observed for

[1] This chapter is mainly based on the publication "X. Wang, L. Q. Chen, E. Bonaccurso, J. Venzmer, *Dynamic wetting of hydrophobic polymers by aqueous surfactant and superspreader solutions*, Langmuir, **29**, 14855-14864 (2013)".

superspreader solutions with very high concentrations (10 CMC). The incompatible exponents may stem from the different trisiloxane surfactants and solids used by researchers. Several studies reported that high relative humidity (e.g. 90 %) promotes the superspreading process of superspreader solutions [8, 30, 67, 162]. The problem is that due to the low time resolution of the video camera used in previous studies, it is impossible to investigate the early wetting stage within several milliseconds when the drop just contacts the solids. Open questions are whether the early wetting dynamics of aqueous surfactant solutions is also dominated by inertia, just as that of simple liquids. How do the substrate wettability, surfactant concentration and RH influence the wetting dynamics of different surfactant solutions? Will a comparative study about superspreader and non-superspreaders help to clarify the mechanism of superspreading? These questions lead to a systematic study of the early wetting dynamics of aqueous surfactant solutions on hydrophobic solids.

4.2 Results and Discussion

The liquids used in this work are water, aqueous CTAB and SDS solutions at 0.1-3 CMC, aqueous TSS10/2 and TSS6/3 solutions at 0.05-1 wt%. The solids are PP, PS, PC, PMMA, Parafilm®, PDMS and hydrophobized glass slides. The experimental results are discussed based on the classification of surfactants. The effects of substrate wettability, surfactant concentration and RH on superspreading are also discussed.

4.2.1 Aqueous Surfactant Solutions of CTAB and SDS

All drops of CTAB or SDS solutions spread out spontaneously after contacting the PP substrates. Figure 4-1 shows the wetting radius as a function of the time of aqueous solutions of CTAB and SDS. When a small amount of surfactant is added to the water, the drops initially spread with an average velocity $U \sim 0.15\, m/s$, which is faster than that of water ($\sim 0.1\, m/s$). It is known that the early wetting dynamics of simple liquids is dominated by inertia and that the wetting radius grows with time according to a power law [58, 59, 81]. The log-log plots in Figure 4-1a & b indicate that in presence of surfactants, the wetting radius follows a power law as well. For all liquids, only one inertia-dominated wetting stage is found, which lasts approx. $10\, ms$ after

drop deposition. After that, CTAB and SDS solutions do not spread further on the PP substrates. The observations are in good agreement with previous reports [126, 167], where the authors showed "conventional" ionic surfactants do not promote rapid spreading of water drops on substrates as hydrophobic as PP.

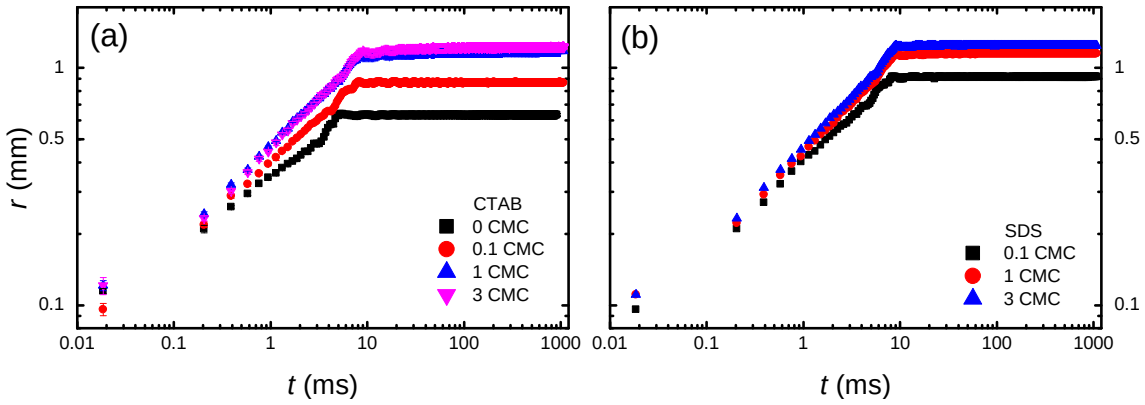

Figure 4-1 Wetting radius vs. time of water and aqueous solutions of CTAB (a) and SDS (b) on the PP substrates in a log-log representation (0 CMC denotes water). The data is averaged from at least six repeated experiments. The error bars show that the experiments are reproducible.

As mentioned in Chapter 2, the actual duration τ of the early inertial wetting stage of simple liquids on solids shows a linear dependence on the characteristic inertial time τ_c. With surfactant addition, it is experimentally found that τ also linearly depends on τ_c, as shown in Figure 4-2. A linear fitting gives a slope of ~ 2.66, which is close to the value of ~ 2.82 reported in Ref. [81]. This indicates that the addition of surfactant has no effect on the duration of the inertial wetting stage, only influences the contact radius.

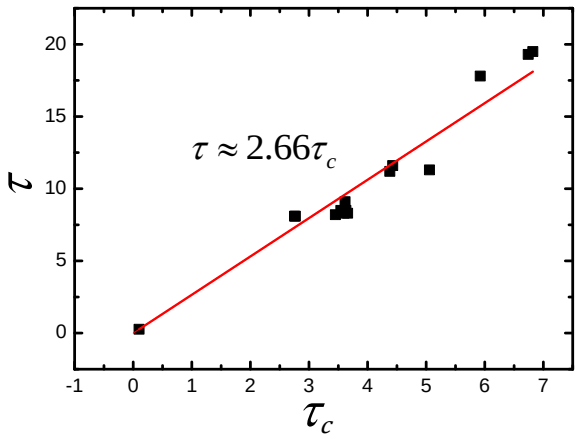

Figure 4-2 Inertial wetting time of drops of various liquids on PP substrates as a function of characteristic inertial time τ_c. The solid line is the best fit with a slope of 2.66.

Figure 4-3 summarizes the wetting exponents α and the static contact angles θ_0 for water, CTAB, and SDS during the early wetting stage. The exponent is ~ 0.33 for water, which is consistent with values for hydrophobic solids in previous studies [59, 81]. The fitted exponents for aqueous surfactant solutions are larger than that of water, and they increase with increasing surfactant concentrations. This is due to the decrease of surface tension with surfactant addition (Table 3-1). However, for aqueous solutions above CMC, the wetting dynamics varies little and the wetting exponents remain unchanged. As shown in Figure 4-3a, the static contact angle θ_0 decreases with increasing surfactant concentration and decreasing surface tension. Also, the exponent α depends on the static contact angle θ_0 (Figure 4-3b). The observations are in good agreement with findings that the exponent of inertial wetting stage is only dependent on substrate wettability or liquid surface tension [59, 81].

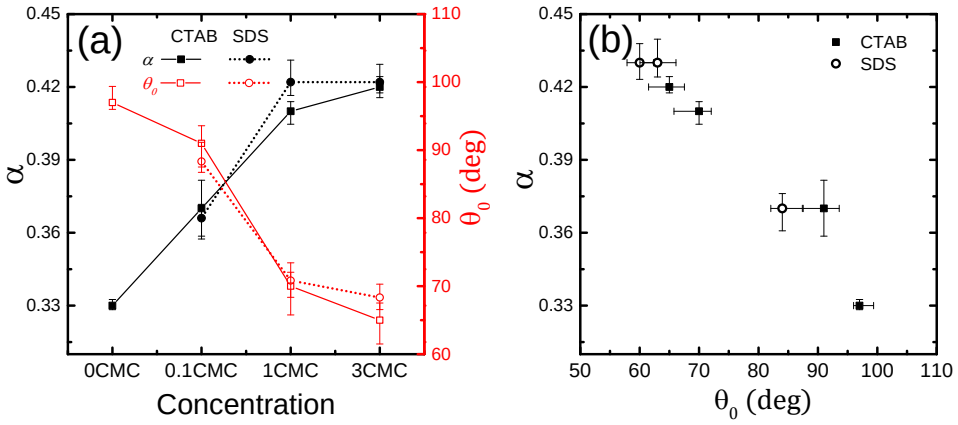

Figure 4-3 (a) Exponent α and static contact angle θ_0 are plotted as a function of surfactant concentration. (b) Exponent α vs. static contact angle θ_0 for water, CTAB and SDS (0.1 - 3 CMC).

4.2.2 Aqueous Trisiloxane Surfactant Solutions

Inertial Wetting Stage

The wetting dynamics of two trisiloxane surfactant solutions (TSS10/2 and TSS6/3) is discussed in this part. The log-log plots of wetting radius vs. time of the trisiloxane-laden drops in the time window $0 - 1\ s$ are shown in Figure 4-4. For CTAB and SDS solutions, only inertial wetting before the drops reach equilibrium is observed (Figure 4-1). In contrast, the wetting process of both aqueous trisiloxane surfactant solutions can be subdivided into two stages: an early wetting followed by another wetting stage, setting in after $\sim 12\ ms$. The early wetting stage, with an average velocity of $\sim 0.15\ m/s$, is also dominated by inertia and follows a power law with exponent ~ 0.42 (Figure 4-4). The close similarity in the curves of r vs. t is observed over the entire concentration range studied (0.05-1 wt%). Moreover, the duration of the early stage τ is linearly dependent on the characteristic inertial time τ_c, which is observed also for water, CTAB, and SDS (Figure 4-2). Therefore, it is reasonable to conclude that the surfactant types and concentrations do not influence the duration of the early inertia-dominated wetting stage in the concentration range used.

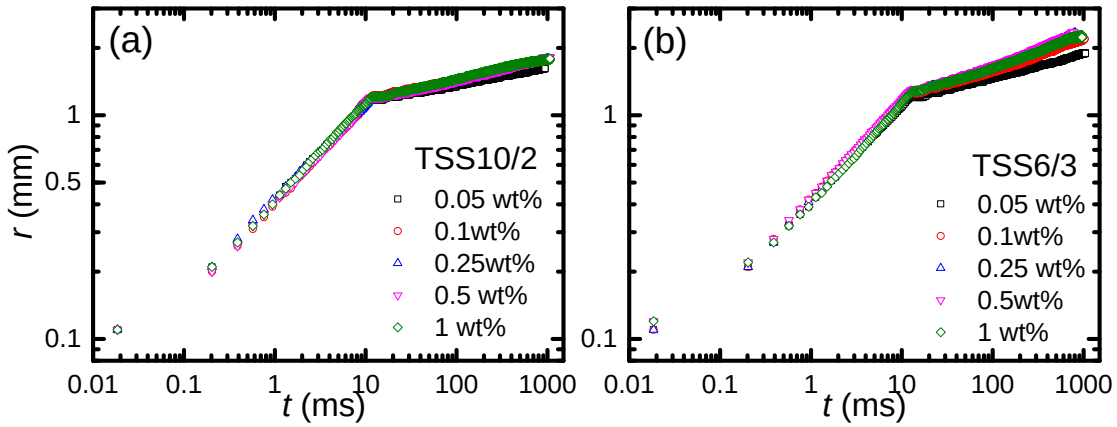

Figure 4-4 Log-Log plots of wetting radius r vs. time t of TSS10/2-laden drops (a), and TSS6/3-laden drops (b) on PP substrates.

Viscous Wetting Stage

For aqueous TSS10/2 solutions (Figure 4-4a), the wetting process slows down after the early inertial stage and the wetting dynamics is similar for different concentrations. Compared with TSS10/2-laden drops, the wetting velocity of TSS6/3-laden drops is faster at $t \gtrsim 12\,ms$, and the effect of concentration becomes more evident (Figure 4-4b). The wetting stage at $t \gtrsim 12$ ms can also be fitted with power laws. Figure 4-5 shows the exponents of aqueous TSS10/2 and TSS6/3 surfactant solutions with different concentrations. For TSS10/2 solutions, the wetting radius shows a time-dependence of $r \sim t^{1/10}$. In contrast, aqueous TSS6/3 solutions have a higher scaling coefficient of $r \sim t^{1/7}$. Considering the dynamic wetting models outlined in Chapter 2, it shows that the wetting dynamics of TSS10/2 solutions is better described by the HDT, while the MKT better describes the wetting dynamics of TSS6/3 solutions. To verify this, both HDT and MKT, embedded in G-dyna software, are used to fit the experimental data of TSS10/2 and TSS6/3 solutions. As inertial wetting is not included in the theory, the data between 0 and 12 ms is masked and only the wetting stage at $t \gtrsim 12\,ms$ is fitted.

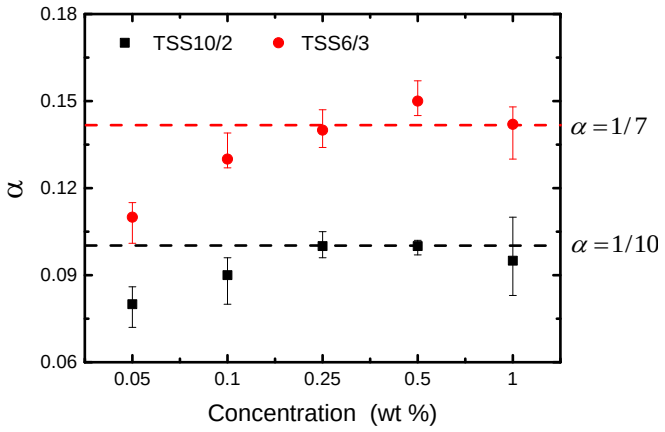

Figure 4-5 Exponent α for trisiloxane surfactant solutions at different concentrations.

Figure 4-6 shows the dynamic contact angle θ vs. velocity U of the TPCL for drops of TSS10/2 and TSS6/3 solutions at concentration 0.1 wt% on PP substrates. After the inertial stage, the wetting of both drops continues with a contact angle of ~ 68° and a velocity of $\sim 0.01\, m/s$ (top right corner of the graph), and then proceeds towards smaller contact angles and lower velocities. For aqueous solutions with low surfactant concentrations used here, the density and viscosity are close to that of water. Therefore, the values used in the fitting process are those of water, and the corresponding HDT and MKT parameters are listed in Table 4-1.

As shown in Figure 4-6, the MKT provides a good fitting to the experimental results over the whole data set of TSS10/2 0.1 wt%, while the HDT is only accurate for the low velocity ($\sim 0.003\, m/s$) stage. The obtained values of the parameters from the MKT fitting are reasonable, and the fitted values of θ_0^{MKT} deviate little from the experimentally determined values θ_0^{exp} (see Table 4-1). The derived value of $ln\,(L/L_s)$ from the fitting with HDT leads to a subatomic slip length, which has therefore limited physical meaning [174, 175]. In comparison, the fitting to the experimental results of TSS6/3 solutions with the MKT and HDT are poor, and the obtained parameter values, K_0 and $ln\,(L/L_s)$, are physically unsound. In spite of these parameters, the HDT fitting seems to agree with the experimental results of TSS10/2 and TSS6/3 solutions at low velocities (small values of contact angle). Similar observation could be found in Ref. [176], the findings in which showed the HDT was valid for small contact angles (low velocity data) in the presence of surfactants.

Moreover, the hydrodynamic regime is preceded by a molecular kinetic regime at high velocities [176]. Such conclusion fails to work for the TSS6/3 solution; since the MKT fitting to the TSS6/3 solution is not acceptable at high velocities (Figure 4-6). Nevertheless, Hopf *et al.* [177] reported that for surfactant-containing system, the HDT was in accord with the experimental results for a high TPCL velocity, while the MKT model held only for low velocities. The authors in Ref. [178] also observed a deviation from the theoretical trend given by MKT at high velocities. These discrepancies may result from different surfactant properties that will influence the surfactant transfer to the air/liquid and to solid/air interfaces, thus affecting the dynamic contact angles during the advancement of TPCL.

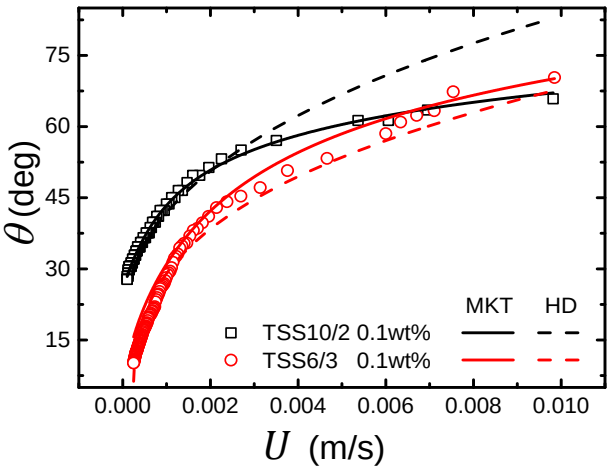

Figure 4-6 Dynamic contact angle vs. velocity of TPCL for the drops of trisiloxane surfactant solutions at 0.1 wt%. The best fitting of MKT and HDT are represented by different lines. Fitting parameters are listed in Table 4-1.

The experimental wetting data of trisiloxane solutions at other concentrations are also fitted with HDT and MKT. All the fitting parameters are summarized in Table 4-1. Overall, the two theories prove to be inappropriate to describe the wetting of TSS6/3 solutions. Reasonable agreement is obtained with MKT and TSS10/2 solutions, and poor agreement is obtained with the HDT and TSS10/2 solutions. This result is disappointing based on the previous observations that the experimental wetting

exponents correspond to those predicted by the HDT (for TSS10/2 solutions) and MKT (for TSS6/3 solutions) for fully wetting liquids.

Table 4-1 Parameters $ln\,(L/L_s)$, K_0 [Mhz], λ [nm], θ_0^{HDT}[deg] fitted by HDT, θ_0^{MKT} [deg] fitted by MKT, and θ_0^{exp}[deg] from experimental results with aqueous surfactant solutions at different concentrations.

Surfactant solutions	$ln\,(L/L_s)$	θ_0^{HDT}	K_0	λ	θ_0^{MKT}	θ_0^{exp}
TSS10/2 0.05 wt%	1052	35	0.32	1.48	28	34
TSS10/2 0.1wt%	820	26	0.24	1.55	26	25
TSS10/2 0.25 wt%	635	16	0.32	1.48	17	24
TSS10/2 0.5 wt%	927	23	0.2	1.46	18	22
TSS10/2 1 wt%	654	21	0.25	1.55	20	25
TSS6/3 0.05 wt%	203	13	8.5E6	0.01	~ 0	15
TSS6/3 0.1 wt%	469	~ 0	0.8E6	1.16	~ 0	8
TSS6/3 0.25 wt%	79	~ 0	3.6E10	3.8E-4	~ 0	5
TSS6/3 0.5 wt%	119	6	0.6E6	0.25	~ 0	6
TSS6/3 1 wt%	82	1	3.5E8	1.7E-3	~ 0	7

This leads to the conclusion that both dynamic wetting theories (HDT, MKT) – originally developed for simple liquids – cannot be generally applied to experiments with surfactant solutions. In fact, because of the presence of surfactants in the drops, surface tension gradient and dynamic surface tension effects result from different molecular mobility and interfacial adsorption, while the HDT and the MKT do not take into account dynamic interfacial tensions that are more pronounced at larger wetting velocities. However, the suitability of the MKT for the description of the spreading of TSS10/2 solutions - but not of the TSS6/3 solutions - may imply that the effect of dynamic surface tension is more important in the superspreading process, and that the dynamics of surfactant molecules at the TPCL is generally different for the two trisiloxane surfactants. This was also suggested in Refs. [9-11, 150], where the authors proposed that the non-superspreading surfactants formed micellar aggregates in solutions, while the superspreaders formed easily “unzippable” bilayer

microstructures at the TPCL, especially in case of a L_3 or L_α phase. The bilayer configuration of the TSS6/3 trisiloxane molecules enables their direct and rapid transfer to the air/water interface and to the solid at the TPCL. This idea was also supported by experimental observations in other studies [12, 163]: non-superspreaders with long hydrophilic groups formed micellar solutions, rather than a L_3 or L_α phase formed by superspreaders. The question remains about the driving force that causes advection of the more easily "unzipping" bilayers to the TPCL region.

Superspreading Stage

As shown in Figure 4-4b, the wetting of aqueous TSS6/3 solutions at different concentrations accelerates after $\sim 100\,ms$, which implies that the wetting process is not just controlled by the viscosity and the surface tension of the liquid, but driven by one or more additional effects. For comparison with the superspreading TSS6/3 solutions, the wetting dynamics of TSS10/2 0.1 wt% is also shown. Drops with TSS10/2 stop spreading with a measurable static contact angle of $\sim 12°$ on the PP substrates. Contrarily, drops of TSS6/3 solutions - at all concentrations - completely wet the PP substrates, with a hardly measureable contact angle close to 0°. Not only the final contact angles, but the wetting dynamics between 1 and 10 s of TSS10/2 and TSS6/3 solutions at studied concentrations are remarkably different as well. One reason may lie in the different length of the hydrophilic EO chain of TSS10/2 and TSS6/3. Only trisiloxane surfactants with intermediate EO chain length exhibit superspreading behavior on hydrophobic solids [26, 150, 161]. It was also reported that surfactants forming turbid solutions performed better than surfactants forming clear micellar solutions [8, 10]. A visual inspection of TSS6/3 and TSS10/2 solutions shows that the TSS6/3 solutions are milky or turbid above a concentration of ~ 0.1 wt%. TSS10/2 solutions are clear even at a concentration of ~ 0.5 wt%, owing to their increased solubility because of their longer hydrophilic tails. The measurements of aggregate size in trisiloxane surfactant solutions are performed by Andreas Geißler (Ernst-Berl-Institute for Macromolecular Chemistry and Paper Chemistry, Technische Universität Darmstadt) with dynamic light scattering (Zetasizer Nano ZS, Malvern Instruments Ltd., UK). The results reveal that aggregates range from 30 to 800 nm in the TSS6/3 solutions, while the aggregates in the TSS10/2 solutions have sizes of

~ 10 *nm* and are monodisperse. The non-uniform aggregates in TSS6/3 solutions may be associated with the known bilayer L_3 or L_α phases of superspreaders, while the uniform micellar phase in TSS10/2 solutions is common to those known for most "conventional" surfactants [9].

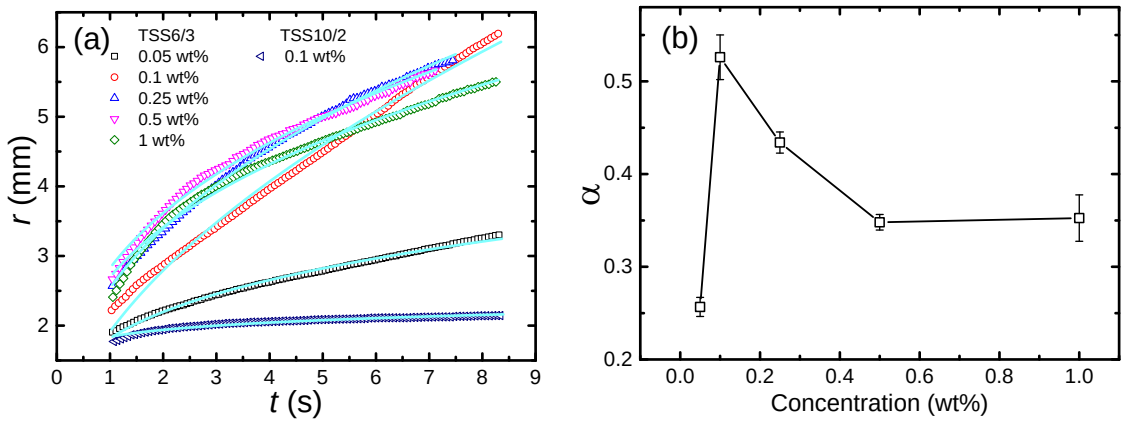

Figure 4-7 (a) Wetting radius vs. time of trisiloxane surfactant solutions at various concentrations on PP substrates in the late wetting stage. Solid lines represent the power law fittings to the experimental results. The wetting exponents for aqueous TSS6/3 solutions at different concentrations are plotted in (b).

In the present work the final wetted area of aqueous superspreader solutions with different concentrations cannot be determined because of the limits of the optical imaging technique. When superspreading occurs, the final drop profile is so thin that it is impossible to distinguish it from the transparent PP substrate and the contour of the wetted area is not circular any more. Therefore, the investigations are limited to approx. 10 *s*, when all drops still show circular contours. However, as shown in Figure 4-7a, drop radii within 10 *s* differ for all solutions investigated. Different concentrations of TSS6/3 solutions influence the wetting dynamics and the wetted area. Solutions with concentration of 0.05 wt% spread slowest and wet the least, while solutions with higher concentrations spread faster to larger wetted areas. At the beginning ($t < 3\,s$), the wetting velocity and wetted area increase with surfactant concentrations, but keep identical above a certain concentration (0.1 wt%). Deceleration of the wetting process is observed after 3 *s* for solutions at concentration

above 0.1 wt%. Considering the entire wetting process, the average wetting velocity and wetted area are maximum at the concentration of 0.1 wt%. Similar results were reported in literature [10, 13, 30], although the trisiloxane surfactants and hydrophobic solids employed are different from the ones in this study. The wetting velocity during the first 10 s was investigated as a function of concentration in Ref. [30]. In that article it was found that at low concentrations, the wetting velocity was proportional to surfactant concentration, but above a certain limit (0.1 wt%) the velocity became constant.

The wetting radius in the superspreading stage can also be fitted with power laws. Although some curves cannot be perfectly fitted over the whole time range from 1 to 10 s, fitting is acceptable with a correlation coefficient above 0.98. The exponents of the power laws for TSS6/3 solutions spreading at all concentrations range from 1/4 to 1/2 (Figure 4-7b). These results are in fair agreement with previous work [13, 24, 155, 173]. The wetting dynamics of simple liquids on completely wettable solids is well described by Tanner's law $r \sim t^{1/10}$ [64]. Thus, TSS6/3 solutions show a faster spreading than simple liquids; hence, the HDT and MKT do not allow drawing conclusions on the wetting mechanisms active here. Since the surface tension gradient can lead to $r \sim t^{1/4}$ [43, 142], it has been considered to drive faster spreading of aqueous surfactant solutions after a time of $\sim 1\ s$ [8, 13, 17, 22, 24].

The dependence of the surface tension gradient on surfactant concentrations can be explained in this way. At a low concentration (0.05 wt%), the rate of surfactant diffusion from the bulk to the newly created fresh drop surface is slow, as the surfactant concentration gradient is small. Eventually, a radial surface tension gradient can be formed and leads to a power law wetting dynamics of $r \sim t^{1/4}$. By increasing the surfactant concentration to 0.1 wt%, the larger surface tension gradient provides a stronger driving force. As a consequence a higher velocity and a larger extent of wetting are observed. A further increase of surfactant concentration leads to a higher wetting velocity at the beginning due to a stronger driving force. However, the wetting in the late stage slows down, because the surfactant diffusion from the bulk is fast enough to replenish surfactant in the newly created drop surface. Therefore, the air/water interface is saturated rapidly with surfactants, and the

surface tension gradient fades more quickly. As a result, a critical concentration (0.1 wt %) does exist for the wetting system at which the wetting velocity and the area wetted by a drop are maximum due to a balance between surface tension gradient driving the drop spreading and the rate of surfactant diffusion to the air/water interface reducing the surface tension gradient. The different exponents of surfactant solutions with different concentrations – lying between 1/4 and 1/2 - imply that the surface tension gradient is probably established in the radial and in the height direction, as suggested also in Ref. [24]. These arguments offer a reasonable interpretation of the results shown in Figure 4-7a. A sufficient surface tension gradient to sustain the wetting process of drops is maintained for the longest time for aqueous solutions with a characteristic concentration of 0.1 wt%. For these reasons, these drops continue wetting rapidly and constantly, and cross the wetting curves of the drops with higher concentrations (Figure 4-7a). Although the above considerations just offer a qualitative picture, they suggest that the surface tension gradient is a major driving force in the superspreading stage.

4.2.3 Influence of Substrate Wettability on Superspreading

Apart from PP, other solids (e.g. PC, PS, PMMA etc.) are also used to study the wetting dynamics of aqueous trisiloxane solutions. The log-log plots in Figure 4-8 show the wetting radius vs. time of aqueous trisiloxane surfactant solutions on hydrophobized glass slides. Aqueous TSS10/2 and TSS6/3 solutions at different concentrations behave similarly to the early wetting dynamics ($t < 12\,ms$) on PP substrates, a. Power law fitting is applied to the wetting data and yields an exponent of approx. 0.43. This suggests that the early wetting stage of aqueous trisiloxane surfactant solutions on the hydrophobized glass slides is dominated by inertia. After the early stage, TSS10/2 solutions and TSS6/3 solutions reach an equilibrium state with a finite static contact angle. This is different from the wetting dynamics on PP substrates, on which a viscosity-dominated wetting stage and superspreading stage are observed with TSS6/3 solutions.

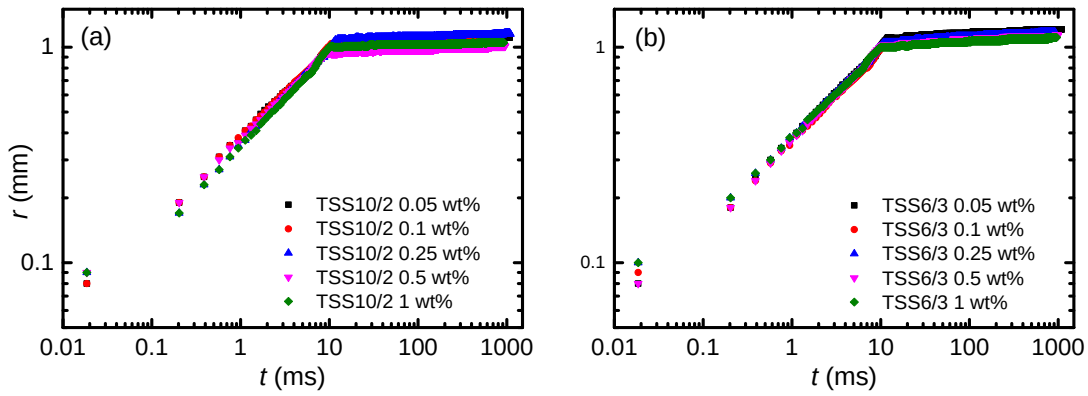

Figure 4-8 Log-log plots of drop wetting radius vs. time of aqueous TSS10/2 surfactant solutions (a) and aqueous TSS6/3 surfactant solutions (b), at various concentrations on the hydrophobized glass slides.

Further experiments of aqueous TSS6/3 solutions demonstrate that superspreading occurs on solids as PS, PC and PMMA, but on Parafilm® and PDMS solids, only partial wetting occurs. Table 3-2 shows that PS, PC and PMMA have higher wettability than PP, while Parafilm®, PDMS and the hydrophobized glass slide have lower wettability than PP. Thus it is reasonable to conclude that superspreader (TSS6/3) solutions fail to superspread on solids too hydrophobic, such as Parafilm®. Potential influences of wettability and surface roughness of the solids cannot be neglected. Therefore, for the purpose of studying superspreading, surfactants, solids and experimental conditions must be selected properly to make the superspreading phenomenon occur.

4.2.4 Influence of Relative Humidity on Superspreading

The experiments are performed at different RH ranging from 10% to 90%. Both superspreader and non-superspreader solutions are used to comparatively study the influence of relative humidity on surfactant-enhanced wetting and superspreading on PP substrates. Log-log plots of the wetting radius vs. time are shown in Figure 4-9. In the case of TSS10/2 0.1 wt% solution, the wetting radius is the smallest at 10% RH (Figure 4-9a). For RH>10% the relative humidity does not play a role in surfactant drop wetting dynamics. This observation also holds true for TSS10/2 solutions at other concentrations. Considering the standard error of plotted data, it leads to the

conclusion that the wetting process of TSS10/2 solutions is not sensitive to RH at RH>10%. This is probably due to the fact that at very low RH (e.g. 10% RH), the formation of a precursor water film from vapor on PP substrates is unfavorable. Therefore, the surface tension gradient between the precursor film and the bulk of the spreading drop is inhibited [35, 162, 179]. When RH is above 10%, the formation of a precursor film is possible, however, the micelle aggregates in TSS10/2 solutions is not favorable for establishing surface tension gradient sufficient to promote fast wetting [30]. Therefore, the wetting velocity of trisiloxane TSS10/2 solutions is not enhanced by varying the relative humidity from 40% to 90%.

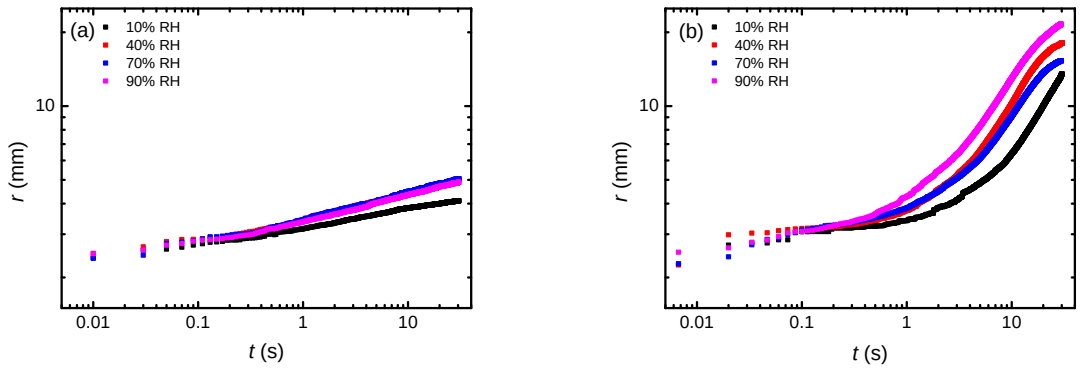

Figure 4-9 Log-log plots of wetting radius vs. time of aqueous TSS10/2 solution at 0.1 wt% (a) and aqueous TSS6/3 solution at 0.1 wt% (b) at different RH. The data is averaged from repeated experiments with standard error less than 1 *mm*.

In contrast to the TSS10/2 0.1 wt% solution, the dependence of wetting radius on RH of TSS6/3 0.1 wt% solution is remarkable (Figure 4-9b). A similar trend is found in the wetting dynamics of TSS6/3 solutions at all concentrations studied. At 10% RH the wetting radius is the smallest, while at 90% RH it is the largest. Similar observation could be found in previous work [8, 67, 162] which reported that the wetting radius increased with increasing RH. The surface tension gradient between the bulk of the drop and the precursor film formed at atmospheric RH was proposed to fasten wetting process of superspreader solutions [8, 162]. From thermodynamics view, however, a precursor film in contact with the leading edge of the drop is not favorable for drop spreading, since it is detrimental to allowing the spreading

coefficient to be positive [9]. Due to evaporation at low RH, the formation of a lamellar phase of the surfactant at the substrate or the leading edge of the drop could hinder drop spreading [30]. The wetting radius is larger at 40% RH than that at 70% RH (Figure 4-9b). The result is surprising, because it was reported that wetting area increased with increasing RH [8, 30, 67, 162]. This unexpected dynamics probably occurs because there is more than one effect involved in superspreading. At 40% and 70% RH, the surface tension difference between the bulk drop and the precursor film may promote drop spreading. At the same time evaporation occurring at the TPCL is more pronounced at 40% RH than at 70% RH. The local surfactant concentration can be lower at 70% RH than that at 40% RH, and therefore 40% RH is more favorable for a positive spreading coefficient, and thus drop spreading.

RH and the formation of a precursor film at the leading edge of a spreading drop do play a role in the wetting process of TSS6/3 solutions, but not of TSS10/2 solutions (Figure 4-9). This suggests that the sensitivity of the trisiloxane surfactants to relative humidity is different. It was reported that the sensitivity was caused by specific interactions between the hydrophilic part of the surfactant molecules and water [31]. Surfactants with long hydrophilic chains prefer to interact with water [26, 150, 161]. Considering the similar chemical structure of TSS6/3 and TSS10/2 but different aggregates in solutions [30], the comparative results confirm that the bilayer aggregates (e.g. lamellar phase) are essential in superspreading [9, 10, 160]. Moreover, since these TSS10/2 and TSS6/3 solutions are well above the CMC and have similar static surface tension, their different behaviors indicate the importance of dynamic adsorption of surfactant during wetting. Venzmer *et al.* [30] suggested that surfactant adsorption on the solid/liquid interface could influence the wetting dynamics. For micelle-forming surfactants, hemimicelles are formed at the substrate, which is less optimal for lowering the interfacial tension γ_{sl} (Figure 2-14a). In contrast, the adsorption of bilayer-forming surfactants on the solid/liquid interface is favorable for reducing interfacial tension γ_{sl} (Figure 2-14b). This promotes a positive spreading coefficient over a longer time, which is responsible for drop spreading. From the above discussion, it becomes clear that the explanations to the underlying mechanism governing superspreading are still uncertain, and some of them are in

contradiction with each other. However, this leads us to conclude that not one single factor, but a combination of different factors, e.g. RH, precursor film, surfactant aggregates, and the dynamic surface tension, work cooperatively for inducing superspreading.

4.3 Summary

The early wetting dynamics ($t < 12\,ms$) of aqueous surfactant solutions is mainly controlled by capillary and inertial forces, and the type of surfactant and its concentration do not play a role. For CTAB and SDS solutions, only this wetting stage is observed. A viscosity-dominated wetting stage ($12\,ms \lesssim t < 1\,s$) is observed for trisiloxane surfactant solutions on PP substrates. Only TSS6/3 solutions show a so-called superspreading stage ($t \gtrsim 1\,s$). The major driving force in the superspreading stage is the surface tension gradient that depends on the competing process of the growth rate of fresh air/water interface and the diffusion rate of surfactant from bulk to the air/water interface. During the superspreading stage, a critical concentration 0.1 wt % exists for the system at which the wetting velocity and the area wetted by a drop are maximum. TSS6/3 solutions fail to exhibit superspreading behavior on solids with wettability lower than that of PP. The influence of RH on the wetting dynamics of non-superspreading TSS10/2 solutions is negligible, but in case of superspreading TSS6/3 solutions, RH does play a pronounced role. Therefore, interplay of several factors, such as RH, precursor film, surfactant aggregates, evaporation and surfactant diffusion, works together for the superspreading phenomenon to occur.

5 Surfactant-enhanced Wetting on Polymers and Water Subphases[2]

This chapter includes two parts. In the first part of surfactant-enhanced wetting of water drops on polypropylene polymers, the experiments are performed by bringing a small surfactant-laden drop into contact with the apex of a large water drop sitting on PP. The spreading of surfactant on the curved air/water interface of the sessile drop, and subsequent wetting of the sessile drop on PP are investigated. In the second part, surfactant-enhanced wetting on flat water subphases with marker microparticles floating on top is addressed. Upon drop deposition, a train of capillary waves is observed when surfactant spreads along either the curved air/water interface or the flat air/water interface. The results show that surfactants influence the propagation velocity of capillary waves. The spreading of sessile drops on PP substrates or the movement of marker microparticles on flat water subphases are initiated by surfactant, rather than the propagating capillary waves. Though the dynamics of the early wetting of such non-homogeneously mixed water/surfactant drops on the PP substrates is different from that of homogeneously mixed drops introduced in Chapter 4, the dynamics of wetting at $t \gtrsim 12\,ms$ is similar and is dominated by viscosity in both cases. The experimental results in the second part can be consistently explained with the known prediction of surfactant spreading on liquid subphases.

5.1 Motivation

In order to understand the drop spreading under the action of a surface tension gradient, some authors conducted experiments on spreading of water drops sitting on polystyrene substrates by bringing Silwet® L-77 surfactant-laden drops into contact with the sessile drops [13, 17]. A large initial difference in surface tension between the two coalescing drops promoted the rise of surface tension gradient, and thus triggered the spreading of the sessile drop immediately [13]. Details in Ref. [17] revealed that it was favorable to deliver pesticide to crops after dew formation. However, this study was restricted to very low surfactant concentrations (2.5×10^{-3}

[2] This chapter is mainly based on the manuscript "X. Wang, E. Bonaccurso, J. Venzmer, S. Garoff, *Surfactant-enhanced spreading on a water subphase*, submit to Langmuir".

wt%, 7.5×10^{-4} wt%), at which the surface tension gradient equilibrated very rapidly and only partial wetting occurred. Moreover, the limited temporal resolution of the video camera (30 fps) did not allow capturing the spreading process of surfactant along the curved air/water interface of the sessile drop [13, 17]. Wetting of liquids on liquid subphases is important in coating processes and physiological applications. For example, the adsorption of aerosols into the lungs is critically dependent on the ability of one liquid to wet another liquid subphase [40]. Surfactants are naturally present in a healthy mammalian lung to reduce surface tension forces, and thus allow breathing without too much effort. The surfactant deficiency can lead to airway closure, decreased lung compliance and mechanical damage of the airway linings. In this case, externally surfactants (synthetic or animal derived) are required to be instilled into the deficient lung either directly through an endotracheal tube, or through inhalation of surfactant in aerosol forms [48, 55]. In order to ameliorate these techniques, numerous researchers performed investigations of the wetting of localized surfactant on flat liquid subphases with infinite radii of curvature [40-48]. Nevertheless, the number of studies of surfactant spreading on curved air/water interfaces is limited. The question is whether the surfactant spreading on air/water interfaces with different geometries and sizes shows similarities. This chapter aims to relate surfactant spreading in these two configurations with the high-speed video. The wetting process on PP of sessile water drops triggered by the deposition of small surfactant-laden drops is studied as well.

5.2 Results and Discussion

The concentrations of aqueous SDS solutions used are 0.5-1.5 wt%. All TSS10/2 and TSS6/3 surfactant solutions have concentrations from 0.1 wt% up to 10 wt%. The spreading of surfactant along curved air/water interfaces and the spreading of sessile drops on PP substrates are shown first. Then, surfactant-enhanced wetting on flat water subphases is discussed.

5.2.1 Surfactant-enhanced Wetting on Polypropylene Polymers

Spreading of Surfactant-laden Drops on Curved Air/Water Interfaces

Figure 5-1 shows the snapshots of the dynamic wetting profiles of a sessile water drop on a PP substrate triggered by local addition of a small water or surfactant-laden drop on its apex. In the first column of Figure 5-1, when a small water drop is brought into contact with a large sessile water drop, interfacial waves (red arrow) are initiated at the neck region and propagate downward along the curved air/water interface to the bottom of the sessile drop. Below a critical wavelength $\lambda_c^* = 2\pi\sqrt{\gamma/\rho g}$, the propagation of waves is dominated by surface tension only and the effect of gravity can be neglected [85, 180, 181]. For the air/water interface, $\lambda_c^* \sim 17\,mm$. This is much larger than drop size of the order of $1\,mm$. Therefore, we call the interfacial waves along the curved air/water interface capillary waves. In the surfactant-free system, the capillary waves reach the bottom of the sessile drop after $\sim 2.2\,ms$. The coalescence with the small water drop induces no motion of the TPCL of the large sessile drop, as shown in the superimposed drops contour sequence (last row in Figure 5-1). Only oscillations of the contact angle of the sessile drop around its static value occur. Therefore, the energy transported by the capillary wave alone is not sufficient for initiating the movement of the TPCL. If the dispensed small drop contains surfactant, the transfer of surfactant to the large sessile drop generates a surface tension difference between apex and bottom of the sessile drop. It was reported that under the action of the surface tension gradient the water drop starts to spread "immediately", based on experimental observations with a camera able of capturing up to 30 fps [13, 17]. Results from the high-speed video imaging show, however, that the contact line of the sessile drop does move only after a lag-time of $\sim 1.6\,ms$, which corresponds to the time needed by the capillary waves to propagate from drop apex to drop bottom in the system with surfactant. This lag-time was not observed in Refs. [13, 17] due to limited time resolution. The present work reveals an early stage, in which the TPCL is pinned even with a surface tension gradient established by dispensing surfactants with spherical micelles (SDS, TSS10/2) and with bilayer aggregates (TSS6/3). The different chemical structures and solubility of surfactants initially lead to similar "distortions" in the drop profiles, as shown in the last three columns of Figure 5-1.

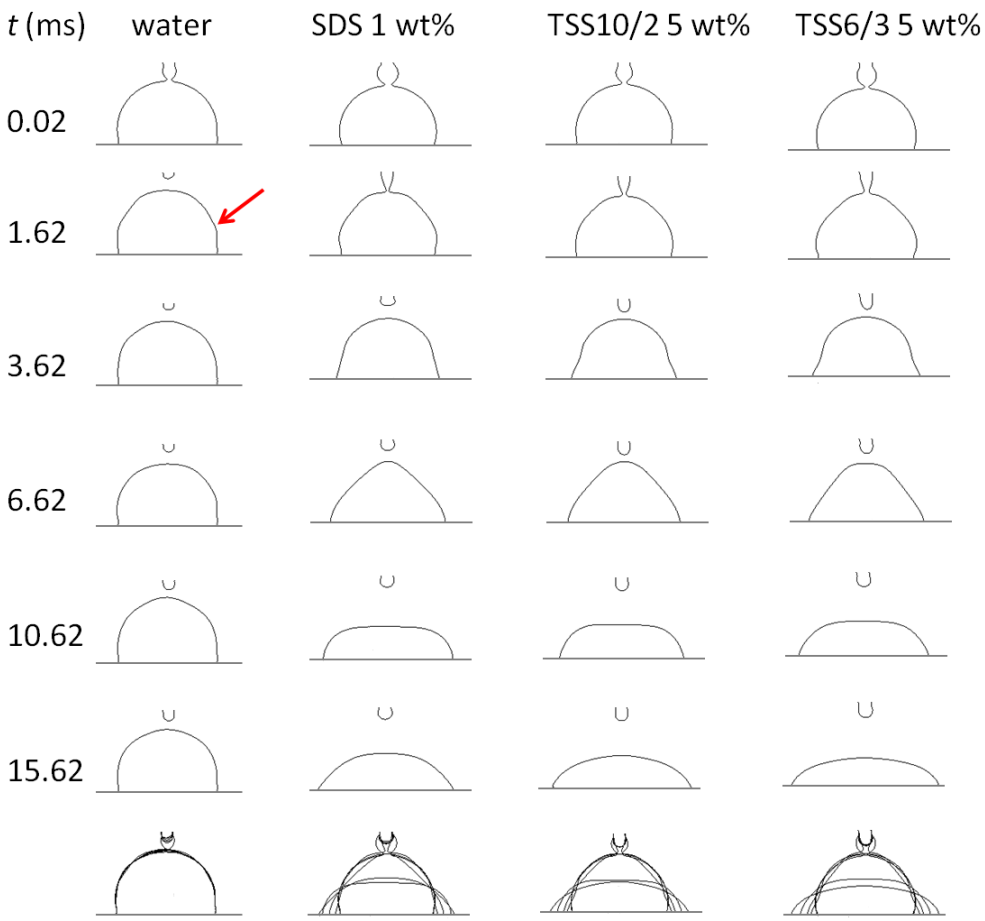

Figure 5-1 Snapshots of drop contours during spreading of large sessile water drops on PP substrates triggered by local dispensing of small drops on top. The last row corresponds to the superposition of all profiles.

Figure 5-2 depicts the possible surfactant coverage at the air/water interface of the sessile drop before the drop rim starts to move. When a dispensed small surfactant-laden drop comes into contact with the large sessile drop with height $h{\sim}1.5\,mm$, a region of low surface tension at the drop apex is created and the transfer of surfactant to the sessile drop occurs immediately (Figure 5-2a). The coalescence of the surfactant-laden drop and sessile drop also generates capillary waves propagating along the curved air/water interface of the sessile drop. The surface tension at the leading edge of the sessile water drop is $\gamma_w{\sim}72\,mN/m$, and the surface tension of a trisiloxane-laden drop dispensed at the apex of the sessile drop is $\gamma_s{\sim}22\,mN/m$. Consequently, the resulting surface tension gradient $\nabla\gamma$ between apex and bottom of the $\sim 1.5\,mm$ high drop is $\sim 33\,N/m^2$. The spreading coefficient of the coalescent

drop on the PP substrate ($S = 30 - (\gamma_{sl} + 72)$, with unknown value of γ_{sl}) is negative. Immediately upon deposition (i.e. at $t = 0$), the TPCL is still pinned, implying that the magnitude of $\nabla\gamma$ is not sufficient to initiate drop spreading. Figure 5-2b shows that at a critical time t_c the surfactant is transferred to the drop and most of the air/water interface is covered by surfactant. The surfactant distribution is not uniform: dense distribution close to the drop apex while sparse distribution close to the drop rim. The surface tension gradient over a small critical height l_c~100 μm at t_c~1 ms, e.g. will greatly increase to ~ 500 N/m^2, which may be sufficient enough to drive the drop rim to spread. Under such circumstances, however, the spreading coefficient at the drop rim is still negative. Figure 5-2c shows the case where the air/water interface is fully covered by surfactant at t~1.6 ms. If the surfactant is uniformly distributed, the surface tension gradient will become zero. The presence of surfactant at the drop rim decreases the liquid surface tension, thus creating a positive spreading coefficient. According to thermodynamics, the unbalanced capillary force at the TPCL will drive the drop to spread.

Both mechanisms that can initiate spreading of the sessile drop, either the strong surface tension gradient close to the contact line or a positive spreading coefficient, requires that surfactant is transported to the TPCL in a finite time after surfactant delivery. The bulk diffusion coefficient of SDS is reported to be D~8×10^{-10} m^2/s [182] and that of trisiloxane surfactants less than D~1×10^{-10} m^2/s [65, 161]. Surface diffusion coefficient and bulk diffusion coefficient are assumed to be of the same order of magnitude [183]. Therefore, the experimentally found lag-time ~ 1.6 ms is too short for the surfactant molecules to reach the TPCL by bulk or surface diffusion. This suggests another surfactant transfer mechanism at the air/water interface. The surfactant dispensed with the small drop may spread along the interface as surfactant monolayer, as suggested by Joos *et al.* [141] (Section 2.2.2).

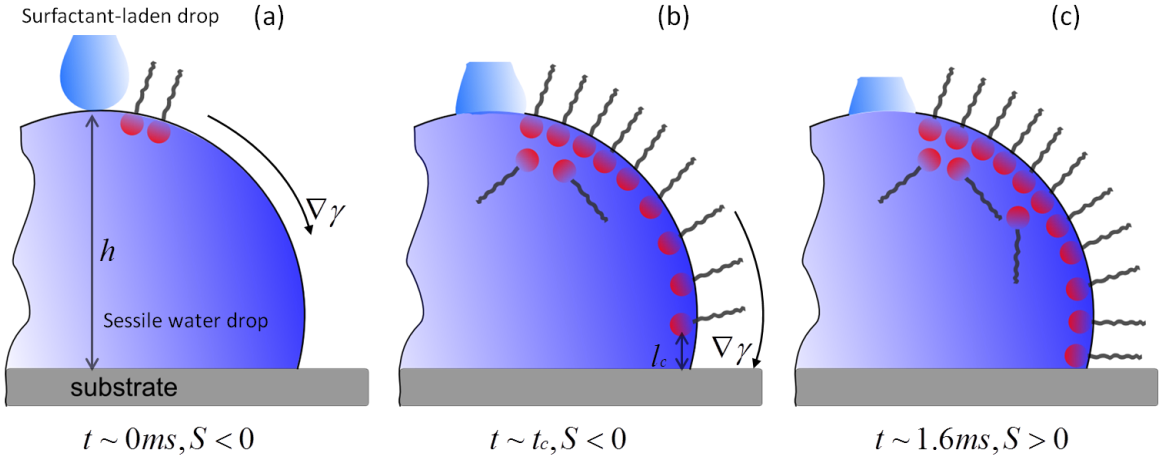

Figure 5-2 Schematic representation of surfactant coverage at the curved air/water interface before the sessile drop spreads. (a) Upon contact transfer of surfactant to the sessile drop occurs immediately, establishing a surface tension gradient $\nabla\gamma$. (b) The air/water interface is gradually covered by surfactant, establishing a strong $\nabla\gamma$ over a critical height l_c~100 μm at a critical time t_c~1 ms. (c) The air/water interface is fully covered by surfactant at t~1.6 ms, and the $\nabla\gamma$ becomes zero.

For a sessile water drop with volume 5 μl, the distance between drop apex and drop bottom along the surface is $\xi \sim 2.2\, mm$. Substituting this value into the above Eqs. (2.26) & (2.28), the spreading velocity v is $\sim 1\, m/s$ and the time needed to spread over distance ξ is $\sim 1.7\, ms$ for trisiloxanes and $\sim 1.9\, ms$ for SDS. Therefore, the prediction from the model in Ref. [141] agreed well with the experimental results on sessile water drops, despite the fact that the curved drops have a geometry different from flat liquid subphases. With this simple estimation one can conclude that the surfactant molecules reach the TPCL almost at the same time as the capillary waves do, which corresponds to the experimentally observed lag-time of $\sim 1.6\, ms$. Therefore, it is hard to decide whether the strong surface tension gradient in Figure 5-2b or the positive spreading coefficient in Figure 5-2c initiates the spreading of the sessile drop. In fact, the experimental setup is not capable of directly tracing the adsorption of surfactant at the air/water interface. Further investigations are necessary for validating the molecular picture of surfactant transfer. Nevertheless, these results lead to the conclusion that the spreading of the drop rim after the initial lag-time results

from the presence of surfactant close to or directly at the TPCL, which leads to either a strong surface tension gradient or a positive spreading coefficient. It is also possible that both mechanisms operate cooperatively, but with different magnitudes at different times.

The measured velocity of the capillary waves propagating from drop apex to drop rim is of the order of $\sim 1\ m/s$. This velocity is close to the propagation velocity of capillary waves reported in Ref. [184]. Figure 5-3 shows that the measured propagation velocity of the capillary waves depends on the surfactant types. The velocity of capillary waves in the sessile drops with volume 5 μl is highest when the dispensed small drops contain trisiloxanes, medium when they contain SDS, and lowest when they are water. Similar findings were shown in Ref. [184], where the authors observed that during the coalescence process of two drops the shape and dynamics of the capillary waves were influenced by spatial variations of the strength of surface tension. This can be explained by the effect arising from surface tension gradient, which superimposes to the capillary waves and speeds up their propagation velocity. The capillary waves propagated faster when a larger surface tension gradient was present [184]. Since trisiloxanes decrease the surface tension of water more strongly than SDS (Table 3-1), the surface tension gradient is larger. As a result, the propagation velocity of the capillary waves is enhanced mostly by trisiloxanes. Despite its practical significance the reason why a stronger surface tension gradient accelerates the propagation of capillary waves remains, however, unclear at this time.

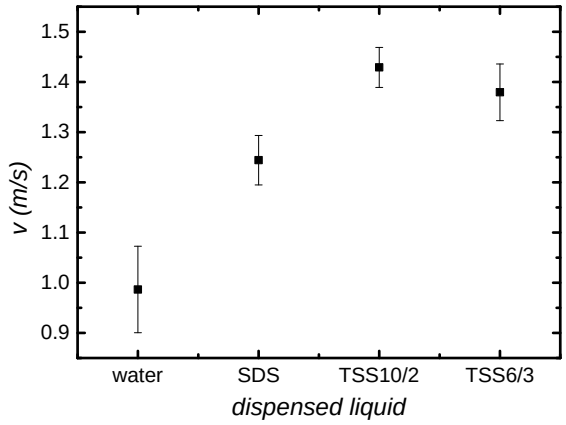

Figure 5-3 Velocity of capillary waves induced by coalescence of small water drops and drops containing three different surfactants.

Wetting of Sessile Water Drops on PP Substrates

The dispensed small surfactant-laden drops cause sessile water drops to spread after $\sim 1.6\,ms$. Figure 5-4 shows the log-log representation of the wetting radius r as a function of time t. Time $t = 0$ is set to the time when the sessile drops start to spread. The lag-time during which the TPCL is pinned is not shown in the figure. The surfactant concentration in the mixed water/surfactant drop is in the range from 0.04 to 0.6 wt%. The wetting radius of the sessile water drop on the PP substrate remains constant when a small water drop is dispensed (Figs. 5-1 & 5-4), while small surfactant-laden drops initiate the wetting of sessile drops. With the ongoing wetting process, the dispensed small surfactant-laden drop detaches from the needle and coalesces with the sessile water drop. During the first two stages ($0 \lesssim t < 4\,ms, 4 \lesssim t \lesssim 12\,ms$), the wetting dynamics of different surfactants at different concentrations does not differ. The kink visible at $\sim 4\,ms$ in Figure 5-4 indicates the sessile drop start to spread with a higher velocity of $\sim 0.05\,m/s$. The power law fitting to all wetting curves within the time range $4 \lesssim t \lesssim 12\,ms$ yields an exponent $\sim 1/4$. Another kink can be observed in the wetting curves of dispensed different small drops at $\sim 12\,ms$. Subsequently, all drops show different wetting dynamics. SDS-laden drops stop spreading and reach equilibrium (i.e. the contact angles of the drops do not change further), while trisiloxane-laden drops continue spreading, but with dynamics different from the previous stage. The wetting radii of TSS6/3- and TSS10/2-laden drops can be described by power laws with exponent $\sim 1/7$ and $\sim 1/10$, respectively. This indicates the wetting stage is dominated by viscosity. Since these exponents are also obtained in spontaneous wetting of trisiloxane-laden drops on PP substrates in Chapter 4, some of the results are plotted together for comparison.

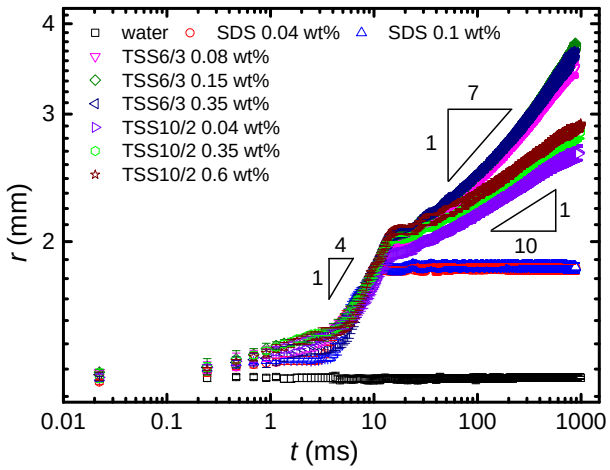

Figure 5-4 Log-log representation of the drop wetting radius r as a function of time t. The small error bars tell that the experiments are reproducible. $t = 0$ is taken as the time when the sessile drop starts to spread.

The wetting radii r are normalized by the initial drop radii r_0 (r/r_0) and plotted in Figure 5-5 vs. time t in a log-log coordinate. Figure 5-5a and Figure 5-5b show the wetting curves of TSS10/2-laden drops and TSS6/3-laden drops, respectively. As depicted in Figure 5-5a, the spontaneous wetting of TSS10/2-laden drops shows a pronounced difference at $t < 12\ ms$ with TSS10/2-enhanced wetting of sessile water drops, while the wetting dynamics at $t \gtrsim 12\ ms$ are similar. This result also applies to the wetting of TSS6/3-laden drops (Figure 5-5b). $12\ ms$ is a too short time for the dispensed small surfactant-laden drop to mix homogeneously with the sessile drop. Since wetting dynamics at $t \gtrsim 12\ ms$ is similar for homogeneously and non-homogeneously mixed surfactant solutions, it implies that only the interfacial surfactant concentration plays a role in the wetting. The presence of bilayer aggregates (lamellae or vesicles) in aqueous surfactant solutions was suspected to be a requirement for superspreading to take place [9, 10]. The dispensed surfactant spreads quickly and simultaneously adsorbs at the air/water interface of the sessile drop. In the bulk of the sessile drop there are thus no surfactant aggregates, which are only at the air/water interface. Therefore, the experiments show that the location of the surfactant reservoir is not crucial to superspreading. In contrast to the scenario

proposed in Ref. [10], the surfactant aggregates in the bulk of sessile drop is not a necessity for superspreading. The surfactant aggregates that are locally dispensed at the drop apex can induce superspreading by spreading along the air/water interface to the TPCL.

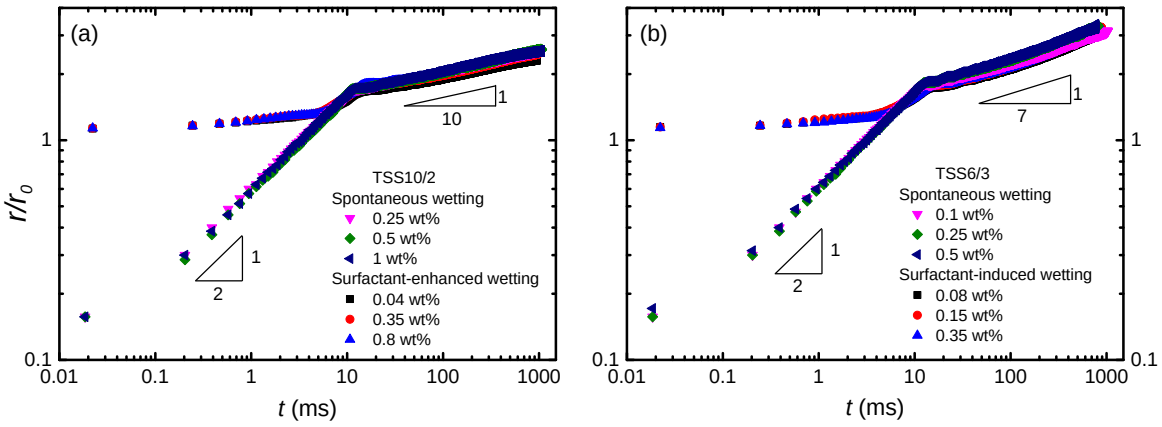

Figure 5-5 Comparison of the wetting radii r normalized by initial radii r_0 as a function of time t. (a) TSS10/2-laden drops, (b) TSS6/3-laden drops.

For further studying the effect of surfactant aggregates on wetting, a small surfactant-laden drop is injected at the bottom of a sessile water drop on PP. The syringe needle is carefully prepared before injecting the small surfactant-laden drop inside the sessile drop so that no surfactant contacts the water during injection. The small surfactant-laden drop is carefully injected close to the drop base inside the sessile drop to deliver surfactant aggregates in the bulk as well. This will establish a surface tension gradient along the solid/water, and not the air/water interface. An immediate spreading of the sessile drop is not observed, which instead occurs up to 1 *min* after injection only. This longer lag-time is required for surfactant aggregates to diffuse to the air/water interface or to drop rim, either establishing a strong surface tension gradient or promoting a positive spreading coefficient. This control experiment confirms that the presence of surfactant in the bulk or at the solid/water interface does not initiate the spreading of sessile drops, while the surfactant at the air/water interface has an earlier effect. Superspreading can be induced either by surfactant transfer to the TPCL from a homogeneously mixed drop or from a dispensed small drop at the air/water interface.

5.2.2 Surfactant-enhanced Wetting on Flat Water Subphases

Wetting of Water Drops on Water Subphases

When a water drop is brought into contact with the water surface, the drop spreads spontaneously and the disturbance on the water surface excites interfacial waves that manifest themselves as concentric rings ahead of the bulk drop. Figure 5-6a shows a typical picture of the propagating wave crests and the drop contact line represented by the yellow dotted line. The position of the contact line is clear in the earliest images where the drop is still attached to the needle. By tracking that feature in the images from one frame to the next, the position of the contact line between the deposited drop and water subphases can be determined until the drop becomes too flat and the feature in the image disappears. PMMA microparticles are deposited on the water subphases before drop deposition as reference markers. As discussed in Section 5.2.1, waves with wavelengths smaller than the critical wavelength $\lambda_c^* \sim 17\ mm$ are dominated by surface tension. The critical wavelength is much larger than the wavelength $\lambda^* \sim 1\ mm$ observed in Figure 5-6a. Therefore, the effect of gravity can be neglected in the experiments, and the interfacial waves on the flat water subphases are termed capillary waves. Further, since the subphase depth is greater than one third of the wavelength, the wave velocities and wave characters are not affected by the finite depth of the subphase [185]. Thus, the results can be compared with the theory for capillary waves on a deep pool. Capillary waves generated by small perturbations on water surfaces with the shortest wavelength have the highest velocity so that the distance between circles decreases with the radius, as described elsewhere [185-187]. The wave pattern shown in Figure 5-6a is consistent with the character of capillary waves for which shorter waves propagate faster.

Figure 5-6b shows the propagation of the capillary wave crests, the advancing of the drop contact line, and the position of PMMA microparticles as a function of time. The marker microparticles show no motion in response to the drop deposition. The contact line moves at a slower velocity than any of the capillary waves. The propagation of the capillary wave front at later times ($t \gtrsim 30\ ms$) is not shown, since it is not discernible due to the reduced optical contrast as the crest height decreases by damping. Only the inner four crests and the outermost crest (capillary wave front) are plotted in order to

avoid overcrowding of the figure. The data shows the trend that the distance between crests decreases with the radius, which is consistent with the descriptions of propagation of capillary waves [185-187]. Since the minimum wave velocity arising from the dispersion relations for the capillary waves is $v_{min} = (4g\gamma_w/\rho)^{1/4} = 0.23\ m/s$, there should be no waves inside a circle with radius $v_{min}t$ [187]. This inner region, free of capillary waves, is seen in the data. The first crest expands with a velocity of $\sim 0.34\ m/s$, greater than the predicted minimum wave velocity. The fastest capillary wave front propagates at a velocity of $\sim 0.6\ m/s$ and its position vs. time follows a power law with an exponent of ~ 0.65. In fact, power laws can characterize all wave crests with exponents within the experimental error of ± 0.02.

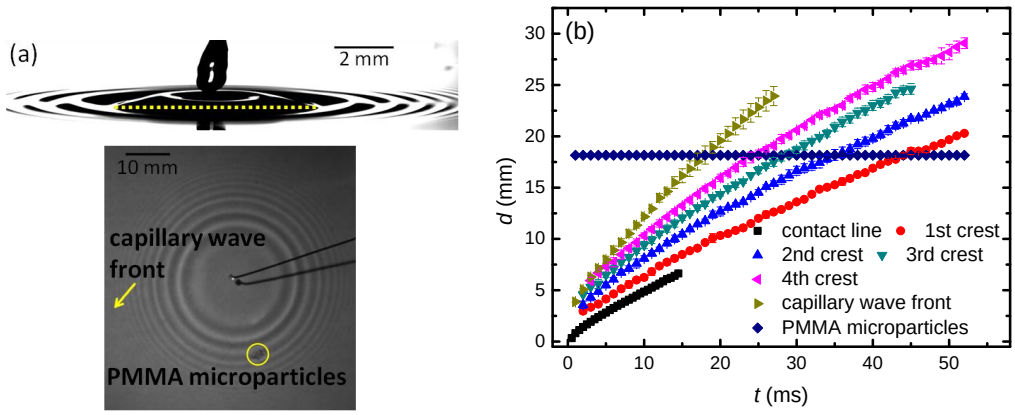

Figure 5-6 (a) Representative images of the wetting of a water drop on a water subphase. The train of capillary waves is shown in both the side-view (top) and top-view image (below). The yellow dotted line in the side-view image represents the drop contact line. (b) The time evolution of contact line, the inner four and the outermost capillary wave crests, and PMMA microparticles with reference to drop deposition point ($d = 0$). Error bars represent estimated uncertainty in position measurements.

The angular frequency ω of capillary waves can be determined from the dispersion relation $\omega^2 = \gamma_w k_*^3/\rho$ [181], with $k_* = 2\pi/\lambda^*$. The phase velocity obtained from the dispersion relation is $v_p = \omega/k_* \sim 0.67\ m/s$ for waves at the air/water interface, using the wavelength measured from recorded images. This is in agreement with the measured velocity of the propagating waves in Figure 5-6b. The group velocity,

$v_g = \partial\omega/\partial k_*$, is $\sim 1\ m/s$ in the experiments. Comparing the measured group velocity and phase velocity, one can obtain $v_g \sim 1.5 v_p$, which agrees well with theory for capillary waves [181].

Wetting of Surfactant-laden Drops on Water Subphases

When a surfactant-laden drop touches the water surface, the surface tension gradient induces liquid flow on the drop surface and on the subphase beyond the drop; and the drop spreads along the air/water interface. This behavior is reproduced by the experiments performed in this work (Figure 5-7).

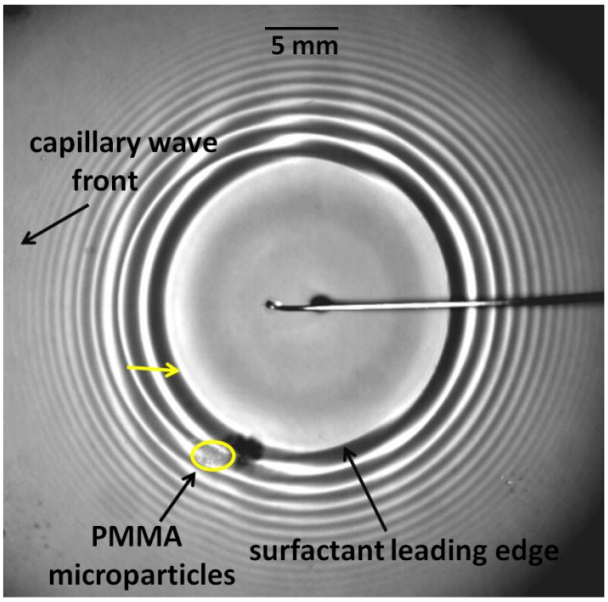

Figure 5-7 Representative image of the spreading of a surfactant-laden drop (TSS10/2 0.1 wt%) on a water subphase. The train of concentric capillary waves is visible, and the dark shadow on the upper right side of the PMMA microparticles is the reflection of the microparticles at the Petri dish bottom.

Similar to the case of water drops, interfacial capillary waves are triggered as well by drops of surfactant solutions and propagate along the air/water interface. It is observed that when the innermost bright ring (indicated by a yellow arrow in Figure 5-7) reaches the PMMA microparticles, they begin to move outwards. This behavior is the same for all different surfactants used in the experiments. The initiation of the movement by the inner ring and the absence of microparticles' movement for

deposition of water drops suggest that the innermost bright ring marks the position of the surfactant leading edge propagating along the air/water interface. There is a recognizable feature – a deformation in the subphase - in the recorded videos at this position. This subphase deformation is predicted to accompany the surfactant leading edge in models of liquid flows driven by surface tension gradient [45, 53, 142].

Figure 5-8 shows the distance $d(t)$ of different features of the observation from the drop deposition point: the drop contact line, the capillary wave crests, the surfactant leading edge and the PMMA microparticles. The contact line lags behind the surfactant leading edge and the capillary wave crests. This observation is consistent with other studies where the authors theoretically predicted [138] or experimentally observed [41, 48, 52, 137, 145, 188] that the surfactant leading edge moves faster than the drop contact line. The PMMA microparticles are accelerated as the surfactant leading edge arrives at their positions. Figure 5-8 also shows the trend that the distance between crests decreases with the radius, just as discussed above in the case of water drops. The capillary waves propagating ahead of the surfactant leading edge do not move the microparticles outwards. The flow field under the surface with the capillary waves [189] is different from that under the surface distorted by the surfactant leading edge [48]. Therefore, different tractions on the microparticles are applied by capillary waves and the surfactant leading edge.

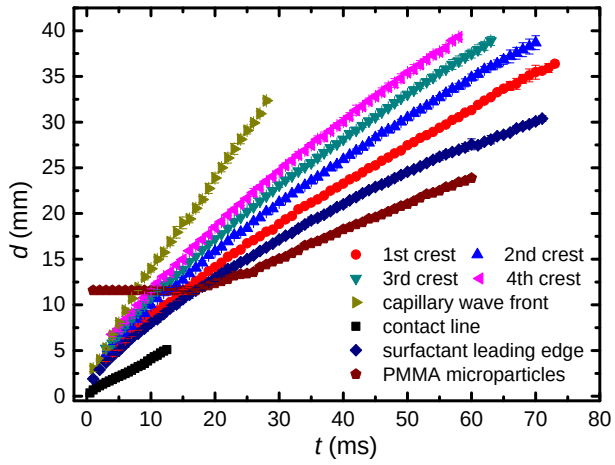

Figure 5-8 Distance of drop contact line, capillary wave crests, surfactant leading edge, and PMMA microparticles from the drop deposition point ($d = 0$).

The transient surface tension measurements (Section 3.2) made at some positions beyond where the microparticles are moved during the entire spreading event (on the time scale of a second) show that surfactant moves out to the distance beyond the microparticles. This reinforces the suggestion that the inner ring observed is the surface distortion that accompanies the leading edge of surfactant. The cartoons in Figure 5-9 demonstrate the overall process when a surfactant-laden drop is deposited on a water subphase. It should be noted that the size of the drop and the marker microparticle is not to scale with respect to the features (e.g. amplitude, wavelength) of the waves, since the amplitude of the waves is not known. The microparticle shows no motion in the direction of wave propagation in response to the capillary waves and the drop contact line is behind the surfactant leading edge (Figure 5-9b). The net force exerted on the microparticle is the sum of the force from the surface tension gradient across the microparticle and the viscous drag force on the partially submerged microparticle. Therefore, as the surfactant leading edge passes the microparticle, the surface tension force across the contact line of the microparticle accelerates it. The inertial mass of the microparticle opposes this motion, so the surfactant leading edge goes past it. But there is a surface tension gradient behind the surfactant leading edge and this continues to drive the microparticle forward. The water flow just under the air/water interface is equal to the surfactant velocity because the gradient in velocity going downwards from the interface occurs on a larger length scale (depth of the water subphase $\sim 3\,mm$) compared to the microparticle size (diameter $\sim 108\,\mu m$). The surface tension gradient across the microparticle changes “slow enough” at the location of the microparticle (of the order of seconds), and the water flow can adjust on a much shorter timescale (some inertia-capillary time of the order of milliseconds). As time progresses beyond the recording time of the high-speed video camera, the microparticle eventually slows down and stops. This suggests that all forces are slowly decreasing over longer times, the surface tension gradient and the viscous drag on the microparticle [52]. Such slowly varying surface tension force across the microparticle is compatible with the model of the liquid flows driven by surface tension gradient [41].

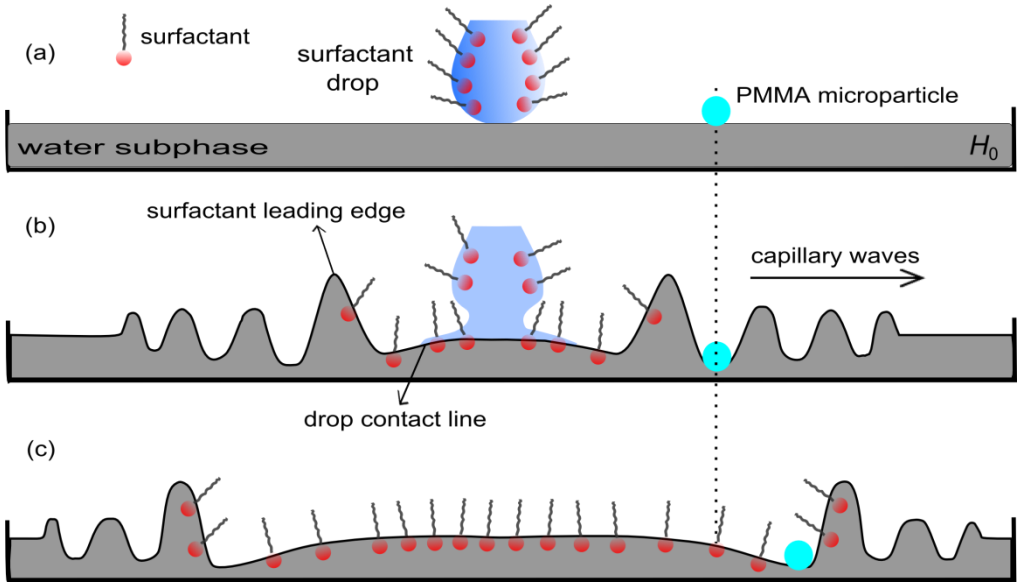

Figure 5-9 (a) A small drop of aqueous surfactant solution is deposited on water subphase of thickness H_0 with PMMA microparticle floating on top. The size of marker microparticle is not to scale with the amplitude or wavelength of the waves. (b) Capillary waves propagating ahead of surfactant leading edge cannot move the PMMA microparticle outwards. The drop contact line is behind the surfactant leading edge. (c) When the surfactant leading edge passes the microparticle, it starts to move outwards. The vertical dotted line indicates the initial position of the microparticle.

Figure 5-10a illustrates the time evolution of capillary wave fronts triggered by different surfactant-laden drops deposited on water subphases. The dynamics of the capillary wave fronts all follows power laws with exponent ~ 0.71 for SDS-laden drops, and ~ 0.82 for drops containing the two trisiloxanes. In the case of deposited water drops, there is no surface tension gradient along the air/water interface and the exponent is ~ 0.65, as discussed above. The capillary wave crests propagate at velocities between 0.8 m/s and 1.1 m/s, depending on the types of surfactant. With surfactants, the velocity of capillary waves is larger than that for water drops. These results are consistent with that in section 5.2.1, which show that surface tension gradient acts as an additional force and accelerates the propagating capillary waves. This confirms previous investigations revealing that the surface tension gradient

generated by a non-uniform surfactant concentration on water could decrease the propagation (e.g. amplitude and wavelength) of the capillary waves [190-192].

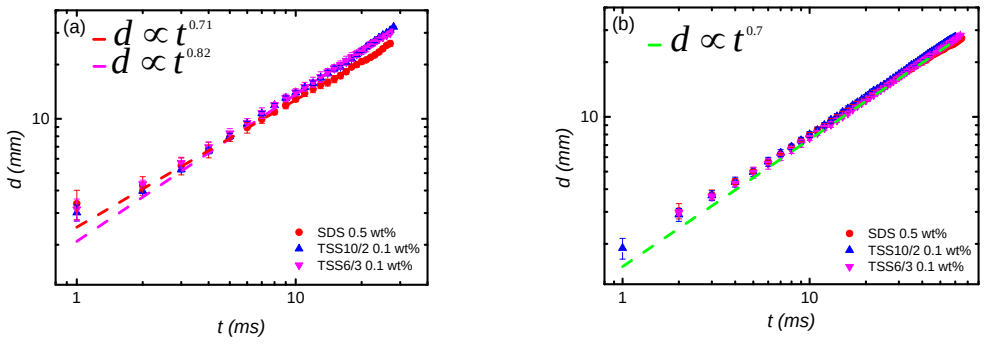

Figure 5-10 Log-log plots of the time evolution of capillary wave fronts triggered by different surfactant-laden drops deposited on water subphases (a), and the evolution of the surfactant leading edges of surfactant-laden drops (b).

In addition to elucidating the propagation dynamics of the capillary waves, the surfactant leading edges of all drops are tracked (Figure 5-10b), which show a similar power law behavior. As predicted in Ref. [145], the dynamics of the surfactant leading edge can be described with power laws with exponents depending on surfactant solubility. Exponents of 0.75 and 0.5 have been derived for insoluble surfactants and soluble surfactants, respectively. The power law fitted for the experimental data results in a general law $d \propto t^{0.7}$ (dashed line in Figure 5-10b). A smaller exponent (0.5) is expected for aqueous SDS-laden drops, since SDS is highly soluble in water [145]. However, for SDS with diffusion coefficient D of $8 \times 10^{-10}\ m^2/s$, the estimation of Péclet number $Pe \sim SH_0/\mu D \approx 10^5 \gg 1$ indicates that spreading is primarily dominated by surface convection, and surface diffusion can be neglected. In fact, considering the time scales of drop spreading studied here ($\sim 60\ ms$), it is safe to assume that SDS and water do not mix during this time. Therefore, the exponent value of 0.7 is larger than the theoretically predicted value 0.5 for soluble SDS and closer to the value for insoluble surfactants [145]. The fitted exponent 0.7 is close to the experimentally obtained value for trisiloxane-laden drops spreading on a thin water subphase [46] and SDS-laden drops spreading on liquid/liquid interface [47]. Several authors have observed a more rapid wetting

promoted by superspreading trisiloxane surfactants with respect to other trisiloxane surfactants on hydrophobic mineral oil subphases [146, 148]. However, in my work the superspreader (TSS6/3) and non-superspreader (TSS10/2) spread similarly on water subphases, at least within the time scales studied. This means that the unique ability of superspreaders to promote fast and extensive spreading on hydrophobic solids does not play a role on water subphases. In fact, due to the miscibility between trisiloxane-laden drops and water subphases, there is no channel for the action of superspreaders to develop. The unbalanced interfacial surface tension is the only driving force for drop spreading, which is the same for both trisiloxane solutions. Therefore, TSS6/3 and TSS10/2 solutions behave similarly on water subphases.

5.3 Summary

In this chapter, surfactant-enhanced wetting of sessile water drops on PP substrates is studied. This is achieved by bring surfactant-laden drops to the apex of sessile drops. It is found that surfactant spreads along the curved air/water interface before the sessile drop starts spreading. Wetting experiments of surfactant-laden drops on flat air/water interfaces with marker microparticles floating on top are performed for comparison. Capillary waves are excited by drop deposition on water and propagate along the curved air/water interface and the flat air/water interface. It is found that surfactants influence the propagation velocity of capillary waves in both sets of experiments. However, up to now the reason behind the phenomenon remains elusive. The motion of the sessile drop rim on PP substrates and the motion of marker microparticles at the flat air/water interface are initiated when surfactant passes by. The dynamics of sessile drops in the wetting stage ($t \gtrsim 12\,ms$) is similar to that in the spontaneous wetting of surfactant-laden drops on the same PP substrates (Chapter 4). The transport of microparticles by surfactants have potential practical applications in controlling aerosol drug delivery.

6 Impact Dynamics of Surfactant-laden Drops[3]

This chapter addresses the impact process – wetting, recoiling and further wetting - of surfactant-laden drops on polypropylene substrates. Regardless of the drop impact velocity, inertial and capillary forces mainly control the early wetting stage of all drops. But, different from the spontaneous wetting in Chapter 4, surfactants influence the wetting dynamics of this early stage. After the drops reach a maximum wetting radii, they start recoiling and reduce their wetted radii. However, despite reducing the static surface tension of water, not all surfactants promote drop spreading to a larger radius than the water drops during the early wetting stage. A new time scale is introduced to rescale the early wetting stage to a universal master curve. After the recoiling process, only superspreader-laden drops re-start wetting the PP substrates and the wetting dynamics is dominated by viscosity.

6.1 Motivation

Most previous work on drop impact dynamics has focused on simple liquids, for which the surface tension remains constant whatever the deformation of the drop. During drop impact, surfactant additives can hinder/slow down recoiling and bouncing of the drop, thus enhancing the deposition efficiency. Motivated by the applications in crop spraying and ink-jet printing, researchers experimentally investigated impact dynamics of surfactant-laden drops on solids [193-200]. In their pioneering work Mourougou-Candoni *et al.* [200] found that the time taken by surfactant molecules to diffuse through the liquid to the air/liquid interface could be comparable to the expansion time of the impacting drop, suggesting that the interface might not be fully saturated with surfactant molecules at all times. However, till now the understanding of the influence of surfactants on drop impact dynamics still remains partly elusive. One reason is that the surface tension of surfactant-laden drops is a dynamic quantity

[3] This chapter is based on the publication "X. Wang, L.Q. Chen, E. Bonaccurso, *Comparison of spontaneous wetting and drop impact dynamics of aqueous surfactant solutions on hydrophobic polypropylene surfaces: scaling of the contact radius*, Colloid and Polymer Science, DOI: 10.1007/s00396-014-3410-x (2014)".

that changes continuously during drop impact. This comparative study in impact dynamics of surfactant-laden drops, some of which have similar properties (e.g. static surface tension), allows exploring more aspects about drop impact.

6.2 Results and Discussion

The concentrations of aqueous SDS solutions are 0.025 wt% and 0.5 wt%. For TSS10/2 and TSS6/3 surfactant solutions, the concentrations range from 0.05 wt% up to 2 wt%. The impact phenomena are discussed and compared with the spontaneous wetting of surfactant-laden drops (Chapter 4).

6.2.1 Impact Phenomena

Figure 6-1 shows the impact process of different aqueous drops on PP substrates at a velocity of $u_0 \sim 2.4\, m/s$. Once a drop contacts the substrate, firstly it expands to a maximum spreading diameter and then recoils and oscillates till it comes to rest eventually. During the expansion process, the drop shape changes from a “spherical cap” to a “flat pancake”, and a maximum spreading diameter is reached within approx. $3\, ms$. Surfactants do not affect the drop shapes during the expansion stage, but they do during the recoiling stage. The water drop recoils so strongly on PP that secondary drops are ejected and partial rebound occurs (Figure 6-1a). After several strong oscillations the water drop eventually equilibrates on the substrate as a “spherical cap”. Drop of SDS solution at 0.025 wt% with a lower surface tension than water (Table 3-1) shows similar oscillations as water, but the oscillation amplitude is smaller. Similar observations were reported elsewhere [194, 197, 198]. No significant recoiling is observed for drops of SDS solutions at 0.5 wt% and trisiloxane-laden drops. This is because the surface tensions of these liquids are much lower than that of water (Table 3-1). Over the entire range of impact velocities studied ($0.6 - 3\, m/s$), the phenomenon of complete rebound is not observed for any trisiloxane-laden drops.

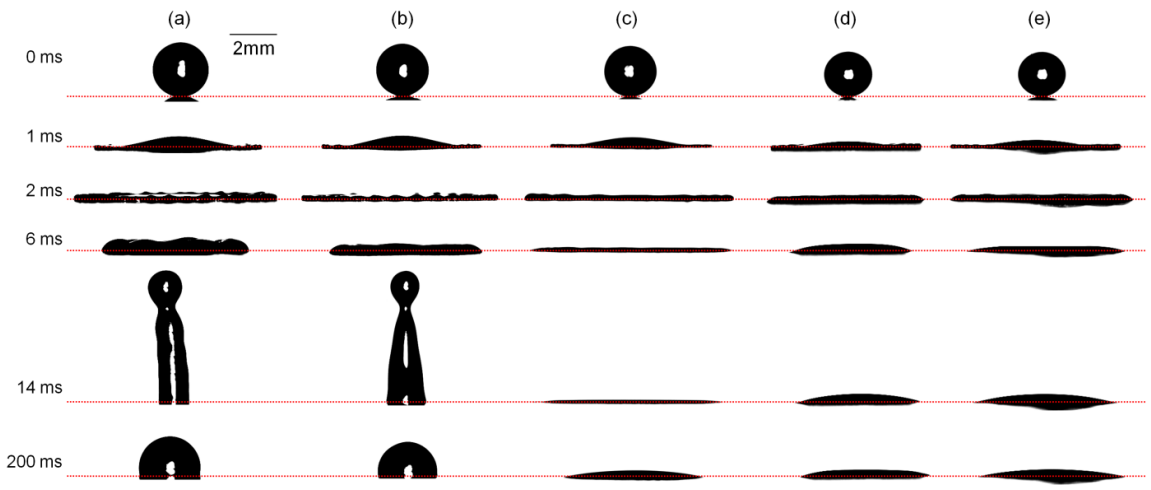

Figure 6-1 Snapshots of drop shapes evolution during impact, recoiling, and wetting on PP substrates represented by the dashed red lines. The impact velocity of drops of (a) water, (b) SDS 0.025 wt%, (c) SDS 0.5 wt%, (d) TSS10/2 0.1 wt% and (e) TSS6/3 0.1 wt%, is ~ 2.4 m/s.

6.2.2 Inertia-dominated Impact Stage

In the inertial wetting stage the spreading diameter grows with time as approx. $t^{1/2}$. This is valid for drop impact and gentle deposition (spontaneous wetting) [58, 109]. One of the parameters to characterize drop impact is the spreading factor, which is the ratio of spreading diameter and initial drop diameter. Figure 6-2 shows the spreading factor vs. time in the early stages of all drops that impact on PP substrates at a velocity of ~ 2.4 m/s. Drop expansion terminates after ~ 3 ms. The wetting curves of different drops are fitted with power laws, yielding exponents lying between 0.4 and 0.5. For all other impact velocities ($0.6 - 3\ m/s$) or concentrations ($0.025 - 2$ wt%) studied, the fitted exponents are also within this range. This is consistent with the results reported in Ref. [109] and indicates that the drop expansion stage is dominated by inertia.

The general wetting dynamics of all drops in this early wetting stage is thus similar. However, different drops attain different expansions, as indicated by the maximum spreading factor β_{max} (marked by two horizontal lines in Figure 6-2). Drops of SDS solutions at concentration 0.025 wt% have similar β_{max} as water (~ 3.9). Drops of SDS 0.5 wt% achieve a slightly larger β_{max} of ~ 4.1. This is consistent with the results

reported in Ref. [198]. Drops with TSS10/2 and TSS6/3 show a smaller β_{max} (~ 3.54 for TSS10/2-laden drops, ~ 3.36 for TSS6/3-laden drops) than other drops, although they have the lowest surface tensions (Table 3-1). Thus, surfactant addition to water does not necessarily always promote a larger β_{max}.

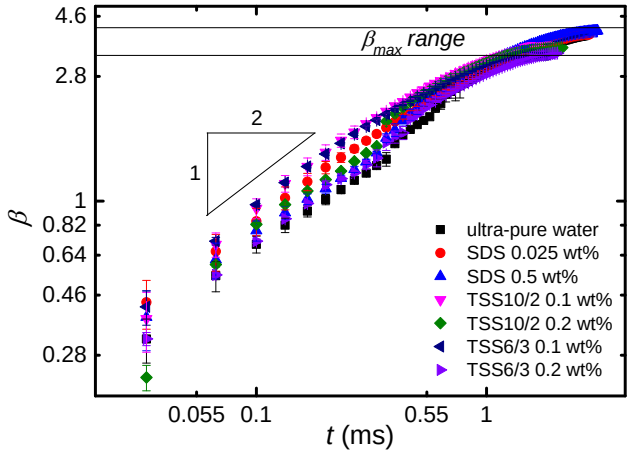

Figure 6-2 Evidence of early inertial wetting stage: log-log representation of the spreading factor of water drops and surfactant-laden drops impacting on PP substrates at a velocity of ~ 2.4 m/s.

Maximum Spreading Factor β_{max}

The maximum spreading factor β_{max} reached by different drops is different. Figure 6-3 shows the dependence of β_{max} on the Weber number. In general a larger β_{max} is obtained at higher We, as was also reported elsewhere [110, 194]. Clanet *et al.* [110] proposed that on partial wetting solids, a competition between inertial and capillary forces of low-viscosity drops caused the β_{max} to scale as $We^{1/4}$. Their experimental data collapsed on a single curve, which was well fitted by $\beta_{max} \propto We^{0.27\pm0.02}$. The data in Figure 6-3 scatters into two groups where the fitting $\beta_{max} \propto We^{1/4}$ with a prefactor 0.85 is shown. Although the whole data set of all drops does not collapse on a single curve, the scaling relations are close to that predicted in Ref. [110]. Generally, the fitted exponents range between $0.23 - 0.29$ for different drops. With similar We, SDS-laden drops behave similarly to water drops. In contrast, trisiloxane-laden drops show smaller β_{max} than water and SDS-laden drops. Similar findings are

found in Ref. [194], where the authors showed that with the same We the drops of trisiloxane Silwet® L-77 solutions promote a smaller β_{max} than water drops and "conventional" surfactant-laden drops. The influence of surfactant properties on β_{max} can be rationalized in this way: during the expansion process, new surfactant-free air/liquid interface is created when the drop is deformed. The surface tension of this fresh interface is close to that of water and decreases with time as the surfactant molecules diffuse to and adsorb at the interface. The ability of surfactant molecules to diffuse and repopulate the newly created interface is governed by their mobility [201]. The diffusion coefficients in solutions are reported to be $8 \times 10^{-10}\ m^2/s$ for SDS and less than $1 \times 10^{-10}\ m^2/s$ for trisiloxanes. Therefore, replenishment of the interface by SDS molecules is approx. one order of magnitude faster than by trisiloxane molecules and thus a larger β_{max} is reached by aqueous SDS solutions.

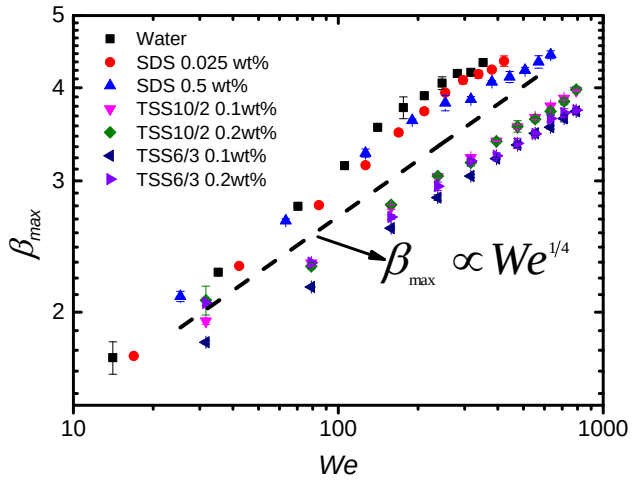

Figure 6-3 The maximal spreading factor of impacting drops as a function of the Weber number (log-log scale). The dashed line indicates the fitting $\beta_{max} \propto We^{1/4}$ with a prefactor of 0.85.

Characteristic Inertial Time

Two distinct time scales are associated with the early wetting stage of drop impact. One is the characteristic time, d_0/u_0, taken by one drop to move one diameter d_0 at the impact velocity u_0. It is employed in many studies addressing the early wetting stage of drop impact [109, 196, 197]. The other one is the characteristic inertial time

$\sqrt{\rho r_0^3/\gamma}$, which also describes the inertia-dominated stage of spontaneous wetting [58, 59, 81]. Since the ratio of the two time scales is itself a function of the Weber number, in principle the choice of one or the other time scale makes no difference. The time scale $\sqrt{\rho r_0^3/\gamma}$ is chosen here to characterize the inertial wetting stage of the impact process.

Figure 6-4a shows the dependence of the dimensionless time t_0^* (the ratio of the real time t at which β_{max} is reached to the characteristic time $\sqrt{\rho r_0^3/\gamma}$) vs. Weber number. For each liquid the data follows a similar trend. In general, t_0^* significantly increases at low We (especially below $We = 250$), while a plateau is observed at high We (above $We = 400$). However, t_0^* of the SDS-laden drops is larger than that of trisiloxane-laden drops. This is likely due to the lower surface tension of trisiloxane-laden drops (Table 3-1).

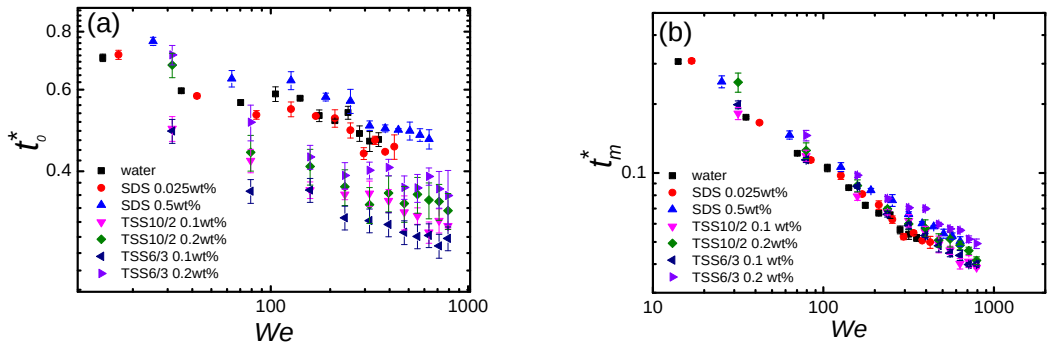

Figure 6-4 (a) Log-log plot of dimensionless time t_0^* (the ratio of real time t for maximum spreading factor to the characteristic inertial time $\sqrt{\rho r_0^3/\gamma}$) as a function of We. (b) Log-log plot of dimensionless time t_m^* (the ratio of real time t for maximum spreading factor to the characteristic inertial time $\sqrt{\rho r_{max}^3/\gamma}$) as a function of We.

When a drop attains its maximum spreading factor, just before recoiling starts the wetting radius on the substrate is r_{max}, which is influenced by surfactant (Figs. 6-1 & 6-3). So the characteristic inertial time by this characteristic length is modified from $\sqrt{\rho r_0^3/\gamma}$ to $\sqrt{\rho r_{max}^3/\gamma}$. Figure 6-4b plots the dimensionless time t_m^* (ratio of the real time t at which β_{max} is reached to the characteristic time $\sqrt{\rho r_{max}^3/\gamma}$) vs. Weber

number We. All experimental data collapses into a single curve, which suggests that the dimensionless time t_m^* depends only on We, but not on the physical and chemical properties of the impacting drops. Therefore, it is safe to conclude that the time scale $\sqrt{\rho r_{max}^3/\gamma}$ better characterizes the inertial wetting stage of impacting drops – of simple liquids or of surfactant solutions – than the time scale $\sqrt{\rho r_0^3/\gamma}$.

6.2.3 Recoiling and Subsequent Wetting/Equilibrium Stage

When a drop impacts on a solid, the inertial force drives the drop to spread. The kinetic energy is mainly converted into the solid/liquid interfacial energy and liquid surface energy dissipation. Once the drop reaches β_{max}, its kinetic energy reduces to zero and thus the stored liquid surface energy causes the drop to recoil afterwards. Figure 6-5 shows the spreading factor β of aqueous drops as a function of time t in a log-log coordinate. The recoiling process shows that drop recoiling is influenced, and mainly slowed down, by surfactants. Drops of water and with SDS 0.025 wt% recoil faster and more violently than drops with SDS 0.5 wt% and with trisiloxanes 0.1 wt%. This demonstrates that drops with lower surface tension recoil more slowly and to a smaller extent, as the surface energy stored in such drops is less. Other researchers reported similar findings [194, 197].

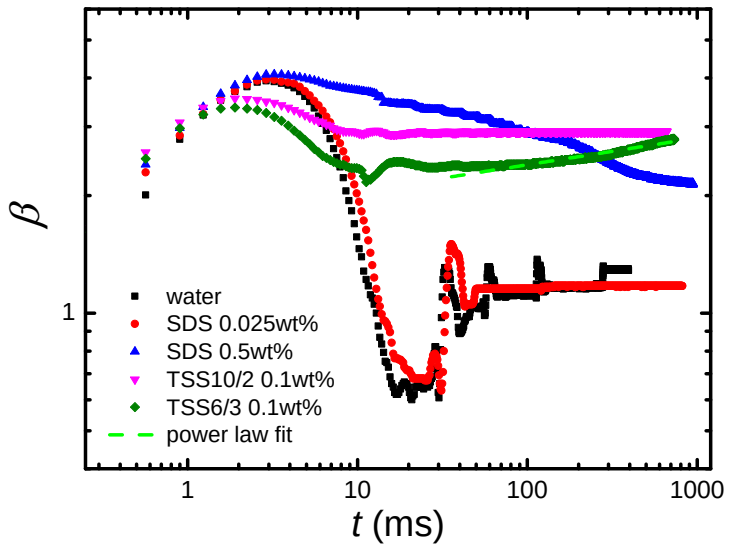

Figure 6-5 Log-log plot of the spreading factor β of drops impacting on PP substrates at a velocity of $\sim 2.4\, m/s$ as a function of time t.

Drops of water, SDS 0.025 wt%, and TSS10/2 0.1 wt% equilibrate after recoiling, i.e. contact angle and wetting radius remain constant, while drops of SDS 0.5 wt% continue recoiling. Even more different, TSS6/3-laden drops recommence wetting the PP substrates after recoiling. The way to explain this behavior comes from the fact that the quickly formed air/water interface area during the first milliseconds of drop impact does not allow the trisiloxane molecules to replenish the interface completely. Therefore, the surface tension of the drop is high, which causes the drop to recoil. Due to the drop recoiling, the surface area shrinks again and is thus covered by an excess of surfactant molecules, which reduces the drop surface tension. This lower surface tension and slower wetting dynamics afterwards induce the further wetting, which is now controlled by surface tension and viscosity rather than by inertia, and which hinders a renewed overshooting. The power law fitting to the wetting curve of TSS6/3 0.1 wt% yielded a wetting exponent $\alpha \sim 0.07$ (Figure 6-5). This implies that surfactants influence the impact process of water drops, similarly as some polymers do [202-204], and considerably reduce the oscillations by providing some sorts of dissipation channel. Therefore, the impact process is shortened and capillarity-driven wetting of the drop can re-start afterwards. This further wetting stage of TSS6/3-laden drop can be approx. described by Tanner's law [64]. As discussed in Chapter 4, the viscosity-dominated wetting stage of TSS6/3-laden drops is described by a power law with an exponent $\sim 1/7$, which is higher than the exponent found for the same drops after impacting on a similar substrate. This is probably because in impact process more kinetic energy is dissipated by viscous force during drop expansion and recoiling, and due to drop oscillations. Consequently, the wetting process after drop recoiling is slowed down and needs some transition time to fully recover to Tanner's law. This agrees with the observation in Figure 6-5 that the evolution of the wetting radius is not exactly described by a power law, but that it is still accelerating in the end. Considering the similar chemical structures and static surface tensions of the TSS10/2 and TSS6/3 solutions, their different temporal evolutions after recoiling are surprising. The reason might lie in the peculiar properties of TSS6/3, which on the

contrary to TSS10/2 shows a superspreading stage on PP substrates even at a low concentration (e.g. 0.1 wt%) (Chapter 4).

6.3 Summary

The early impact stage of aqueous surfactant solutions on PP substrates is inertia-dominated, as in spontaneous wetting. However, surfactant additives influence the impact dynamics of the early stage. SDS-laden drops promote a larger maximum spreading factor than water drops, while trisiloxane-laden drops do not. The experimental data showed that - regardless of surfactant concentrations and types - the introduced characteristic time scale $\sqrt{\rho r_{max}^3/\gamma}$ allows rescaling all inertial wetting data onto a general master curve, while rescaling with the characteristic inertial time scale $\sqrt{\rho r_0^3/\gamma}$ does not work. Surfactant additives also play a significant role in the recoiling process during drop impact. Compared with water drops, the reduced surface tension of drops due to surfactant addition results in weaker surface oscillations and less recoiling. After recoiling TSS6/3-laden drops show a further viscosity-dominated wetting stage, while other surfactant-laden drops reach equilibrium. The plausible reasons for the peculiar behavior of surfactant TSS6/3 may lie in its specific properties that make it a superspreader.

7 Conclusion and Outlook

In this experimental Ph. D. project, the dynamic wetting of drops containing cationic CTAB, anionic SDS, and nonionic trisiloxane surfactants on hydrophobic solids and on water subphases is investigated with high-speed video imaging. The influence of surfactant types, surfactant concentrations, substrate wettability, as well as the atmospheric relative humidity on the wetting process is addressed. The findings in the Ph. D. thesis contribute to a deeper understanding of rapid surfactant-enhanced wetting and superspreading.

For spontaneous wetting of aqueous surfactant solutions, the early wetting stage of all surfactant-laden drops is dominated by inertia, and surfactant does not play a role in this stage. The inertial time scale $\sqrt{\rho r_0^3/\gamma}$ characterizes the duration of the early wetting stage. For CTAB and SDS solutions only this wetting stage is observed, while solutions of two trisiloxanes (TSS10/2, TSS6/3) show a viscosity-dominated stage following the early inertial stage. In this viscous stage, concentrations of trisiloxane TSS6/3 come into effect. Only the TSS6/3-laden drops show a superspreading stage, during which the wetting dynamics strongly depends on RH, surfactant concentration, and substrate wettability. The wetting velocity is higher at 90% RH than that at 10% RH. Maximum wetting radius and wetting velocity are observed at a characteristic concentration of 0.1 wt% for superspreading, which is due to a balance between surface tension gradient driving the drop spreading and the rate of surfactant diffusion to the air/water interface reducing the surface tension gradient. The surface tension gradient is also present in the wetting process of non-superspreader solutions. However, it may fade out quickly due to faster diffusion of surfactants to the air/water interface. It is found that TSS6/3 solutions only superspread on hydrophobic solids whose wettability is within a narrow range. Therefore, surfactants, substrates and atmospheric RH have to be selected properly for superspreading to occur.

The early wetting stage of surfactant-laden drops impacting on polypropylene substrates at different velocities is dominated by inertia. However, surfactant types and concentrations influence the maximum wetting radius r_{max} in this stage. The inertial time scale $\sqrt{\rho r_{max}^3/\gamma}$ which takes the r_{max} of the drop upon impact into

account allows rescaling the duration of the early wetting stage to a universal master curve. Surfactant-laden drops with low surface tension recoil less than water drops. After recoiling, superspreader-laden drops - but not other surfactant-laden drops - show a viscosity-dominated wetting stage on polypropylene substrates.

The surface tension gradient is proven to be a driving force for the transport of microparticles on water subphases. It is found that the superspreading property of TSS6/3 solutions on hydrophobic solids is not effective on water subphases. Surfactants influence the propagation velocity of capillary waves that are excited by drop deposition at the air/water interface. The reasons behind the phenomenon, however, remain elusive.

7.1 Outlook

During this study other new issues arise. Therefore, additional research is certainly necessary to explore more aspects of surfactant-enhanced wetting and superspreading. Several key aspects are pointed out for future research:

- As discussed in section 4.2.3, superspreader solutions only superspread on solids whose wettability is within a narrow and well-defined range. The different wettability of solids may influence surfactant adsorption at the solid/liquid interface, thus affecting wetting. Therefore, investigation of surfactant adsorption on different solids is important. The experimental setup can be designed to immerse solids into aqueous superspreader solutions, and then to measure the adsorbed amount of surfactant at the solid/liquid interface by ellipsometry technique.
- Relative humidity has a remarkable effect on the wetting dynamics of superspreader solutions. The wetting velocity of superspreading solutions is higher at 40% RH than that at 70% RH. Why is it like this? What is the role of the precursor film in superspreading? What is the difference of the precursor film formed at different RH? An experimental study of the precursor film on polypropylene substrates at different RH may help to answer the questions. The analysis of the precursor films can be performed with ellipsometry and interferometry techniques.

- Marker microparticles with different wettability deposited at the air/water interface can be transported by a surface tension gradient. How do the inertia of the microparticles and their engulfment in the water subphase influence the transport process? How is the transport distance affected by different surface tension gradients? Systematic experiments are needed to answer these questions so that the transport process of microparticles can be controlled. Further experimental work about this topic can be supplemented by using atomic force microscope. A designed arrangement together with colloidal probe technique can be used to determine the forces acting on individual microparticles at the air/water interface while the surfactant spreads along the water subphase.

The new aspects revealed in this Ph. D. thesis represent solid steps forward towards understanding fundamentals of the early wetting dynamics of aqueous surfactant solutions. Different wetting dynamics are observed for ionic and nonionic surfactants. This may provide advice on controlling the wetting stages with solutions of surfactants that have different physicochemical properties. The early wetting dynamics of surfactant-laden drops on hydrophobic solids has been assessed and shows that surfactant in solutions becomes effective after a characteristic time. The superspreading dynamics depends on substrate wettability, surfactant concentration and atmospheric RH. These findings can offer practical guidance in some applications. Using trisiloxane superspreaders in agricultural chemicals is effective and economical, since even at a low concentration (e.g. 0.1 wt%) superspreaders enable the chemicals to rapidly penetrate into waxy plant leaves and cover greater leaf areas without drop rebound. By choosing appropriate conditions, e.g. optimal surfactant concentration and atmospheric RH, the farmers can take the advantages of superspreaders to the largest extent. The surface tension gradient can transport microparticles along liquid subphases. This has potential practical applications in cosmetic and pharmaceutical fields, even though the toxicological profile of trisiloxanes makes them unsuitable for use in skin care products and aerosol drugs. Understanding the physicochemical root for superspreading may enable the synthetic chemists to design new, more benign superspreading surfactants.

Bibliography

[1] J. Bieleman, Additives for coatings, in, Wiley-VCH, Weinheim, Germany, 2000.

[2] M. Knoche, Organosilicone surfactant performance in agricultural spray application-a review, Weed Res., 34(3) (1994) 221-239.

[3] J.D. Nalewaja, G.R. Goss, R.S. Tann, Pesticide formulations and application systems, in, Philadelphia, 1998.

[4] M. Griese, Pulmonary surfactant in health and human lung diseases: state of the art, Eur. Respir. J., 13(6) (1999) 1455-1476.

[5] G.J. Murphy, G.A. Policello, R.E. Ruckle, Formulation considerations for trisiloxane based organosilicone adjuvants, Brighton Crop Protection Conference-Weeds, 1 (1991) 355-362.

[6] B. Kanner, W.G. Reid, I.H. Petersen, Synthesis and properties of siloxane-polyether copolymer surfactants, Ind. Eng. Chem. Prod. R. D, 6(2) (1967) 88-92.

[7] E.G. Schwarz, W.G. Reid, Surface active agent—their behavior and industrial use, Ind. Eng. Chem., 56(9) (1964) 26-31.

[8] S. Zhu, W.G. Miller, L.E. Scriven, H.T. Davis, Superspreading of water-silicone surfactant on hydrophobic surfaces, Colloids Surf., A, 90(1) (1994) 63-78.

[9] J. Venzmer, Superspreading-20 years of physicochemical research, Curr. Opin. Colloid Interface Sci., 16(4) (2011) 335-343.

[10] R.M. Hill, Superspreading, Curr. Opin. Colloid Interface Sci., 3(3) (1998) 247-254.

[11] C. Maldarelli, On the microhydrodynamics of superspreading, J. Fluid Mech., 670 (2011) 1-4.

[12] R.M. Hill, M.T. He, H.T. Davis, L.E. Scriven, Comparison of the liquid-crystal phase-behavior of 4 trisiloxane superwetter surfactants, Langmuir, 10(6) (1994) 1724-1734.

[13] A.D. Nikolov, D.T. Wasan, A. Chengara, K. Koczo, G.A. Policello, I. Kolossvary, Superspreading driven by Marangoni flow, Adv. Colloid Interface Sci., 96(1-3) (2002) 325-338.

[14] E. Sieverding, G.D. Humble, I. Fleute-Schlachter, A new herbicide adjuvant based on a non-superspreading trisiloxane surfactant, J. Plant Dis. Protect, (2006) 1005-1011.

[15] Y. Zhang, G.Y. Zhang, F. Han, The spreading and superspeading behavior of new glucosamide-based trisiloxane surfactants on hydrophobic foliage, Colloids Surf., A, 276(1-3) (2006) 100-106.

[16] K.P. Ananthapadmanabhan, E.D. Goddard, P. Chandar, A study of the solution, interfacial and wetting properties of silicone surfactants, Colloids Surf., 44 (1990) 282–297.

[17] A. Chengara, A.D. Nikolov, D.T. Wasan, Spreading of a water drop triggered by the surface tension gradient created by the localized addition of a surfactant, Ind. Eng. Chem. Res., 46(10) (2007) 2987-2995.

[18] A. Nikolov, D. Wasan, Superspreading: role of the substrate surface energy, in: R.G. Rubio, Y.S. Ryazantsev, V.M. Starov, G.-X. Huang, A.P. Chetverikov, P. Arena, A.A. Nepomnyashchy, A. Ferrus, E.G. Morozov (Eds.) Without Bounds: A Scientific Canvas of Nonlinearity and Complex Dynamics, Springer Berlin Heidelberg, 2013, pp. 301-314.

[19] M.J. Rosen, Y.F. Wu, Superspreading of trisiloxane surfactant mixtures on hydrophobic surfaces. 1. Interfacial adsorption of aqueous trisiloxane surfactant-N-alkyl pyrrolidinone mixtures on polyethylene, Langmuir, 17(23) (2001) 7296-7305.

[20] Y.F. Wu, M.J. Rosen, Superspreading of trisiloxane surfactant mixtures on hydrophobic surfaces 2. Interaction and spreading of aqueous trisiloxane surfactant-N-alkyl-pyrrolidinone mixtures in contact with polyethylene, Langmuir, 18(6) (2002) 2205-2215.

[21] N.V. Churaev, N.E. Esipova, R.M. Hill, V.D. Sobolev, V.M. Starov, Z.M. Zorin, The superspreading effect of trisiloxane surfactant solutions, Langmuir, 17(5) (2001) 1338-1348.

[22] N. Kumar, A. Couzis, C. Maldarelli, Measurement of the kinetic rate constants for the adsorption of superspreading trisiloxanes to an air/aqueous interface and the relevance of these measurements to the mechanism of superspreading, J. Colloid Interface Sci., 267(2) (2003) 272-285.

[23] A. Kabalnov, Thermodynamics of superspreading, Eur. Phys. J. E, 2(3) (2000) 255-264.

[24] S. Rafai, D. Sarker, V. Bergeron, J. Meunier, D. Bonn, Superspreading: aqueous surfactant drops spreading on hydrophobic surfaces, Langmuir, 18(26) (2002) 10486-10488.

[25] M.J. Rosen, L.D. Song, Superspreading, skein wetting, and dynamic surface tension, Langmuir, 12(20) (1996) 4945-4949.

[26] E. Ruckenstein, Effect of short-range interactions on spreading, J. Colloid Interface Sci., 179(1) (1996) 136-142.

[27] Y.Y. Shen, A. Couzis, J. Koplik, C. Maldarelli, M.S. Tomassone, Molecular dynamics study of the influence of surfactant structure on surfactant-facilitated spreading of droplets on solid surfaces, Langmuir, 21(26) (2005) 12160-12170.

[28] D.R. Beacham, O.K. Matar, R.V. Craster, Surfactant-enhanced rapid spreading of drops on solid surfaces, Langmuir, 25(24) (2009) 14174-14181.

[29] J.D. Halverson, C. Maldarelli, A. Couzis, J. Koplik, Wetting of hydrophobic substrates by nanodroplets of aqueous trisiloxane and alkyl polyethoxylate surfactant solutions, Chem. Eng. Sci., 64(22) (2009) 4657-4667.

[30] J. Venzmer, S.P. Wilkowski, Trisiloxane surfactants-mechanisms of spreading and wetting, in: Pesticide Formulations and Application Systems, American Society for Testing and Materials ASTM STP, 1998, pp. 140-151.

[31] M. He, R.M. Hill, Z. Lin, L.E. Scriven, H.T. Davis, Phase-behavior and microstructure of polyoxyethylene trisiloxane surfactants in aqueous solution, J. Phys. Chem. , 97(34) (1993) 8820-8834.

[32] M. von Bahr, F. Tiberg, B.V. Zhmud, Spreading dynamics of surfactant solutions, Langmuir, 15(20) (1999) 7069-7075.

[33] M. von Bahr, F. Tiberg, V. Yaminsky, Spreading dynamics of liquids and surfactant solutions on partially wettable hydrophobic substrates, Colloids Surf., A, 193(1-3) (2001) 85-96.

[34] A. Marmur, M.D. Lelah, The spreading of aqueous surfactant solutions on glass, Chem. Eng. Commun., 13(1-3) (1981) 133-143.

[35] S.M. Troian, E. Herbolzheimer, S.A. Safran, Model for the fingering instability of spreading surfactant drops, Phys. Rev. Lett., 65(3) (1990) 333-336.

[36] B. Frank, S. Garoff, Surfactant self-assembly near contact lines: control of advancing surfactant solutions, Colloids Surf., A, 116(1–2) (1996) 31-42.

[37] A. Nikolov, D. Wasan, Superspreading mechanisms: An overview, Eur. Phys. J. Sepc. Top., 197(1) (2011) 325-341.

[38] P.G. de Gennes, Wetting: statics and dynamics, Rev. Mod. Phys., 57(3) (1985) 827-863.

[39] V.G. Levich, V.S. Krylov, Surface-tension-driven phenomena, Annu. Rev. Fluid Mech., 1 (1969) 293-316.

[40] M.S. Borgas, J.B. Grotberg, Monolayer flow on a thin-film, J. Fluid Mech., 193 (1988) 151-170.

[41] D.P. Gaver, J.B. Grotberg, Droplet spreading on a thin viscous film, J. Fluid Mech., 235 (1992) 399-414.

[42] D. Halpern, J.B. Grotberg, Dynamics and transport of a localized soluble surfactant on a thin-film, J. Fluid Mech., 237 (1992) 1-11.

[43] O.E. Jensen, J.B. Grotberg, Insoluble surfactant spreading on a thin viscous film-shock evolution and film rupture, J. Fluid Mech., 240 (1992) 259-288.

[44] O.E. Jensen, The spreading of insoluble surfactant at the free-surface of a deep fluid layer, J. Fluid Mech., 293 (1995) 349-378.

[45] A.D. Dussaud, O.K. Matar, S.M. Troian, Spreading characteristics of an insoluble surfactant film on a thin liquid layer: comparison between theory and experiment, J. Fluid Mech., 544 (2005) 23-51.

[46] K.S. Lee, V.M. Starov, T.J.P. Muchatuta, S.I.R. Srikantha, Spreading of trisiloxanes over thin aqueous layers, Colloid J. Ussr, 71(3) (2009) 365-369.

[47] S. Berg, Marangoni-driven spreading along liquid-liquid interfaces, Phys. Fluids, 21(3) (2009).

[48] A.B. Afsar-Siddiqui, P.F. Luckham, O.K. Matar, The spreading of surfactant solutions on thin liquid films, Adv. Colloid Interface Sci., 106 (2003) 183-236.

[49] N.D. DiPietro, C. Huh, R.G. Cox, The hydrodynamics of the spreading of one liquid on the surface of another, J. Fluid Mech., 84 (1978) 529-549.

[50] A.F.M. Leenaars, J.A.M. Huethorst, J.J. Vanoekel, Marangoni drying-a new extremely clean drying process, Langmuir, 6(11) (1990) 1701-1703.

[51] S. Obrien, On Marangoni drying-nonlinear kinematic waves in a thin-film, J. Fluid Mech., 254 (1993) 649-670.

[52] K. Koch, B. Dew, T.E. Corcoran, T.M. Przybycien, R.D. Tilton, S. Garoff, Surface tension gradient driven spreading on aqueous mucin solutions: a possible route to enhanced pulmonary drug delivery, Mol. Pharm., 8(2) (2011) 387-394.

[53] K.S. Lee, V.M. Starov, Spreading of surfactant solutions over thin aqueous layers at low concentrations: Influence of solubility, J. Colloid Interface Sci., 329(2) (2009) 361-365.

[54] J. Ahmad, R.S. Hansen, A simple quantitative treatment of the spreading of monolayers on thin liquid films, J. Colloid Interface Sci., 38(3) (1972) 601-604.

[55] D.L. Shapiro, R.H. Notter, Surfactant replacement therapy, New York, 1989.

[56] J.B. Grotberg, O.E. Jensen, Biofluid mechanics in flexible tubes, Annu. Rev. Fluid Mech., 36 (2004) 121-147.

[57] W.T. Tsai, L.Y. Liu, Transport of exogenous surfactants on a thin viscous film within an axisymmetric airway, Colloids Surf., A, 234(1-3) (2004) 51-62.

[58] A.L. Biance, C. Clanet, D. Quere, First steps in the spreading of a liquid droplet, Phys. Rev. E, 69(1) (2004).

[59] J.C. Bird, S. Mandre, H.A. Stone, Short-time dynamics of partial wetting, Phys. Rev. Lett., 100(23) (2008).

[60] L. Chen, E. Bonaccurso, M.E.R. Shanahan, Inertial to viscoelastic transition in early drop spreading on soft surfaces, Langmuir, 29(6) (2013) 1893-1898.

[61] J. Drelich, D. Chibowska, Spreading kinetics of water drops on self-assembled monolayers of thiols: Significance of inertial effects, Langmuir, 21(17) (2005) 7733-7738.

[62] K.G. Winkels, J.H. Weijs, A. Eddi, J.H. Snoeijer, Initial spreading of low-viscosity drops on partially wetting surfaces, Phys. Rev. E, 85(5) (2012).

[63] A.M. Cazabat, M.A. Cohen-Stuart, Dynamics of wetting: effects of surface roughness, J. Phys. Chem., 90 (1986) 5845-5849.

[64] L.H. Tanner, Spreading of silicone oil drops on horizontal surfaces, J. Phys. D Appl. Phys., 12(9) (1979) 1473-1484.

[65] J. Radulovic, K. Sefiane, M.E.R. Shanahan, Dynamics of trisiloxane wetting: effects of diffusion and surface hydrophobicity, J. Phys. Chem. C, 114(32) (2010) 13620-13629.

[66] N. Ivanova, V. Starov, D. Johnson, N. Hilal, R. Rubio, Spreading of aqueous solutions of trisiloxanes and conventional surfactants over PTFE AF coated silicone wafers, Langmuir, 25(6) (2009) 3564-3570.

[67] X. Zhu, Surfactant fluid microstructure and surfactant aided spreading, University of Minnesota, 1992.

[68] T. Young, An essay on the cohesion of fluids, Philos. Trans. R. Soc. Lond., 95 (1805) 65-87.

[69] R.G. Cox, The spreading of a liquid on a rough solid surface, J. Fluid Mech., 131 (1983) 1-26.

[70] T.D. Blake, The physics of moving wetting lines, J. Colloid Interface Sci., 299(1) (2006) 1-13.

[71] J. De Coninck, M.J. de Ruijter, M. Voue, Dynamics of wetting, Curr. Opin. Colloid Interface Sci., 6(1) (2001) 49-53.

[72] Y.D. Shikhmurzaev, On metastable regimes of dynamic wetting, J. Phys.: Condens. Matter, 14(3) (2002) 319-330.

[73] D. Bonn, J. Eggers, J. Indekeu, J. Meunier, E. Rolley, Wetting and spreading, Rev. Mod. Phys., 81(2) (2009) 739-805.

[74] L. Leger, J.F. Joanny, Liquid spreading, Rep. Prog. Phys., 55(4) (1992) 431-486.

[75] V.E.B. Dussan, On the spreading of liquids on solid surfaces: static and dynamic contact lines, Annu. Rev. Fluid Mech., 11 (1979) 371-400.

[76] P.G.d. Gennes, F. Brochard-Wyart, D. Quere, Capillarity and wetting phenomenon: drops, bubbles, pearls, waves, Springer, New York, 2004.

[77] H.W. Fox, W.A. Zisman, The spreading of liquids on low energy surfaces. 1. polytetrafluoroethylene, J. Colloid Sci., 5(6) (1950) 514-531.

[78] W.A. Zisman, Contact angle, wettability and adhesion, American Chemical Society, Washington, 1964.

[79] R. Tadmor, Line energy and the relation between advancing, receding, and young contact angles, Langmuir, 20(18) (2004) 7659-7664.

[80] E. Chibowski, K. Terpilowski, Surface free energy of sulfur - Revisited I. Yellow and orange samples solidified against glass surface, J. Colloid Interface Sci., 319(2) (2008) 505-513.

[81] L. Chen, G.K. Auernhammer, E. Bonaccurso, Short time wetting dynamics on soft surfaces, Soft Matter, 7(19) (2011) 9084-9089.

[82] O.A. Soboleva, B.D. Summ, E.A. Raud, Transition from inertial to viscous spreading of a drop, Colloid J. Ussr, 51(6) (1989) 1049-1052.

[83] L. Chen, E. Bonaccurso, Effects of surface wettability and liquid viscosity on the dynamic wetting of individual drops, Phys. Rev. E, 90(2) (2014).

[84] J.B. Keller, P.A. Milewski, J.M. Vanden-Broeck, Merging and wetting driven by surface tension, Eur. J. Mech. B-Fluid, 19(4) (2000) 491-502.

[85] H. Lamb, Hydrodynamics, Dover, New York, 1932.

[86] O. V.Voinov, Hydrodynamics of wetting, Fluid Dyn., 11 (1976) 714–721.

[87] R.G. Cox, The dynamics of the spreading of liquids on a solid surface part. 1 viscous flow, J. Fluid Mech., 168 (1986) 169-194.

[88] T.D. Blake, J.M. Haynes, Kinetics of liquid/liquid displacement, J. Colloid Interface Sci., 30(3) (1969) 421-423.

[89] T.D. Blake, K.J. Ruschak, Maximum speed of wetting, Nature, 282(5738) (1979) 489-491.

[90] A.M. Cazabat, Wetting-from macroscopic to microscopic scale, Adv. Colloid Interface Sci., 42 (1992) 65-87.

[91] D. Seveno, A. Vaillant, R. Rioboo, H. Adao, J. Conti, J. De Coninck, Dynamics of wetting revisited, Langmuir, 25(22) (2009) 13034-13044.

[92] R.L. Hoffman, Study of advancing interface. 1 interface shape in liquid-gas systems, J. Colloid Interface Sci., 50(2) (1975) 228-241.

[93] M. Fermigier, P. Jenffer, An experimental investigation of the dynamic contact-angle in liquid-liquid systems, J. Colloid Interface Sci., 146(1) (1991) 226-241.

[94] A.M. Cazabat, S. Gerdes, M.P. Valignat, S. Villette, Dynamics of wetting: from theory to experiment, Interface Sci., 5(2-3) (1997) 129-139.

[95] R.E. Powell, W.E. Roseveare, H. Eyring, Diffusion, thermal conductivity, and viscous flow of liquids, Ind. Eng. Chem., 33(4) (1941) 430-435.

[96] M.J. de Ruijter, J. De Coninck, T.D. Blake, A. Clarke, A. Rankin, Contact angle relaxation during the spreading of partially wetting drops, Langmuir, 13(26) (1997) 7293-7298.

[97] J. Eggers, E. Villermaux, Physics of liquid jets, Rep. Prog. Phys., 71(3) (2008).

[98] O. Planchon, E. Mouche, A physical model for the action of raindrop erosion on soil microtopography, Soil Sci. Soc. Am. J., 74(4) (2010) 1092-1103.

[99] G.D. Martin, S.D. Hoath, I.M. Hutchings, Inkjet printing-the physics of manipulating liquid jets and drops, J. Phys. Conf. Ser., 105 (2008) 012001-012014.

[100] J. Madejski, Solidification of droplets on a cold surface, Int. J. Heat Mass Transfer, 19(9) (1976) 1009-1013.

[101] S. Sikalo, E.N. Ganic, Phenomena of droplet-surface interactions, Exp. Therm. Fluid Sci., 31(2) (2006) 97-110.

[102] J. Fukai, Z. Zhao, D. Poulikakos, C.M. Megaridis, O. Miyatake, Modeling of the deformation of a liquid droplet impinging upon a flat surface, Phys. Fluids A Fluid Dyn., 5(11) (1993) 2588-2599.

[103] J. Fukai, Y. Shiiba, T. Yamamoto, O. Miyatake, D. Poulikakos, C.M. Megaridis, Z. Zhao, Wetting effects on the spreading of a liquid droplet colliding with a flat surface-experiment and modeling, Phys. Fluids, 7(2) (1995) 236-247.

[104] F.H. Harlow, J.P. Shannon, The splash of a liquid drop, J. Appl. Phys., 38(10) (1967) 3855-3866.

[105] A.M. Worthington, On the forms assumed by drops of liquids falling vertically on a horizontal plate, Proc. R. Soc. Lond., 25(171-178) (1876) 261-272.

[106] M. Rein, Phenomena of liquid-drop impact on solid and liquid surfaces, Fluid Dyn. Res., 12(2) (1993) 61-93.

[107] R. Rioboo, C. Tropea, M. Marengo, Outcomes from a drop impact on solid surfaces, Atomization Spray, 11(2) (2001) 155-165.

[108] S. Chandra, C.T. Avedisian, On the collision of a droplet with a solid-surface, R. Soc. Lond. Proc. Ser. A Math. Phys. Eng. Sci., 432(1884) (1991) 13-41.

[109] R. Rioboo, M. Marengo, C. Tropea, Time evolution of liquid drop impact onto solid, dry surfaces, Exp. Fluids, 33(1) (2002) 112-124.

[110] C. Clanet, C. Beguin, D. Richard, D. Quere, Maximal deformation of an impacting drop, J. Fluid Mech., 517 (2004) 199-208.

[111] D. Bartolo, C. Josserand, D. Bonn, Retraction dynamics of aqueous drops upon impact on non-wetting surfaces, J. Fluid Mech., 545 (2005) 329-338.

[112] J.F. Scamehorn, Phenomena in mixed surfactant systems, in, American Chemical Society, Washington, DC, 1986.

[113] D.J. Shaw, Introduction to colloid and surface chemistry, in, Elsevier Science, 1992.

[114] M.J. Rosen, Surfactants and interfacial phenomenon, in, John Wiley & Sons, Inc., New Jersey, 2004.

[115] P.C. Hiemenz, Principles of colloid and surface chemistry, in, Marcel Dekker, New York, 1977.

[116] L.L. Schramm, E.N. Stasiuk, D.G. Marangoni, 2 Surfactants and their applications, Annu. Rep. Sect. C (Phys. Chem.), 99(0) (2003) 3-48.

[117] H.J. Butt, K. Graf, M. Kappl, Physics and Chemistry of Interfaces, Wiley, 2006.

[118] D. Myers, Surfaces, interfaces, and colloids, 2nd ed., Wiley-VCH, 1999.

[119] K.L. Mittal, Micellization, solubilization, and microemulsions, 2nd ed., Plenum Press, New York, 1977.

[120] T. Charles, The hydrophobic effect: formation of micelles and biological membranes, Wiley, New York, 1980.

[121] J.N. Israelachvili, D.J. Mitchell, B.W. Ninham, Theory of self-assembly of hydrocarbon amphiphiles into micelles and bilayers, J. Chem. Soc. Faraday Trans., 72(0) (1976) 1525-1568.

[122] R. Strey, R. Schomacker, D. Roux, F. Nallet, U. Olsson, Dilute lamellar and L3 phases in the binary water-C12E5 system, J. Chem. Soc. Faraday Trans., 86(12) (1990) 2253-2261.

[123] V. Yaminsky, T. Nylander, B. Ninham, Thermodynamics of transfer of amphiphiles between the liquid-air interface and a solid surface-wetting tension study of Langmuir-Blodgett films, Langmuir, 13(6) (1997) 1746-1757.

[124] V.M. Starov, S.R. Kosvintsev, M.G. Velarde, Spreading of surfactant solutions over hydrophobic substrates, J. Colloid Interface Sci., 227(1) (2000) 185-190.

[125] M. Cachile, A.M. Cazabat, Spontaneous spreading of surfactant solutions on hydrophilic surfaces: CnEm in ethylene and diethylene glycol, Langmuir, 15(4) (1999) 1515-1521.

[126] V. Dutschk, K.G. Sabbatovskiy, M. Stolz, K. Grundke, V.M. Rudoy, Unusual wetting dynamics of aqueous surfactant solutions on polymer surfaces, J. Colloid Interface Sci., 267(2) (2003) 456-462.

[127] W.D. Harkins, A. Feldman, Films. The spreading of liquids of liquids and the spreading coefficient, J. Am. Chem. Soc., 44(12) (1922) 2665-2685.

[128] J.A. Moriarty, L.W. Schwartz, E.O. Tuck, Unsteady spreading of thin liquid-flims with small surface-tension, Phys. Fluids A Fluid Dyn., 3(5) (1991) 733-742.

[129] J.J. Haitsma, U. Lachmann, B. Lachmann, Exogenous surfactant as a drug delivery agent, Adv. Drug Deliv. Rev., 47(2-3) (2001) 197-207.

[130] K.J. Ruschak, Coating flows, Annu. Rev. Fluid Mech., 17 (1985) 65-89.

[131] J. Fay, The spread of oil slicks on a calm sea, in: D. Hoult (Ed.) Oil on the sea, Springer US, 1969, pp. 53-63.

[132] D.W. Camp, J.C. Berg, The spreading of oil on water in the surface-tension regime, J. Fluid Mech., 184 (1987) 445-462.

[133] D.P. Hoult, Oil spreading on sea, Annu. Rev. Fluid Mech., 4 (1972) 341-&.

[134] A.D. Dussaud, S.M. Troian, Dynamics of spontaneous spreading with evaporation on a deep fluid layer, Phys. Fluids, 10(1) (1998) 23-38.

[135] G. Karapetsas, R.V. Craster, O.K. Matar, Surfactant-driven dynamics of liquid lenses, Phys. Fluids, 23(12) (2011).

[136] R. Sharma, R. Kalita, E.R. Swanson, T.E. Corcoran, S. Garoff, T.M. Przybycien, R.D. Tilton, Autophobing on liquid subphases driven by the interfacial transport of amphiphilic molecules, Langmuir, 28(43) (2012) 15212-15221.

[137] R. Sharma, T.E. Corcoran, S. Garoff, T.M. Przybycien, E.R. Swanson, R.D. Tilton, Quasi-immiscible spreading of aqueous surfactant solutions on entangled aqueous polymer solution subphases, ACS Appl. Mater. Interfaces, 5(12) (2013) 5542-5549.

[138] V.M. Starov, A. deRyck, M.G. Velarde, On the spreading of an insoluble surfactant over a thin viscous liquid layer, J. Colloid Interface Sci., 190(1) (1997) 104-113.

[139] D.W. Fallest, A.M. Lichtenberger, C.J. Fox, K.E. Daniels, Fluorescent visualization of a spreading surfactant, New J. Phys., 12 (2010).

[140] M. Foda, R.G. Cox, The spreading of thin liquid films on a water-air interface, J. Fluid Mech., 101 (1980) 33-51.

[141] P. Joos, J. Pintens, Spreading kinetics of liquids on liquids, J. Colloid Interface Sci., 60(3) (1977) 507-513.

[142] D.P. Gaver, J.B. Grotberg, The dynamics of a localized surfactant on a thin-film, J. Fluid Mech., 213 (1990) 127-148.

[143] O.E. Jensen, Self-similar, surfactant-driven flows, Phys. Fluids, 6(3) (1994) 1084-1094.

[144] P. Joos, J. Vanhunsel, Spreading of aqueous surfactant solutions on organic liquids, J. Colloid Interface Sci., 106(1) (1985) 161-167.

[145] K.S. Lee, V.M. Starov, Spreading of surfactant solutions over thin aqueous layers: Influence of solubility and micelles disintegration, J. Colloid Interface Sci., 314(2) (2007) 631-642.

[146] T. Stoebe, Z.X. Lin, R.M. Hill, M.D. Ward, H.T. Davis, Superspreading of aqueous films containing trisiloxane surfactant on mineral oil, Langmuir, 13(26) (1997) 7282-7286.

[147] T.F. Svitova, R.M. Hill, C.J. Radke, Spreading of aqueous dimethyldidodecylammonium bromide surfactant droplets over liquid hydrocarbon substrates, Langmuir, 15(21) (1999) 7392-7402.

[148] T.F. Svitova, R.M. Hill, C.J. Radke, Spreading of aqueous trisiloxane surfactant solutions over liquid hydrophobic substrates, Langmuir, 17(2) (2001) 335-348.

[149] A. Chauhan, T.F. Svitova, C.J. Radke, A sorption-kinetic model for surfactant-driven spreading of aqueous drops on insoluble liquid substrates, J. Colloid Interface Sci., 222(2) (2000) 221-232.

[150] T. Stoebe, Z.X. Lin, R.M. Hill, M.D. Ward, H.T. Davis, Surfactant-enhanced spreading, Langmuir, 12(2) (1996) 337-344.

[151] T. Svitova, R.M. Hill, Y. Smirnova, A. Stuermer, G. Yakubov, Wetting and interfacial transitions in dilute solutions of trisiloxane surfactants, Langmuir, 14(18) (1998) 5023-5031.

[152] N.A. Ivanova, Z.B. Zhantenova, V.M. Starov, Wetting dynamics of polyoxyethylene alkyl ethers and trisiloxanes in respect of polyoxyethylene chains and properties of substrates, Colloids Surf., A, 413 (2012) 307-313.

[153] J. Radulovic, K. Sefiane, M.E.R. Shanahan, Spreading and wetting behaviour of trisiloxanes, J. Bionic. Eng., 6(4) (2009) 341-349.

[154] Y. Zhang, F. Han, The spreading behaviour and spreading mechanism of new glucosamide-based trisiloxane on polystyrene surfaces, J. Colloid Interface Sci., 337(1) (2009) 211-217.

[155] A. Chengara, A. Nikolov, D. Wasan, Surface tension gradient driven spreading of trisiloxane surfactant solution on hydrophobic solid, Colloids Surf., A, 206(1-3) (2002) 31-39.

[156] X. Tang, J. Dong, X. Li, A comparison of spreading behaviors of Silwet L-77 on dry and wet lotus leaves, J. Colloid Interface Sci., 325(1) (2008) 223-227.

[157] S. Rafai, D. Bonn, Spreading of non-newtonian fluids and surfactant solutions on solid surfaces, Phys. A, 358(1) (2005) 58-67.

[158] M. Knoche, H. Tamura, M.J. Bukovac, Performance and stability of the organosilicone surfactant L-77 effect of PH, concentration, and temperature, J. Agric. Food Chem., 39(1) (1991) 202-206.

[159] A.V. Chengara, A.D. Nikolov, D.T. Wasan, New paradigms for spreading of colloidal fluids on solid surfaces, in: R. Narayanan (Ed.) Interfacial Processes and Molecular Aggregation of Surfactants, 2008, pp. 117-141.

[160] G. Karapetsas, R.V. Craster, O.K. Matar, On surfactant-enhanced spreading and superspreading of liquid drops on solid surfaces, J. Fluid Mech., 670 (2011) 5-37.

[161] T. Svitova, H. Hoffmann, R.M. Hill, Trisiloxane surfactants: surface interfacial tension dynamics and spreading on hydrophobic surfaces, Langmuir, 12(7) (1996) 1712-1721.

[162] Z.X. Lin, R.M. Hill, H.T. Davis, M.D. Ward, Determination of wetting velocities of surfactant superspreaders with the quartz-crystal microbalance, Langmuir, 10(11) (1994) 4060-4068.

[163] T. Stoebe, Z.X. Lin, R.M. Hill, M.D. Ward, H.T. Davis, Enhanced spreading of aqueous films containing ethoxylated alcohol surfactants on solid substrates, Langmuir, 13(26) (1997) 7270-7275.

[164] W.B. Hardy, The spreading of fluids on glass, Phil. Mag. , 38 (1919) 49-54.

[165] K. Morton, O.K.C. Tsui, C.-K. Tung, J.C. Sturm, S.Y. Chou, R. Austin, The anti-lotus leaf effect in nanohydrodynamic bump arrays, New J. Phys., 12 (2010).

[166] H.P. Kavehpour, B. Ovryn, G.H. McKinley, Microscopic and macroscopic structure of the precursor layer in spreading viscous drops, Phys. Rev. Lett., 91(19) (2003).

[167] T. Stoebe, R.M. Hill, M.D. Ward, H.T. Davis, Enhanced spreading of aqueous films containing ionic surfactants on solid substrates, Langmuir, 13 (1997) 7276-7281.

[168] V. Starov, K. Sefiane, On evaporation rate and interfacial temperature of volatile sessile drops, Colloids Surf., A, 333(1–3) (2009) 170-174.

[169] D. Fell, M. Sokuler, A. Lembach, T. Eibach, C. Liu, E. Bonaccurso, G. Auernhammer, H.-J. Butt, Drop impact on surfactant films and solutions, Colloid & Polymer Sci, 291(8) (2013) 1963-1976.

[170] A.M. Khan, S.S. Shah, Determination of critical micelle concentration (Cmc) of sodium dodecyl sulfate (SDS) and the effect of low concentration of pyrene on its Cmc using ORIGIN software, J. Chem. Soc. Pak., 30(2) (2008) 186-191.

[171] G. Loglio, P. Pandolfini, R. Miller, A.V. Makievski, F. Ravera, M. Ferrari, L. Liggieri, Drop and bubble shape analysis as a tool for dilational rheological studies of interfacial layers, in: D. Möbius, R. Miller (Eds.) Studies in Interface Science, Elsevier, 2001, pp. 439-483.

[172] http://www.accudynetest.com/polytable_03.html?sortby=contact_angle.

[173] T. Svitova, R.M. Hill, C.J. Radke, Adsorption layer structures and spreading behavior of aqueous non-ionic surfactants on graphite, Colloids Surf., A, 183 (2001) 607-620.

[174] R. Fetzer, M. Ramiasa, J. Ralston, Dynamics of liquid-liquid displacement, Langmuir, 25(14) (2009) 8069-8074.

[175] P.G. Petrov, J.G. Petrov, A combined molecular-hydrodynamic approach to wetting kinetics Langmuir, 8(7) (1992) 1762-1767.

[176] T. Roques-Carmes, V. Mathieu, A. Gigante, Experimental contribution to the understanding of the dynamics of spreading of Newtonian fluids: Effect of volume, viscosity and surfactant, J. Colloid Interface Sci., 344(1) (2010) 180-197.

[177] W. Hopf, H. Stechemesser, Three-phase contact line movement in systems with and without surfactant, Colloids Surf., 33(0) (1988) 25-33.

[178] J.G. Petrov, B.P. Radoev, Steady motion of the three phase contact line in model Langmuir-Blodgett systems, Colloid & Polymer Sci, 259(7) (1981) 753-760.

[179] S.M. Troian, X.L. Wu, S.A. Safran, Fingering instability in thin wetting films, Phys. Rev. Lett., 62(13) (1989) 1496-1499.

[180] K. Kenyon, Capillary waves understood by an elementary method, J. Oceanogr. , 54(4) (1998) 343-346.

[181] F. Behroozi, N. Podolefsky, Dispersion of capillary-gravity waves: a derivation based on conservation of energy, Eur. J. Phys., 22(3) (2001) 225-231.

[182] C.H. Chang, E.I. Franses, Adsorption dynamics of surfactants at the air/water interface-a critical review of mathematical models, data, and mechanisms, Colloids Surf., A, 100 (1995) 1-45.

[183] A.Q. Shen, B. Gleason, G.H. McKinley, H.A. Stone, Fiber coating with surfactant solutions, Phys. Fluids, 14(11) (2002) 4055-4068.

[184] S.T. Thoroddsen, B. Qian, T.G. Etoh, K. Takehara, The initial coalescence of miscible drops, Phys. Fluids, 19(7) (2007).

[185] E.R. Swanson, S.L. Strickland, M. Shearer, K.E. Daniels, urfactant spreading on a thin liquid film: reconciling models and experiments, J. Eng. Math., (2014).

[186] G. Falkovich, Fluid Mechanics: A Short Course for Physicists, Cambridge University Press, New York, 2011.

[187] J. Lighthill, Waves in Fluids, 2nd ed., Cambridge University Press, New York, 2001.

[188] A.B. Afsar-Siddiqui, P.F. Luckham, O.K. Matar, Unstable spreading of aqueous anionic surfactant solutions on liquid films. 2. Highly soluble surfactant, Langmuir, 19(3) (2003) 703-708.

[189] D.J. Acheson, Elementary Fluid Dynamics, Oxford University Press Inc., New York, 1990.

[190] H.D. Ceniceros, The effects of surfactants on the formation and evolution of capillary waves, Phys. Fluids, 15(1) (2003) 245-256.

[191] X. Liu, J.H. Duncan, G.M. Korenowski, J.S. Kelly, A laboratory study of longitudinal waves in surfactant films in a water wave tank, J. Geophys. Res., 112(C6) (2007).

[192] J.R. Saylor, A.J. Szeri, G.P. Foulks, Measurement of surfactant properties using a circular capillary wave field, Exp. Fluids, 29(6) (2000) 509-518.

[193] P. Marmottant, E. Villermaux, C. Clanet, Transient surface tension of an expanding liquid sheet, J. Colloid Interface Sci., 230(1) (2000) 29-40.

[194] M. Aytouna, D. Bartolo, G. Wegdam, D. Bonn, S. Rafai, Impact dynamics of surfactant laden drops: dynamic surface tension effects, Exp. Fluids, 48(1) (2010) 49-57.

[195] J.J. Cooper-White, R.C. Crooks, D.V. Boger, A drop impact study of worm-like viscoelastic surfactant solutions, Colloids Surf., A, 210(1) (2002) 105-123.

[196] N. Mourougou-Candoni, B. Prunet-Foch, F. Legay, M. Vignes-Adler, K. Wong, Retraction phenomena of surfactant solution drops upon impact on a solid substrate of low surface energy, Langmuir, 15(19) (1999) 6563-6574.

[197] K.P. Gatne, M.A. Jog, R.M. Manglik, Surfactant-induced modification of low Weber Number droplet impact dynamics, Langmuir, 25(14) (2009) 8122-8130.

[198] M. PasandidehFard, Y.M. Qiao, S. Chandra, J. Mostaghimi, Capillary effects during droplet impact on a solid surface, Phys. Fluids, 8(3) (1996) 650-659.

[199] X.G. Zhang, O.A. Basaran, Dynamic surface tension effects in impact of a drop with a solid surface, J. Colloid Interface Sci., 187(1) (1997) 166-178.

[200] N. MourougouCandoni, B. PrunetFoch, F. Legay, M. VignesAdler, K. Wong, Influence of dynamic surface tension on the spreading of surfactant solution droplets impacting onto a low-surface-energy solid substrate, J. Colloid Interface Sci., 192(1) (1997) 129-141.

[201] S.S. Dukhin, G. Kretzschmar, R. Miller, Dynamics of adsorption at liquid interfaces, in, Elsevier, Amsterdam, Holland, 1995.

[202] M.I. Smith, V. Bertola, Effect of polymer additives on the wetting of impacting droplets, Phys. Rev. Lett., 104(15) (2010).

[203] V. Bertola, Effect of polymer additives on the apparent dynamic contact angle of impacting drops, Colloids Surf., A, 363(1-3) (2010) 135-140.

[204] V. Bergeron, D. Bonn, J.Y. Martin, L. Vovelle, Controlling droplet deposition with polymer additives, Nature, 405(6788) (2000) 772-775.

Curriculum Vitae

Name: Xiang Wang

Date of Birth: 27/11/1987

Place of Birth: Shangqiu, Henan Province, China

Education

10/2011-12/2014	**Ph.D. Candidate**, Department of Mechanical Engineering, Technische Universität Darmstadt (TU Darmstadt), Germany
08/2014-09/2014	**Visiting Scholar**, Department of Physics, Carnegie Mellon University, United States of America
09/2009-08/2011	**M.Phil.**, Nano Science and Technology, Hong Kong University of Science and Technology (HKUST), China
10/2005-06/2009	**B.Sc.**, Electronics & Information Science, Department of Mathematics and Physics, Chongqing University (CQU), China

Work Experience

01/2014 - 06/2014	**Bachelor Adviser** at Department of Mechanical Engineering
06/2011 - 08/2011	**Bachelor Adviser** at Department of Physics, HKUST
09/2009 - 08/2011	**Research Assistant** at Micro-/Nano-fluidics Group, HKUST
09.2010 - 06.2011	**Project Coordinator** at Micro-/Nano-fluidics Group, HKUST → Co-raised HKD 1.7 Million from HK government (NAMI Fund) → Structured research plans and business proposals
09/2009 - 04/2011	**Teaching Assistant** at Department of Physics, HKUST
02/2009 - 04/2009	**Intern** at Fuqiang-Huawei Environment Engineering Ltd., China
12/2008 - 01/2009	**Intern** at Mechanical and Electronic Workshop, CQU
02/2007 - 06/2007	**Administration Assistant** at Student Affairs Office, CQU

Publications and Patent

1. X. Wang, E. Bonaccurso, J. Venzmer, S. Garoff, “Surfactant-enhanced spreading on a water subphase”, submitted to Langmuir (2014).
2. Y.G. Wang, X. Wang, L.O. Heim, H. Breitzke, G. Buntkowsky, K. Zhang, “Superhydrophobic surfaces from surface-hydrophobized cellulose fibers with stearoyl groups”, Cellulose, DOI 10.1007/s10570-014-0505-y (2014).
3. X. Wang, L.Q. Chen, E. Bonaccurso, “Comparison of spontaneous wetting and impact dynamics of aqueous surfactant solutions on hydrophobic polypropylene surfaces: scaling of the contact radius”, Colloid and Polymer Science, DOI 10.1007/s00396-014-3410-x (2014).
4. X. Wang, L.Q. Chen, E. Bonaccurso, J. Venzmer, “Dynamic wetting of hydrophobic polymers by aqueous surfactant and superspreader solutions,” Langmuir, **29**, 14855 (2013).
5. X. Wang, S. Li, L. Wang, X. Yi, Y. Hui, J. Qin, W. Wen, “Microfluidic device for controllable chemical release via field-actuated membrane incorporating nanoparticles”, Journal of Nanomaterials, 864584 (2013).
6. J. Li*, X. Wang*, C. Cheng, L. Wang, E. Zhao, X. Wang, W. Wen, Selective modification for polydimethylsiloxane chip by micro-plasma, Journal of Materials Science, **48**, 1330 (2013). (* co-first author with equal contribution)
7. B. Zhou, L. Wang, S. Li, X. Wang, Y. Hui, W. Wen, “Universal logic gates via liquid-electronic hybrid divider”, Lab Chip, **12**, 5211 (2012).
8. M. Zhang, L. Wang, X. Wang, J. Wu, J. Li, X. Gong, J. Qin, W. Li, W. Wen, “Microdroplets-based universal logic gates by electrorheological fluid”, Soft Matter, **7**, 7493 (2011).
9. J. Wu, M. Zhang, X. Wang, S. Li, W. Wen, “A simple approach for local contact angle determination on a heterogeneous surface”, Langmuir, **27**, 5705 (2011).
10. L. Chen, X. Wang, W. Wen, Z. Li, “Critical droplet volume for spontaneous capillary wrapping”, Applied Physics Letters, **97**, 124103 (2010).
11. W. Wen, L. Wang, X. Wang, S. Li, “Liquid-electronic hybrid divider”, US 2013/0037149 A1 (2013).

Conference Presentations

Oral contribution

06.2014 20th International Symposium on Surfactants in Solution, Coimbra, Portugal

Poster contribution

04.2014 The Physics of Soft and Biological Matter, Cambridge, United Kingdom

04.2014 10th Zsigmondy-Colloquium of Kolloid-Gesellschaft e.V., Konstanz, Germany

03.2014 555th WE-Heraeus-Seminar, Bad Honnef, Germany

03.2013 9th Zsigmondy-Colloquium of Kolloid-Gesellschaft e.V., Essen, Germany

03.2012 8th Zsigmondy-Colloquium of Kolloid-Gesellschaft e.V., Darmstadt, Germany

04.2010 East Asian Postgraduate Workshop on Soft Matter, Hong Kong, China

Awards

09.2009 – 08.2011 Postgraduate Studentship, HKUST

12.2009 Excellent Student Scholarship, CQU (ranked 1st for 8 semesters)

06.2009 Excellent Graduate, Chongqing

12.2008 National 1st Prize in Social Survey, China

11.2008 Silver Medal in National Challenge Cup, China

11.2008 National Scholarship for Academic Excellence, China

10.2008 Model of Outstanding Student, Chongqing (The only awardee)

11.2007 Luzhou Laojiao Scholarship

03.2007 Excellent Student Cadre, CQU

03.2006 – 06.2009 1st Class Scholarship for Excellent Academic Performance, CQU